Low Complex, Power Efficient Modulation Schemes for VLC Systems and Hardware Implementation

Submitted in partial fulfilment of the requirements

for the award of the degree of

Doctor of Philosophy

by

Ganesh Miriyala

(Roll No: 718039)

Under the supervision of

Prof. V. Venkata Mani

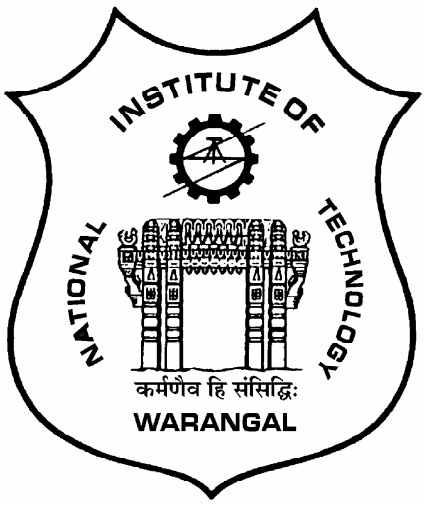

Department of Electronics & Communication Engineering

National Institute of Technology Warangal

Telangana, India - 506004

2024

Dedicated

To

My Family,

Teachers & Friends

Approval Sheet

This thesis entitled **Low Complex, Power Efficient Modulation Schemes for VLC Systems and Hardware Implementation** by **Ganesh Miriyala** is approved for the degree of **Doctor of Philosophy**.

Examiners

Research Supervisor

Dr. V. Venkata Mani
Department of ECE
NIT Warangal, India-506004

Chairman & Head

Dr. P. Sreehari Rao
Department of ECE
NIT Warangal, India-506004

Place:

Date:

Declaration

This is to certify that the work presented in this thesis entitled **Low Complex, Power Efficient Modulation Schemes for VLC Systems and Hardware Implementation** is a bonafied work done by me under the supervision of **Dr. V. Venkata Mani** and was not submitted elsewhere for the award of any degree.

I declare that this written submission represents my own ideas and even considered others ideas which are adequately cited and further referenced the original sources. I understand that any violation of the above will cause disciplinary action by the institute and can also evoke panel action from the sources or from whom proper permission has not been taken when needed. I also declare that I have adhered to all principles of academic honesty and integrity and have not misrepresented or fabricated or falsified any idea or data or fact or source in my submission.

Place:

Date:

Ganesh Miriyala
Research Scholar
Roll No.: 718039

NATIONAL INSTITUTE OF TECHNOLOGY

WARANGAL, INDIA-506004

Department of Electronics & Communication Engineering

CERTIFICATE

This is to certify that the thesis work entitled is a bonafide record of work carried out by **Ganesh Miriyala** submitted to the faculty of **Electronics & Communication Engineering** department, in partial fulfilment of the requirements for the award of the degree of **Doctor of Philosophy** in **Electronics and Communication Engineering, National Institute of Technology Warangal, India-506004**. The contributions embodied in this thesis have not been submitted to any other university or institute for the award of any degree.

Dr. V. Venkata Mani

Research Supervisor

Professor

Department of ECE

NIT Warangal, India-506 004.

Place:

Date:

Acknowledgements

First and foremost, I thank my research supervisor, Prof. V. Venkata Mani for her continuous guidance, encouragement and consistent support throughout my research work. I feel that I am blessed to work with her, who is having immense knowledge, enthusiasm, passion and potential in the area of wireless communication, which benfited me to develop the core concepts on multi carrier modulation techniques. She always stay as a role model with her inspiration, admiration and suggestions at various stages of this duration, at both technical and personal level. She always boosts up my confidence,, extends my wings in understanding the concepts, foresees my capabilities, spends countless hours and adds every little information to extend my boundary limits. Undoubtedly, I couldn't imagine a better supervisor than her to complete successfully my PhD work.

My sincere thanks to chairman of the Doctoral Scrutiny Committee (DSC) and Head of the department Prof. P. Sreehari Rao for his indispensable advices, motivation and essential comments at various stages of this work. I would also like to thank the DSC members, Prof. Padmavathy (External Member-Computer Science & Engineering), Prof. L. Anjaneyulu (Member-Internal-Department of Electronics & Communication Engineering) and Prof. T. Kishore Kumar (Member-Internal-Department of Electronics & Communication Engineering) who has always driven me with their constructive suggestions, fruitful discussions and thought provoking words during my doctoral studies. I further extend my thanks to all the faculty members of the Department of ECE and non teaching staff for their support.

I have been extremely happy and so lucky to have some of the enthusiastic and incredible people in the Wireless Communication Research Laboratory (WCRL), Dr. Sai Krishna Kondoju, Dr. Shravan kumar bandari, Dr. Valluri Sivaprasad, Dr. Vejandla Kishore, Renikunta Mallaiah, Mounika Jammula, Abhay Narasimha, Sandhya, Sai Kiran,

Greeshma, Niharika, Rehena, Gowthami, Hema Latha, Prathyusha and Jahnavi whose friendship is truly valuable, always having a healthy technical debates and having enjoyable non-technical aspects to relax from rigid thoughts. My deep thanks to all the teachers having their blessings and friends who are constantly in touch with me, wishes me to achieve great heights, giving financial help and supporting all events in my life. I also want to acknowledge anonymous reviewers for taking there valuable time to evaluate this thesis and suggesting improvements.

Whatever I accomplish it's only because of my parents Yellesham and Gangamma, my wife Adhya, my mother-in-law Dhasma, brother Bhanu, brother-in-law Satyanarayana and my lucky daughter Hitanshi Aaroohi's everlasting support, care and love. A simple 'thank you' is not just good enough to show my immense love, and gratitude towards them no words to express my gratefulness to them, I wish them a good healthy life ahead. I want to thank them for their unwavering support throughout my education, endless love, and understanding of my goals and for being my side throughout my ups and downs, which kept me moving forward. Finally, thanks to God for giving me an opportunity to meet all these wonderful people and for giving me this life with warm memories.

Ganesh Miriyala

Abstract

The rise of groundbreaking technologies such as massive machine-type communication (MTC), Internet of Things (IoT), and smart cities concepts have significantly emphasized the need for an alternative channel to alleviate the congestion in the Radio Frequency (RF) spectrum for wireless communication. To address this demand, Visible Light Communication (VLC) technology has emerged as a viable solution within the realm of optical wireless communication. VLC transmits information through the Intensity Modulation (IM) of Light Emitting Diode (LED) light and receives it through Direct Detection (DD) using a Photodiode at the receiver. Several variants of Optical Orthogonal Frequency Division Multiplexing (O-OFDM) have been developed within the constraints of this incoherent modulation technique in VLC, employing Hermitian symmetry. However, systems that employ IM/DD and rely on these O-OFDM modulations encounter certain drawbacks in terms of spectral efficiency and energy efficiency and computational complexity. Furthermore, the utilization of O-OFDM schemes results in a high peak-to-average power ratio (PAPR), causing significant signal distortion when transmitted through nonlinear devices in the front end. Additionally, the rapid development of high-speed 5G systems requires waveforms that offer flexibility to meet the demands of vehicular communication technology based on VLC. These challenges emphasize the necessity for advanced multicarrier waveforms that preserve the benefits of O-OFDM variations while effectively addressing the aforementioned issues.

A new PPAPR reduction technique called Top Samples Detection and Appending (TSDA) is proposed for an O-OFDM system. Unlike other PAPR reduction schemes such as Selected Mapping (SLM) and Partial Transmit Sequence (PTS), the TSDA technique does not rely on side information, making it more efficient and practical. The TSDA technique works by identifying and modifying the high-amplitude samples in the OFDM

signal. It employs a two-step process: detection and appending. In the detection, the TSDA algorithm identifies the top samples with the highest magnitudes in each OFDM symbol. These top samples are the primary contributors to the high PAPR. Once the top samples are detected, the appending step modifies these samples by appending top samples at the tail of the actual sequence. This modification effectively reduces the overall PAPR of the signal. Importantly, the TSDA technique achieves this without requiring any additional side information, which simplifies its implementation and reduces computational complexity. To evaluate the effectiveness of the TSDA technique, the proposed method is compared with established PAPR reduction schemes like SLM and PTS. Performance metrics such as PAPR reduction, computational complexity, and bit error rate (BER) are considered in the comparison.

Subsequently, a novel modulation scheme called LADO-OFDM for VLC systems has been introduced. The primary goal of this technique is to mitigate the mutual interference between even subcarriers, which are associated with DC-biased Optical OFDM (DCO-OFDM) and ACO-OFDM, during transmission. This is achieved through the utilization of a pre-distortion technique. To assess the effectiveness of LADO-OFDM, two generalized LED models have been examined. The investigation focuses on the impact of nonlinear clipping distortion on the LED's bias point and dynamic range. By applying pre-distortion to the transmitted signal and adjusting the knee factor in the piecewise polynomial model and Rapps models, respectively, the LED's dynamic range can be linearized, thereby enhancing the performance of the system. The performance of the proposed system is then compared to that of ADO-OFDM in terms of bit error rate (BER) and computational complexity. The comparison is based on simulation results obtained through Monte Carlo BER simulations.

Consequently, a new modulation scheme called Variably-biased Asymmetrically clipped Optical OFDM (VAO-OFDM) for VLC systems is proposed. Unlike traditional constant DC bias methods, VAO-OFDM utilizes a variable bias that is dependent on specific samples. By aligning the frequency components of VAO-OFDM with pre-defined subcarriers, the variable bias does not cause any interference with the initially transmitted symbols. This bias design can helps to mitigate potential signal degradation and improve overall transmission quality. One notable advantage of VAO-OFDM over its counter-

parts is its reduced computational complexity. By incorporating a pre-distortion process, VAO-OFDM achieves a significant decrease in computational requirements compared to ADO-OFDM. This reduction in complexity allows for more efficient implementation and utilization of system resources. To validate the performance of VAO-OFDM, we conducted simulations and presented the corresponding results. Additionally, we also implemented the proposed modulation scheme on an experimental Testbed using LabView software and Universal Software-defined Radio Peripherals (USRPs). These practical validations help to demonstrate the feasibility and effectiveness of VAO-OFDM in real-world VLC systems.

Finally, a novel modulation scheme called Variably-biased Asymmetrically-clipped Optical Conjugate-symmetric Sequency-ordered Complex Hadamard Coded Modulation (VAO-CS-CHCM) is proposed for VLC systems. The objective of this scheme is to enhance power efficiency by leveraging the benefits of a discrete set of amplitudes generated through Conjugate Symmetric Sequency-ordered Complex Hadamard Transform (CS-SCHT). VAO-CS-CHCM introduces a new approach to bias design like in VAO-OFDM, where the bias is dependent on specific sample amplitudes. Additionally, the frequency domain signals of VAO-CS-CHCM are distributed across pre-defined subcarriers, similar to the VAO-OFDM scheme which is initiated in the previous contribution. This VAO-CS-CHCM ensures that the originally transmitted symbols remain unaffected by any interference, resulting in significant gains in power efficiency. Further, the simulation results are presented to evaluate the performance of VAO-CS-CHCM compared to traditional modulation schemes such as VAO-OFDM, DCO-OFDM, ACO-OFDM, and ADO-OFDM over a wide range of bit rates and normalized bandwidths. Additionally, the computational complexity of VAO-CS-CHCM is analyzed in comparison to VAO-OFDM and ADO-OFDM.

Contents

List of Figures

List of Tables

List of Abbreviations

ACO-OFDM Asymmetrically Clipped Optical OFDM

ADO-OFDM Asymmetrically clipped DC-biased Optical OFDM

BER Bit Error Rate

BBT branch-and-bound technique

CAs Complex Additions

CMs Complex Multiplications

CAP Carrier less Amplitude and Phase

CS-SCHT conjugate-symmetric sequency-ordered complex Hadamard transform

CCRR Computational Complexity Reduction Ratio

CC Computational Complexity

CSK Colour Shift Keying

DCC Digital Communications Commission

DCO-OFDM DC-biased Optical OFDM

DD Direct Detection

DFT-s Discrete Fourier transformation spread

DHT Discrete Hartley Transformation

EM Electro-Magnetic

EB Exabytes

FCC Federal Communications Commission

FFT Fast Fourier Transform

F-OFDM Flipped OFDM

GHz Giga Hertz

HCM Hadamard-coded modulation

ICI Inter Carrier Interference

IFFT Inverse Fast Fourier Transform

IoT Internet of Things

IoMT Internet of Medical Things

WPDM Wavelet Packet Division Multiplexing

IM/DD Intensity Modulation/Direct Detection

IM Intensity Modulation

FWHT Fast Walsh-Hadamard Transformation

ITUR International Telecommunication Union Radiocommunication

ISI Inter Symbol Interference

IFFT Inverse Fast Fourier Transform

J-PAM J-ary Pulse Amplitude Modulation

eU-OFDM enhanced Unipolar OFDM

SEE-OFDM Spectral and Energy Efficient-OFDM

KHz Kilo Hertz

LACO-OFDM Layered ACO-OFDM

HACO-OFDM Hybrid ACO-OFDM

LASER Light Amplification by Stimulated Emission of Radiation

LADO-OFDM Low-complex ADO-OFDM

LED Light Emitting Diode

Li-Fi Light Fidelity

MCM Multi Carrier Modulation

MIMO Multiple Input Multiple Output

NI National Instruments

OFDM Orthogonal Frequency Division Multiplexing

OWC Optical Wireless Communication

OOB Out Of Band

OOK On-Off Keying

PAM Pulse Amplitude Modulation

PAM-DMT Pulse Amplitude Modulation Discrete Multi-Tonen

PPM Pulse Position Modulation

PAPR Peak-to-Average-Power Ratio

PD Photodiode

PTS Partial Transmit Sequence

QAM Quadrature Amplitude Modulation

RF Radio Frequency

SE Spectral Efficiency

PE Power Efficiency

SLM Selected Mapping

SCM Single Carrier Modulation

SDP semi-definite programming

TI tone injection

TRAI Telecom Regulatory Authority of India

TSDA Top Samples Detection and Appending

USRP Universal Software Radio Peripheral

U-OFDM Unipolar-OFDM

VAO-OFDM Variably Biased Asymmetrically Clipped Optical OFDM

VLC Visible Light Communication

Wi-Fi Wireless Fidelity

5G Fifth Generation

Chapter 1

Introduction

1.1 Motivations

The need for data rates has been shown to grow exponentially as a result of the current trend in wireless communications, where multiple connected devices are present and demand intracommunication and intercommunication. The use of rapidly developing technologies, such as the Internet of Medical Things (IoMT), the Internet of Things (IoT) and smartphones, is largely responsible for this. In addition, factors including the rise in online activities like e-commerce, gaming, and social networking, as well as the availability of data at lower costs in some populated nations, all contributed to the increase in the data rate needed. According to International Telecommunication Union Radiocommunication (ITUR), by 2030, according to predictions, approximately two-thirds of the global population are expected to have access to the Internet., and non-PC devices would contribute 75 % of the data traffic [2]. The projected growth of global mobile subscriptions is depicted in Fig. 1.1, indicating a rapid increase from 2020 to 2030. The total number of global mobile subscriptions had already reached 6.7 billion in 2013. With advancements in system performance and the introduction of new and widely adopted device types and applications, the future is expected to witness a significant surge in global mobile subscriptions. Projections suggest that by 2025, Global mobile subscriptions have the potential to reach a staggering 13.8 billion in number, and by 2030, it may further increase to 17.1 billion. The development of mobile communications and electronic technologies will lead to enhanced user experiences and more affordable devices, consequently accelerating

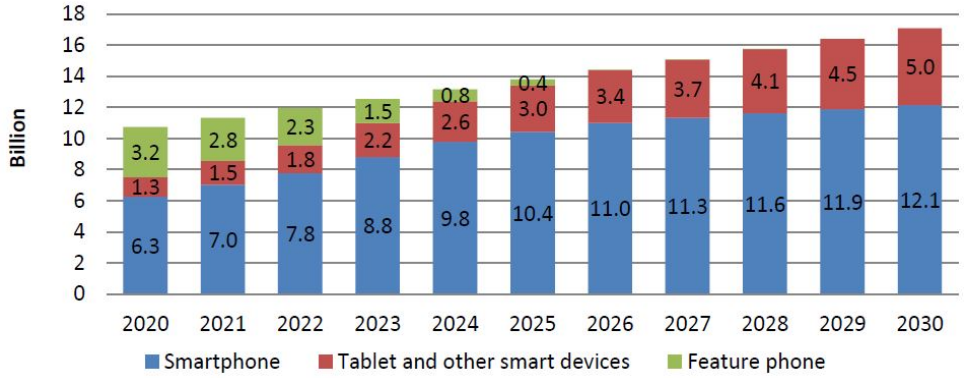

Figure 1.1: Estimation of Global Mobile Subscriptions with different categories

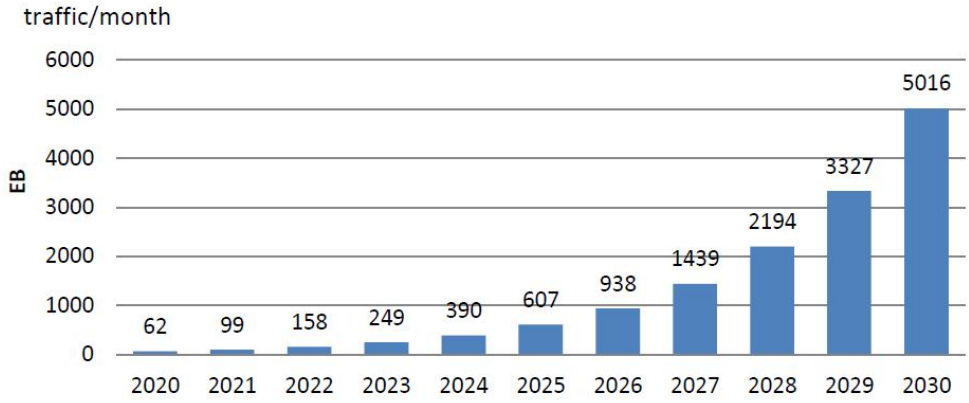

Figure 1.2: Global IMT traffic estimations

the penetration rate of tablets between 2020 and 2030. It is estimated that by 2025, there could be around 10 billion smartphone subscriptions globally, which is expected to grow to approximately 12 billion by 2030. Additionally, subscriptions to tablets and other smart devices are projected to reach approximately 3 billion in 2025 and 5 billion in 2030. However, during the same period, the number of non-smartphone (feature phone) subscriptions is anticipated to decline rapidly. Fig. 1.2 shows the growth of mobile traffic (including M2M traffic) at an annual rate of approximately 55% from 2020 to 2030. The estimated global mobile traffic per month is expected to reach 607 Exabytes (EB) in 2025 and 5,016 EB in 2030.

The electromagnetic spectrum, which spans from 3 Hz to 300 EHz, is divided into various bands. Among them, the Radio Frequency (RF) band occupies a range from 30 Kilo Hertz (KHz) to 300 Giga Hertz (GHz) and is extensively utilized for wireless communications in the present era. Each communication occurring worldwide is allocated

a specific frequency band for a designated period of time. To manage the limited RF spectrum, which is in high demand, global governance is carried out by the International Telecommunication Union (ITU) through licensing, while local regulatory authorities such as the Telecom Regulatory Authority of India (TRAI) in India and the Federal Communications Commission (FCC) in the United States implement auctions. The scarcity of RF spectrum has intensified competition among telecom operators, prompting the Digital Communications Commission (DCC), the primary decision-making body for telecommunications in India, to set the reserve price for the 8.3 GHz band at Rs. 5.22 lakh crore in the upcoming auction for Fifth Generation Fifth Generation (5G) bands [3].

Martin Cooper, widely recognized as the father of mobile telephony and a pioneering figure in wireless communications, made a significant prediction regarding the exponential growth of wireless capacity. According to his foresight, the capacity of wireless communications has doubled every 2.5 years since the inception of wireless transmission in 1895. Analyzing the overall growth in wireless capacity from 1957 to 2008, it was found that a 25-fold increase was achieved through the release of additional spectrum. Another five-fold growth was accomplished through spectrum reformation, while an additional five-fold improvement was attributed to advancements in physical layer designs [4]. Notably, an astounding 1600-fold growth was attained by reducing cell size and transmission distance. However, this achievement also led to an increase in cell density, resulting in co-channel interference limitations in the RF domain. Remarkably, in an effort to mitigate interference, access points for Wireless Fidelity (Wi-Fi) were strategically positioned under stadium seats, leveraging the attenuation properties of the human body [5].

There is a growing focus among scientists and engineers on utilizing millimeter wave bands ranging from 30 GHz to 300 GHz to meet the demands of 5G technology. The exploration of Multiple Input Multiple Output (MIMO) technologies has opened up possibilities for utilizing millimeter bands, which allow for the use of numerous antennas due to their smaller wavelengths. However, the transmission at these higher frequencies faces significant challenges, such as substantial atmospheric losses and limited penetration depth, resulting in shorter transmission distances. Additionally, the implementation of new hardware for this technology incurs substantial costs. Moreover, there are valid concerns regarding the health and safety of humans as well as the balance of ecosystems [6].

Hence, it is imperative to overcome the imminent RF spectrum crunch by leveraging new technologies in the electromagnetic spectrum's next frequency bands to meet the demands of next-generation communications. Within the realm of Optical Wireless Communication (OWC), recent research studies [7] have brought attention to the potential of infrared and white Light Emitting Diode (LED) based OWC systems for indoor wireless networks.

As the global adoption of solid-state lighting infrastructure has revolutionized energy conservation efforts, Visible Light Communication (VLC) is rapidly gaining recognition as a promising communication technology. VLC utilizes the spectrum between 400 nm and 700 nm, facilitated by the widespread use of VLC in solid-state lighting. This technology offers significant bandwidth advantages, operates in unlicensed frequency bands, and poses no harm when eye safety requirements are met. VLC not only provides immense bandwidth in the Terahertz range but also offers additional benefits such as energy efficiency, minimal interference, secure communication, absence of health risks, and cost-effective deployment with existing infrastructure. It is envisioned that leveraging the entire visible spectrum can enable data rates of up to 100 Gbps. However, maximizing spectrum utilization presents considerable challenges due to the limited frequency response of front-end devices, which typically results in a bandwidth limitation of up to 6.8 GHz [8].

The evolution of solid-state lighting began in 1962 with the pioneering works of Holonyak and Bevacqua in New York, where they demonstrated low-intensity light emission using inorganic materials (GaAsP) [9]. This breakthrough paved the way for the development of blue LEDs based on nitride alloys, which were later combined with phosphors to generate white light [10]. Presently, LED-based solid-state lighting has been widely commercialized and finds applications as indicators in traffic monitoring, liquid-crystal displays, backlighting for cell phones, and large indoor and outdoor displays in various public venues. LEDs offer two indispensable features: significant energy savings without environmental harm and the ability to control emitted light properties, including spectrum, color, direction, and polarization. The economic and environmental impact of LEDs is substantial, which led to the authors receiving the 2014 Nobel Prize in Physics [10].

The increased efficiency of LEDs has resulted in a significant expansion of LED

lighting infrastructure worldwide. Unlike traditional lighting technologies, LEDs offer the unique advantage of rapid and imperceptible switching between different intensity levels, allowing for parallel illumination and communication in the emerging VLC technology. VLC utilizes the variation in light intensity emitted by LEDs, known as Intensity Modulation (IM), to transmit information. This information is then detected by a Photodiode (PD) on the receiving end using Direct Detection (DD). Recently, the standard in [11] has been revised to incorporate a high-speed wireless network called Light Fidelity (Li-Fi). Li-Fi aims to provide seamless data connectivity similar to RF networks, with the added benefits of user mobility and handover capabilities. It supports bidirectional communication among multiple users and utilizes photocells with broad spatial usability to enhance Spectral Efficiency (SE). A new standard, IEEE 802.11bb, has been established by a task group within IEEE 802.11 specifically for Li-Fi [12].

In VLC, the transmission of information occurs through LED light in the form of intensity modulation. However, this digital modulation technique poses certain challenges and necessitates specific requirements. Single Carrier Modulation (SCM), commonly utilized in VLC systems, includes techniques such as Pulse Position Modulation (PPM), Pulse Amplitude Modulation (PAM), On-Off Keying (OOK), which are relatively easy to implement [13]. OOK modulation simply switches the LED on and off, allowing for dimming control. However, all SCMs encounter Inter Symbol Interference (ISI) when operating at higher data rates in dispersive optical channels. As a result, researchers have directed their efforts towards Multi Carrier Modulation (MCM) to achieve high-speed OWC systems. One widely accepted MCM technique is Orthogonal Frequency Division Multiplexing (OFDM), which enables simultaneous transmission of data streams through orthogonal sub-carriers and requires simple single-tap equalization at the receiver. In VLC, due to the use of incoherent modulation, the signal used to modulate the LEDs must be real and unipolar. Consequently, Hermitian symmetry is enforced on the sub-carriers to generate the real signal after Inverse Fast Fourier Transform (IFFT) in Optical OFDM. Another well-known technique, called DCO-OFDM [14], introduces a DC bias to convert the real signal into a unipolar form, resulting in significant energy losses.

In later developments, various techniques were explored to address the energy losses in OFDM-based unipolar modulation. These techniques include Asymmetrically Clipped

Optical OFDM (ACO-OFDM) [14], Unipolar-OFDM (U-OFDM) [15], Flipped OFDM (F-OFDM) [16], and Pulse Amplitude Modulation Discrete Multi-Tonen (PAM-DMT) [17]. Except for PAM-DMT, these waveforms utilize Quadrature Amplitude Modulation (QAM) and leverage the frame structure of OFDM to create the unipolar signal. However, they suffer from a reduction in SE of 50% compared to DCO-OFDM. Furthermore, the energy benefits of ACO-OFDM, U-OFDM, and F-OFDM diminish when higher-order QAM constellations are used. On the other hand, PAM-DMT employs PAM as its base modulation and achieves the same SE as DCO-OFDM. Nevertheless, as the Bit Error Rate (BER) performance of J-ary Pulse Amplitude Modulation (J-PAM) is equivalent to J^2-QAM, the Power Efficiency (PE) of PAM-DMT diminishes at higher SE. In contrast, DCO-OFDM achieves the unipolar signal by introducing a DC bias, which reduces the PE of the optical signal. ACO-OFDM, on the other hand, only utilizes the odd subcarriers for symbol transmission, resulting in a decrease in SE. To overcome these challenges, a more efficient modulation scheme called Asymmetrically clipped DC-biased Optical OFDM (ADO-OFDM) was introduced [1]. Additionally, hybrid waveforms combining multiple layers were investigated to improve SE, but they introduced increased Computational Complexity (CC) [18]. However, all OFDM-based waveforms suffer from high Out Of Band (OOB) emissions due to rectangular filtering and the lack of power control. Therefore, achieving high SE, energy efficiency, and improved flexibility remain active areas of research in OWC [19].

On the other hand, the nonlinear behaviour of LED transmitters in the front-end is very crucial. Therefore, the nonlinear clipping distortion introduced by LEDs results in amplitude distortion in the modulated signal, thereby degrading the performance of the communication system [20]. Therefore, it is crucial to study and analyze the impact of clipping noise on VLC systems and explore possible methods to mitigate this distortion. Simultaneously, the validation of a new waveform or modulation through proof-of-concept hardware has become increasingly important. Therefore, the implementation of hardware testbeds based on the Universal Software Radio Peripheral (USRP) has gained popularity in recent times. These testbeds offer flexibility in designing wireless application systems, incorporating the configurable daughter boards [21]. Additionally, in terms of hardware design, the development of driver circuits for front-end LED transmitters is an interesting aspect, and the current work includes a high-speed MOSFET based driver.

1.2 Contributions

- **Contribution I: A new Peak-to-Average-Power Ratio (PAPR) reduction technique in DCO-OFDM for VLC Systems**

  1. Even if OFDM is considered to be able to transmit data at high rates, it is unavoidable that there will be large peaks caused by the super-imposition of a sizable number of subcarriers. Since optical OFDM uses LEDs, the limited dynamic range of LEDs results in the clipping of optical OFDM signal peaks that don't fall within the LED linear range, and making the problem even worse. Consequently, it is necessary to lower PAPR in OFDM, particularly in the optical domain.
  2. The intent of this contribution is to highlight the many PAPR reduction strategies, such as tone injection (TI) based techniques, applying semi-definite programming (SDP), Selected Mapping (SLM), Partial Transmit Sequence (PTS), and branch-and-bound technique (BBT) to discover the best PAPR reduction method.
  3. In addition to sending the candidate signals, it requires side information to use the SLM and PTS approaches, but this results in a reduction in SE and an increase in computational CC compared to traditional methods. As far as we know, there are still several major problems with the method of design for PAPR reduction techniques for VLC systems, such as excessive CC and side information transmission.
  4. In this work, based on Top Samples Detection and Appending (TSDA), a new PAPR reduction scheme is proposed without using the side information, and compares it to other PAPR reduction schemes like SLM and PTS for the same system to lower the amount of PAPR in the optical-OFDM system.
  5. MATLAB software is used to simulate the proposed PAPR reduction technique for the optical-OFDM system. The simulated results indicate that, in comparison to SLM and PTS, the TSDA technique improved PAPR reduction and lowered CC. In contrast to SLM and PTS, the TSDA system does not need any side information.

- **Contribution-II : A nonlinear Modelled Low-complex ADO-OFDM for VLC Systems**

    1. Based on the efficiency paradigm, the ACO-OFDM and DCO-OFDM schemes have significant inherent drawbacks. However, the ACO-OFDM uses only the odd subcarriers for symbol transmission, which reduces SE, whereas the DCO-OFDM results in a unipolar signal by adding the DC bias, which will decrease the PE of the optical signal. To solve these issues, an effective modulation method known as ADO-OFDM was proposed. However, because asymmetrically clipping noise affects the even subcarriers of DCO-OFDM, the ACO-OFDM signal must first be retrieved before being used to produce the DCO-OFDM signal, which adds delay and complexity to the computational process.
    2. This contribution proposes a novel modulation scheme for VLC systems called nonlinear modelled Low-complex ADO-OFDM (LADO-OFDM). The primary objective of this method is to reduce mutual interference between the even subcarriers that correspond to DCO-OFDM and ACO-OFDM at the transmitter section by using the pre-distortion technique.
    3. Two generalized LEDs models are examined to determine how well the proposed LADO-OFDM performs. The impact of nonlinear clipping distortion on the LEDs dynamic range and bias point has been investigated. By predistorting the transmitted signal and raising the knee factor in the piecewise polynomial model and Rapps models, respectively, the LED dynamic range can be linearized to enhance system performance.
    4. The proposed technique performs better in terms of BER when compared to ADO-OFDM, according to simulation results obtained using Monte Carlo BER simulations. The proposed system performs better than ADO-OFDM in terms of BER, CC, and latency.

- **Contribution-III :Variably Biased Asymmetrically Clipped Optical OFDM (VAO-OFDM) for VLC Systems**

    1. Commercially available LEDs demand VLC system implementations with excellent Power Efficiency and minimal CC. ADO-OFDM is a waveform that has

recently started to be used in VLC systems to address spectral and PE issues in the best possible way. However, with ADO-OFDM, all samples are subjected to strong DC bias in order to produce unipolar signals, which reduce PE.

2. In this contribution, a new modulation scheme for VLC systems is proposed. It is called VAO-OFDM with pre-distortion. In contrast to constant DC bias, we design a variable bias for VAO-OFDM that relies on particular samples. Because its frequency components fall on the pre-defined subcarriers, variable bias doesn't cause any interference with the initially sent symbols. Due to the pre-distortion process, the proposed VAO-OFDM has significantly decreased CC than the ADO-OFDM.
3. Finally, simulation results are presented which show that the VAO-OFDM outperforms the ADO-OFM in terms of PE.
4. Further, the VAO-OFDM is also validated on the experimental Testbed with LabView software and the USRPs.

- **Contribution-IV : Conjugate-symmetric Sequency-ordered Hadamard Coded Modulation for VLC Systems**

1. Given that OFDM signals have high amplitude variations, it is suitable for incoherent optical transmission. The direct application of OFDM techniques is still constrained by the aforementioned signal limitations. There are methods for limiting the OFDM signal in addition to the easy addition of a DC offset, which can be achieved in the analogue domain by a bias-T or in the digital domain with a DC offset. These constraints make the waveform's negative component redundant, allowing its negative portions to be clipped without the clipping disclosing any information.
2. However, Fourier transform-based OFDM techniques are vulnerable to non-linearities because they produce continuous waveforms with substantial amplitude fluctuations. However, a modulation system that uses discrete signal amplitudes is simple since it can be composed of several LEDs that are readily switched on or off. The linearity of the transmitter is obtained by superposing the various signals in the medium. Hadamard-coded modulation (HCM) is one of them.

3. In this contribution, conjugate-symmetric sequency-ordered complex Hadamard transform (CS-SCHT), a new signal processing technique, addresses nonlinear distortion while significantly reducing CC as CS-SCHT's inherent advantage.
4. Simulation results are presented for the proposed optical system in which the orthogonal transform technique called CS-SCHT is used.

1.3 Thesis Outline

This thesis is organized into seven chapters, starting with an introduction, a literature survey of the enabling modulation techniques highlighting the challenges, four chapters delineating the contributions, and with the conclusion in the last chapter. The details of each chapter are summarised as,

- Chapter-1 provides the motivations for the accomplishments, contributions of the thesis, and layout.
- Chapter-2 begins with a quick overview of optical wireless communication before providing a thorough analysis of the current modulation techniques for VLC systems and noting the difficulties involved. Also covered in this chapter are an explanation of the USRP-based experimental testbed and the nonlinear behaviour of LEDs.
- Chapter-3: This chapter presents a new method for reducing PAPR in the optical-OFDM system based on TSDA, without the need of side information, and compares it to previous PAPR reduction strategies like SLM and PTS for the same system.
- Chapter-4: In this chapter, presented a novel modulation scheme for VLC systems called nonlinear modelled LADO-OFDM. The primary objective of this method is to reduce mutual interference between the even subcarriers that correspond to DCO-OFDM and ACO-OFDM at the transmitter section by using the pre-distortion technique. Subsequently, two generalized LED models are examined to determine how well the proposed LADO-OFDM performs.
- Chapter-5: In this chapter, presented a novel modulation scheme for VLC systems called VAO-OFDM with pre-distortion. In contrast to constant DC bias, we design a variable bias for VAO-OFDM that depends on specific samples. Because its frequency components fall on the pre-defined subcarriers, variable bias doesn't interfere with the originally sent symbols. The experimental verification and the corresponding result analysis are described.
- Chapter-6: In this chapter, CS-SCHT, a new signal processing technique is adopted, which addresses nonlinear distortion while significantly reducing the CC.

- Chapter-7: This chapter is dedicated to give conclusions on the thesis, and to point out the possible future works.

1.4 Summary

The proliferation of diverse data-accessing devices designed to seamlessly connect via technologies like the IoT has led to an overwhelming burden on the existing RF spectrum. To address the demand for high data rates, VLC technology, a subsidiary of OWC, has emerged as a complementary solution to RF communication in the upcoming 5G era. However, VLC systems are currently hindered by their modulation techniques, particularly in terms of SE and PE. This thesis aims to address these challenges by investigating various multi-carrier waveforms. Moreover, experimental studies and validations of new modulations are also presented. This chapter highlights the motivations and contributions of the present thesis and provides an overview of its structure.

Chapter 2

Review of Literature

2.1 Introduction

The earliest form of light communication can be traced back to the ancient Romans and Greeks, who utilized mirrored surfaces to transmit information over long distances by reflecting sunlight. However, significant advancements in technological optical communication systems began in the late 1790s with the development of semaphore lines by a French scientist. This system laid the foundation for visual telegraphy. In the late 18th century, Alexander Graham Bell demonstrated wireless optics technology by transmitting a voice message using a light beam. However, the progress of optical communications was impeded by the widespread adoption of radio communications. It wasn't until the 1970s when the invention of Light Amplification by Stimulated Emission of Radiation (LASER) and optical fibres revitalized the growth of optical communications. A crucial milestone in modern Optical Wireless Communication (OWC) occurred in the 1970s when Gfeller and Bapst pioneered a short-range free space communication system based on infrared Light Emiting Diode (LED). Their work catalyzed the development of OWC as we know it today [7].

The innovation of blue LED technology by Shuji Nakamura et al. [22] in 1990 revolutionized the field of solid-state lighting, paving the way for energy-efficient illumination infrastructure. It also opened up opportunities to utilize the visible portion of the Electro-Magnetic (EM) spectrum, ranging from $\lambda = 400\ nm$ to $\lambda = 700\ nm$, for communication purposes. Masso Nakagawa [23] was the first to exploit this potential by utilizing Visible

Light Communication (VLC) technology. Subsequently, research groups and major industry bodies in Japan established the VLC Consortium (VLCC) in 2003. The growing competition for limited RF bands in the EM spectrum, along with the cost-effectiveness and efficiency of LED lighting infrastructure, has significantly fueled the development of VLC technology. In a VLC system, various optical sources, including commercially available LEDs, colour LEDs, and LED arrays, are employed as transmitters. Optical detectors such as photodiodes are utilized as receivers. This enables seamless connectivity, facilitates handover, and supports user mobility scenarios. Professor Harald Haas and his group [24] introduced a bidirectional wireless networking solution called Li-Fi, utilizing VLC technology.

The use of incoherent optical components in the transmitter and receiver sections of VLC systems restricts the signalling to Intensity Modulation/Direct Detection (IM/DD). This results in unipolar transmitted signals and necessitates modifications in modulation techniques. SCMs like OOK, PAM, and PPM can be easily implemented for IM/DD systems. However, issues such as ISI significantly impact their performance at high data rates [13]. As a result, various forms of multi-carrier modulations, such as Optical OFDM, have been explored in the literature [25]. These modulation schemes are designed to comply with VLC constraints, provide computationally efficient single-tap equalization, and offer other associated benefits.

The remaining sections of this chapter are organized as follows: Section 2.2 discusses the evolution of OWC and presents a basic wireless optical communication system, outlining the necessary processing steps for practical communication. In Section 2.3, a comprehensive survey of existing modulation schemes is presented, highlighting their advantages and limitations. Section 2.4 focuses on the nonlinear distortion caused by LEDs and their detrimental effect on communication system performance. Furthermore, Section 2.5 describes the main components and details of the experimental setup. In Section 2.6, key practical issues that need to be addressed in real-time VLC systems are explored. Finally, Section 2.7 summarizes the content covered in this chapter.

2.2 Optical Wireless Communications

Optical Wireless Communication, is a long-standing technology that enables the transmission of information through free space using optical signals. In the past, ancient civilizations such as the Greeks and Americans used fire beacons and smoke signals for signalling purposes. Similarly, French sea navigators utilized semaphores for optical communication during the late 17th century. However, the first instance of optical communication can be attributed to Alexander Graham Bell, who conducted an experiment involving modulating sunlight to transmit a voice signal over a distance of approximately 200 meters. Unfortunately, the experiment was unsuccessful due to the unpredictable nature of sunlight and the inaccuracies of the equipment employed.

The emergence of OWC gained prominence in the early 1960s with the advancement of optical sources, particularly lasers. During the 1960s and 1970s, numerous demonstrations of free space optical communication systems took place, utilizing HeNe lasers and GaAs LEDs [13]. As a result, the military in the United States adopted OWC technology for covert communications, and NASA employed it for near-earth satellite communications [26]. Despite achieving a considerable understanding of OWC system construction, practical implementation was limited for several reasons. Firstly, existing RF communication systems at the time were deemed sufficient to meet data requirements. Secondly, the performance of OWC systems was heavily influenced by atmospheric anomalies and the underdeveloped state of optical components. Finally, even under normal atmospheric conditions, accurate tracking and pointing optical systems were not readily available. Collectively, these challenges hindered the widespread adoption of OWC systems in commercial communication networks.

Over time, the significant advancements in optoelectronic devices and related technologies have sparked a renaissance in OWC. Furthermore, the escalating demand for extensive bandwidth, unmet by existing technologies, has contributed to the resurgence of OWC. OWC encompasses a broad spectrum ranging from 100 nm to 1 mm in the electromagnetic spectrum, covering ultraviolet, visible, and infrared regions. The invention of blue LEDs, pioneered by Shuji Nakamura et al., [22] enabled the utilization of the visible portion of the electromagnetic spectrum (ranging from 400 nm to 700 nm) for

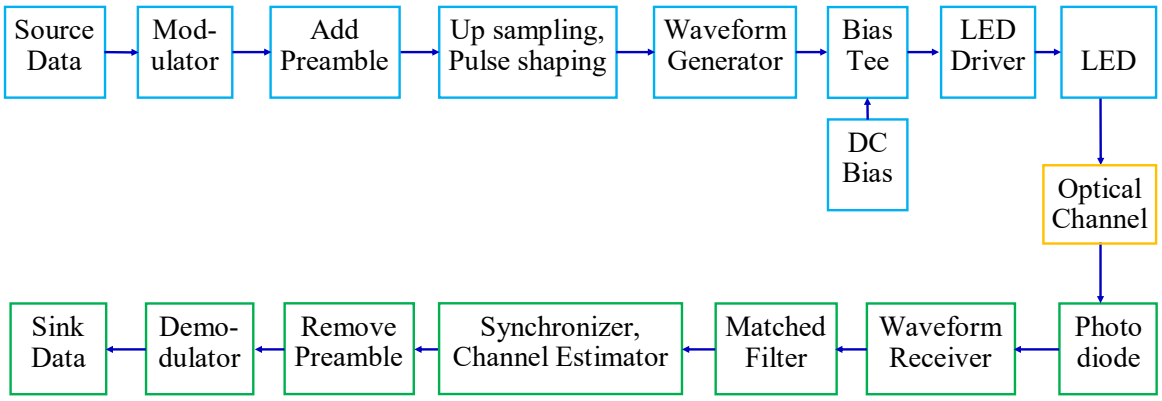

Figure 2.1: Basic block diagram illustration of a practical OWC based VLC system

VLC technology. VLC, a subsidiary of OWC, operates on IM/DD and offers simultaneous illumination and communication capabilities. It should be noted that the contributions discussed in this thesis are primarily focused on VLC within the context of OWC. Figure 2.1 depicts a basic block diagram of a practical VLC system based on OWC, illustrating all the necessary steps for its implementation. The binary information originating from the data source undergoes baseband modulation using either SCM or MCM techniques tailored to meet the requirements of the IM/DD-based VLC system. The literature proposes various modulation techniques for IM/DD systems, which are extensively discussed in the subsequent section. Following the preamble, the baseband modulated signal undergoes upsampling, pulse shaping, and additional processing to overcome ISI and other channel irregularities. The resulting digital signal is then converted to analog form using a waveform generator. A Bias-Tee adds a DC bias to the analog signal, which is then used to modulate the LED through the driver circuit depicted in Figure 2.1. At the receiver end, a P-i-N Photodiode (PD) captures the optical signal emitted by the LED and converts it into an analog electrical signal. Subsequently, the waveform generator performs ADC and transfers the digital signal to the PC. Within the PC, several processing steps, including synchronization, channel estimation, equalization, and demodulation, are executed to retrieve the original information, as illustrated in Figure 2.1.

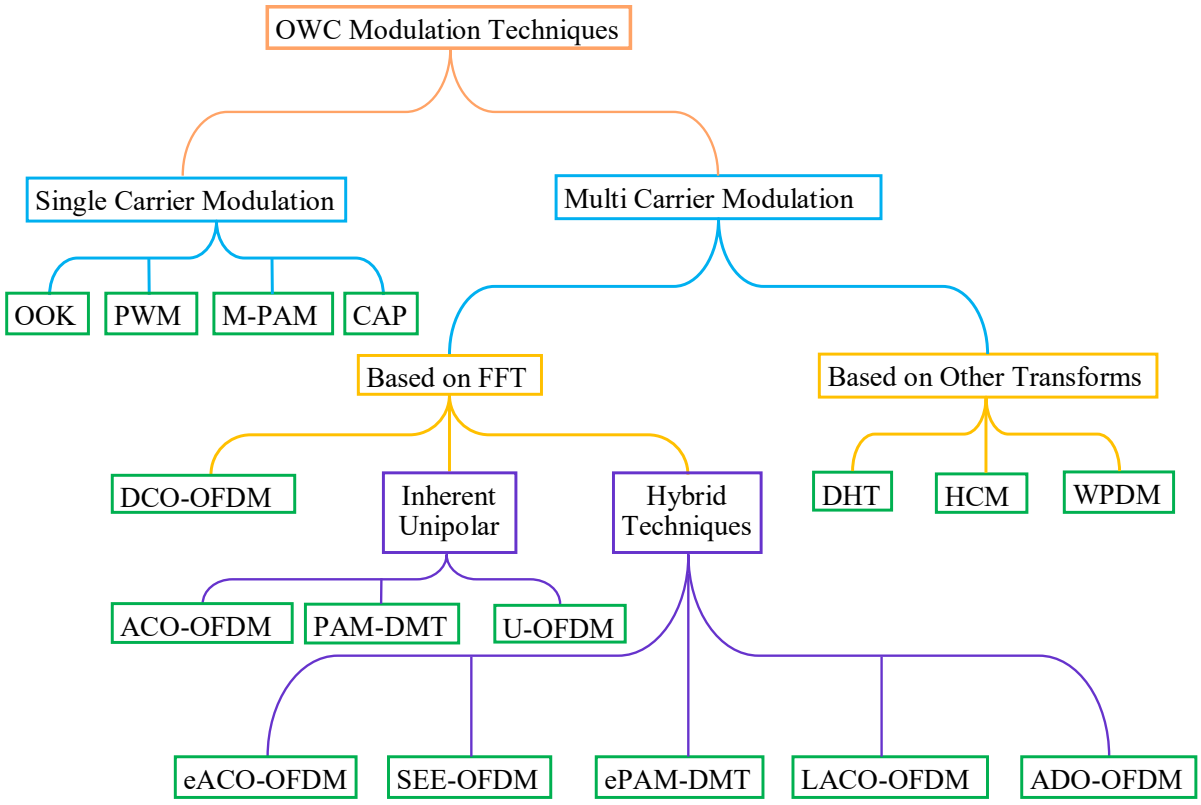

Figure 2.2: Modulation techniques in IM/DD systems

2.3 Modulation Schemes

In order to meet the lighting needs in VLC technology, inexpensive and straightforward system designs often utilize incoherent sources as transmitters. This choice of incoherent sources in VLC systems restricts the modulation schemes to rely on IM/DD. To fulfill the requirements of IM/DD, various modulation schemes have been considered for VLC systems. These modulation techniques can be broadly categorized as depicted in Figure 2.2. The first category encompasses SCM, followed by MCM based on Fourier transform. Additionally, MCM techniques based on other transforms are also explored, and finally, modulation schemes based on color domains are considered.

2.3.1 Single Carrier Modulation (SCM) Schemes

In these schemes for SCM, the dynamic nature of pulse signals is harnessed to transmit information using light. The simplest scheme is OOK, where binary bits are encoded based on the presence or absence of light intensity. Importantly, the system's performance

remains unaffected as the illumination is adjusted to binary levels. Additionally, M-ary PAM is used to encode multiple intensity levels [27]. Other modulation techniques such as PPM and PWM utilize different timing characteristics to convey information. PPM decodes transmitted symbols based on the timing position of the pulse, while PWM extracts symbols using the width of the pulse. PPM has been proven to be more PE than OOK, also requiring higher bandwidth to achieve data rates equivalent to OOK [28]. An alternative approach, called Variable PPM (VPPM), was proposed in the VLC standard IEEE 802.15.7, combining the advantages of PPM and PWM [29].

2.3.2 Multi Carrier Modulation (MCM) Schemes

Multiple studies have conducted performance comparisons between single-carrier and multi-carrier modulations [30, 31]. While variations may arise from the factors and assumptions considered in each study, it is widely acknowledged that single-carrier modulations exhibit limitations at high data rates due to increased ISI. In response to this, a solution called Discrete Fourier transformation spread (DFT-s) OFDM was proposed for VLC systems. DFT-s-OFDM combines the advantages of multi-carrier OFDM waveform with a low PAPR [32]. In this approach, an additional DFT and Inverse DFT block are utilized for signal modulation and demodulation alongside the conventional OFDM. Furthermore, researchers have also investigated a novel modulation technique known as Carrier less Amplitude and Phase (CAP) modulation to enhance SE [33]. However, it is important to note that this technique entails higher CC compared to other single-carrier modulations.

Researchers have been exploring multi-carrier modulations such as OFDM due to the challenges posed by high data rates and the need for complex equalization in traditional systems. OFDM was first used in practical wireless communication systems in the mid-1980s, and its potential for mobile communications and broadcasting was also investigated by industry experts around the same time [34]. While OFDM systems offer numerous benefits, its application to optical wireless systems has only recently gained attention. This development can be attributed to the increasing demand for higher data capacities and advancements in digital signal-processing hardware. Notably, there are certain distinctions between RF-based OFDM systems and optical-based systems, which

Table 2.1: Comparison of RF and Optical based OFDM systems

RF based OFDM system	Bipolar Signal	Information is carried by electric field	Require local Oscillator at receiver	Coherent detection
Optical based OFDM system	Unipolar Signal	Information is carried by optical intensity	No local Oscillator is required	Direct detection

are summarized in Table 2.1. In RF-based OFDM, information is transmitted by modulating an electromagnetic wave, and the signal can be bipolar, allowing for both positive and negative values. However, in optical-based systems, information is transmitted by modulating light intensity in an IM/DD system, and the signal is unipolar. Additionally, unlike RF systems, optical-based systems do not require a local oscillator and employ direct detection at the receiver side.

In the context of OFDM-based multiple subcarrier modulation, the initial step involves dividing the incoming bits into parallel streams. These streams represent the baseband modulated symbols and are subsequently directed to the IFFT block, as depicted in Figure 2.3. In order to obtain a real signal after the IFFT process, the subcarriers are arranged in Hermitian symmetry, and the baseband modulated symbols are allocated to different subcarriers $X(k)$ in various ways, depending on the specific requirements. Consequently, multiple variations of OFDM modulations have been developed for optical-based communication systems. At the transmitter, the time domain signal $x(n)$ is generated by applying the following IFFT equation.

$$x(n) = \frac{1}{K} \sum_{k=0}^{K-1} X(k) e^{j2\pi \frac{k}{N} n}, \tag{2.1}$$

where $x(n)$, with $n = 0, 1, K-1$ are time domain samples and $X(k)$ with $k = 0, 1, K-1$ are frequency domain symbols. Various modulation techniques utilize different methods to convert the cyclic prefixed real signal into a unipolar form after signal generation. This unipolar signal is subsequently employed to modulate the intensity of the LED light, as depicted in Figure 2.3. At the receiver, a Photodiode captures the modulated light and generates the corresponding electrical signal. This electrical signal is then processed

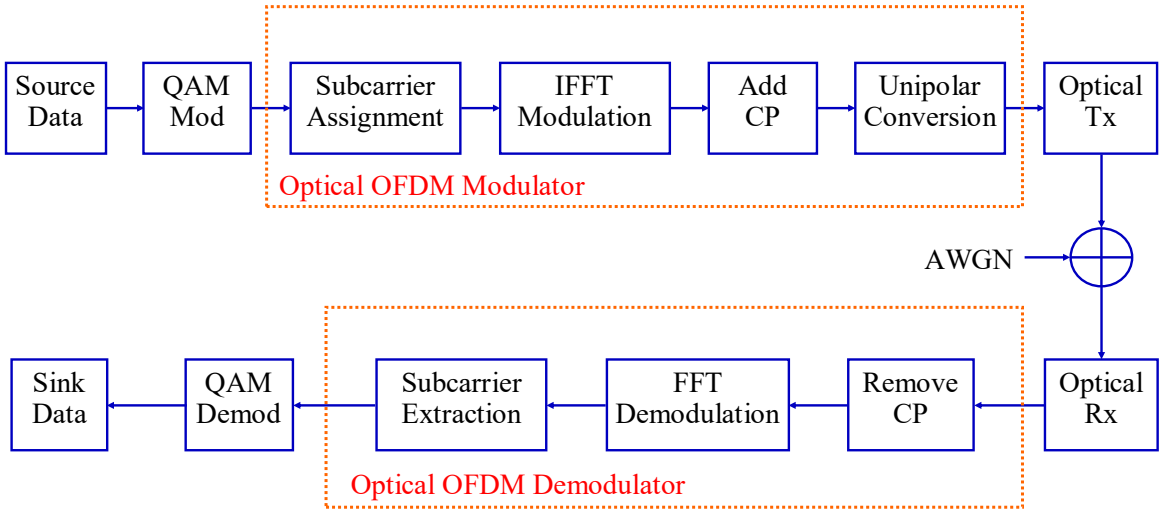

Figure 2.3: A block diagram illustration of Optical OFDM with necessary functions in transmitter and receiver

according to the procedure illustrated in Figure 2.3 to retrieve the original data symbols.

DCO-OFDM

Among all the optical OFDM variants, this modulation technique is widely recognized and favoured. It employs QAM modulation to facilitate the subcarriers in the frequency domain. The symbols, denoted as $X(k)$, are organized in Hermitian symmetry, as follows:

$$X(K - k) = X^*(k) \; for \; k = 1, 2, ... \frac{K}{2} - 1. \tag{2.2}$$

It should be noted that the symbols X(k) on subcarriers $k = 0$ and $k = \frac{K}{2}$ are set to zero. In this context, the asterisk (*) denotes complex conjugation. This implies that the symbols $X(k) = [0, X(1), X(2), ...X(\frac{K}{2} - 1), 0, X^*(\frac{K}{2} - 1), ...X^*(2), X^*(1)]$ are utilized as inputs for IFFT, as given in (2.1), in order to generate a real time-domain signal. To meet the requirements of VLC systems, a DC bias is added to the signal, based on the average power of the real signal provided below, resulting in a unipolar signal.

$$\beta_{dc} = \gamma \sqrt{E\left[x_{cp}^2(n)\right]}, \tag{2.3}$$

where x_{cp} denotes the real signal in the time domain with a cyclic prefix. In (2.3), the symbol $E[.]$ represents the expectation. The value of β_{dc} relies on the clipping factor γ, which represents the ratio of the direct current (DC) component to the standard deviation

of $x_{cp}(n)$, as given in [14]. The addition of a DC bias shift the time-domain signal to the linear portion of the dynamic range of the nonlinear device in the front end. However, due to the high PAPR, it becomes challenging to convert all the time-domain samples into unipolar values. Consequently, the large peaks that exceed the linear range result in clipping noise within the modulated signal.

Inherent Unipolar Modulations

In order to enhance PE by eliminating the need for high DC bias values, novel modulation techniques such as ACO-OFDM [15], PAM-DMT [35], and U-OFDM [36] have been developed . ACO-OFDM and PAM-DMT, similar to DCO-OFDM, employ Hermitian symmetry on the subcarriers to generate real signals. However, there is a fundamental distinction between ACO-OFDM and DCO-OFDM: ACO-OFDM only transmits symbols on odd subcarriers, while PAM-DMT utilizes a symbol structure akin to DCO-OFDM but utilizes PAM modulation instead of QAM. In ACO-OFDM, the frequency domain symbols $X(k) = [0, X(1), 0, X(2), 0, ...X(\frac{K}{2} - 1), 0, X^*(\frac{K}{2} - 1), 0, ...X^*(2), 0, X^*(1)]$ are symmetrically positioned on even subcarriers as X(k), indicating explicitly that the effective number of transmitted symbols is halved compared to DCO-OFDM. Nevertheless, this arrangement concentrates all the information on the positive portion of the time domain signal, rendering the negative portion redundant. Consequently, an asymmetrical clipping of the negative portion facilitates the generation of a unipolar signal in ACO-OFDM without any bias. As a result, by applying an asymmetrical clipping technique to eliminate the negative portion, ACO-OFDM can generate a unipolar signal without introducing any bias. In the context of PAM-DMT, where $X(k) = [0,\ jP(1),\ jP(2), ...,jP(\frac{K}{2} - 1), 0, -jP^*(\frac{K}{2} - 1), ..., -jP^*(2), -jP^*(1)]$ represents pure imaginary symbols and P(k) represents PAM symbols, the time-domain signal exhibits antisymmetry. Exploiting this property, we can achieve a unipolar signal by selectively clipping the negative part, while preserving all the information. However, in both modulation schemes, it is necessary to introduce a small bias to ensure the signal remains within the linear range of the front-end LED. It's important to note that this bias value is significantly lower compared to DCO-OFDM.

Another modulation technique called U-OFDM is being explored as a solution to the PE issue. U-OFDM shares similarities with DCO-OFDM in terms of Hermitian symmetry

and symbol arrangement to achieve a real signal. However, unlike DCO-OFDM, U-OFDM divides the time domain real signal into two consecutive frames of equal length. The first frame consists of positive samples with zeros at the negative sample positions, while the second frame consists of absolute negative samples from the original real signal with zeros at the positive sample positions. This approach generates a unipolar signal without the need for a DC bias. Consequently, the frame length of U-OFDM is twice that of DCO-OFDM.

In conclusion, although these inherent unipolar modulations enhance the PE of IM/DD systems, their SE is lower compared to DCO-OFDM. It is worth mentioning that while PAM-DMT has a SE comparable to DCO-OFDM, the BER performance of J-PAM is equivalent to J^2-QAM.

Other Hybrid Modulations

The aforementioned modulations mentioned above utilize Hermitian symmetry on the frequency domain subcarriers. This approach effectively reduces the transmitted symbols by half, thereby impacting the overall throughput. This reduction is even more significant for inherently unipolar modulations due to their sub-carrier assignment. Consequently, in the search for alternative modulations suitable for IM/DD-based optical systems, several multi-layered and hybrid modulations based on OFDM have been investigated. Examples of such modulations include ADO-OFDM [35], Hybrid ACO-OFDM (HACO-OFDM) [37], Layered ACO-OFDM (LACO-OFDM) [38],enhanced Unipolar OFDM (eU-OFDM) [19], Spectral and Energy Efficient-OFDM (SEE-OFDM) [39], among others. However, all these variants are derived from basic variants like DCO-OFDM and ACO-OFDM, and they achieve the SE of DCO-OFDM at higher modulation depths or with a larger number of layers. Moreover, all of these variants increase both the receiver complexity and CC.

In the meantime, all existing modulation techniques based on OFDM divide the frequency grid while leaving the time grid undivided. As a result, all OFDM variants transmit only one symbol on each sub-carrier. However, this approach leads to high peak values in the time domain real samples after the IFFT, which can distort due to the nonlinear behaviour of the LED. Additionally, the use of rectangular pulses in optical OFDM results in more power being dissipated on out-band carriers, thereby reducing

the energy efficiency of LEDs. Furthermore, since LEDs vary in terms of their dynamic range, it is crucial to have control over the peak power of the modulated waveform in a user-friendly manner, without the need for additional symbols or increased CC. Therefore, there is a pressing need for innovative waveforms that can achieve high SE, and energy efficiency, and provide greater flexibility to enhance the adoption of VLC systems in real-time wireless networks.

MCM based on other Transforms

Extensive surveys have been conducted on OFDM-based MCM using Fast Fourier Transform (FFT) and IFFT. However, there are alternative transformation techniques, such as Discrete Hartley Transformation (DHT) [40], Fast Walsh-Hadamard Transformation (FWHT) [41], and Wavelet Packet Division Multiplexing (WPDM) [42], that have been considered for the modulation techniques of IM/DD systems. DHT-based modulations generate real signals when real constellations are employed on the subcarriers and can utilize DC bias and asymmetrical clipping to produce unipolar signals. Although DHT-based modulation does not rely on Hermitian symmetry, its SE falls short of that achieved by FFT-based OFDM modulations. Subsequently, Hadamard coded modulation HCM was proposed using FWHT, which proves advantageous in high illumination scenarios.

Moreover, an exclusive feature unique to IM/DD systems is colour modulation, where the colour-changing LEDs correspond to the applied intensity level. This characteristic led to the introduction of Colour Shift Keying (CSK) in the IEEE 802.15.7 standard for VLC systems [43]. In colour modulations, information is encoded into the instantaneous intensity of RGB LEDs while meeting the illumination requirements. However, prolonged exposure to these illuminated environments can pose health hazards, such as dizziness, nausea, and other light-related issues.

2.4 Non-linear Distortion of LEDs

In general, OFDM-based multi-carrier modulations are highly sensitive to nonlinear distortion, which impacts the performance of communication systems. Nonlinear elec-

tronic devices, such as RF amplifiers and LEDs, introduce nonlinearity into the envelope variations of OFDM-modulated signals, leading to in-band distortion and Inter Carrier Interference (ICI). To mitigate this distortion, it is crucial to properly adjust the characteristics of the time domain waveform, such as the electrical power driving the LEDs and the biasing point. Achieving this requires a deeper understanding of the nonlinear behaviour of these devices and their effects on performance. LEDs, for instance, exhibit piecewise linearity in their Voltage (V)-Current (I) characteristics due to their fabrication using semiconductor materials like PN diodes and transistors. Only a specific portion of the characteristic curve displays linearity, known as the dynamic range of the LED. To ensure proper operation, LEDs should always be biased in a way that the applied signal lies within their dynamic range. However, due to the limited dynamic range of LEDs, even signals applied within this range can experience clipping at the extremities. This occurs because of the minimum TOV requirement for the LED to emit light at the lower end and the maximum permissible AC current for safe operation. TOV is similar to the cut-in voltage of diodes below which the LED is considered non-conducting. Figure 2.4 provides a detailed illustration of the nonlinear V-I characteristics, highlighting key V-I points. The maximum permissible DC current represents the highest DC bias value that can be applied within the LED's dynamic range. Additionally, Figure 2.4 depicts a linearized characteristic obtained through the pre-distortion technique. The nonlinear behaviour exhibited by LEDs introduces clipping distortion into the modulated signal, significantly impacting system performance. This is particularly critical in multi-carrier modulations where the algebraic sum of symbols generates time-domain samples with large peaks. To mitigate this clipping distortion and limit performance degradation, it is necessary to apply an external bias to the LED within its dynamic range, above the TOV, while considering the maximum permissible DC and AC currents. Identifying the optimal bias point and signal power is essential to reduce clipping noise. This necessitates the use of polynomial models to study the LED's nonlinear behaviour and identify the best operational conditions.

Researchers [44] have proposed a Rapps model that incorporates amplitude distortion and allows for parameter-controlled upper clipping to address this issue. Alternatively, [45] introduced a pre-distortion model to linearize the polynomial approximation of the LED's V-I characteristics. These models are employed to investigate the impact

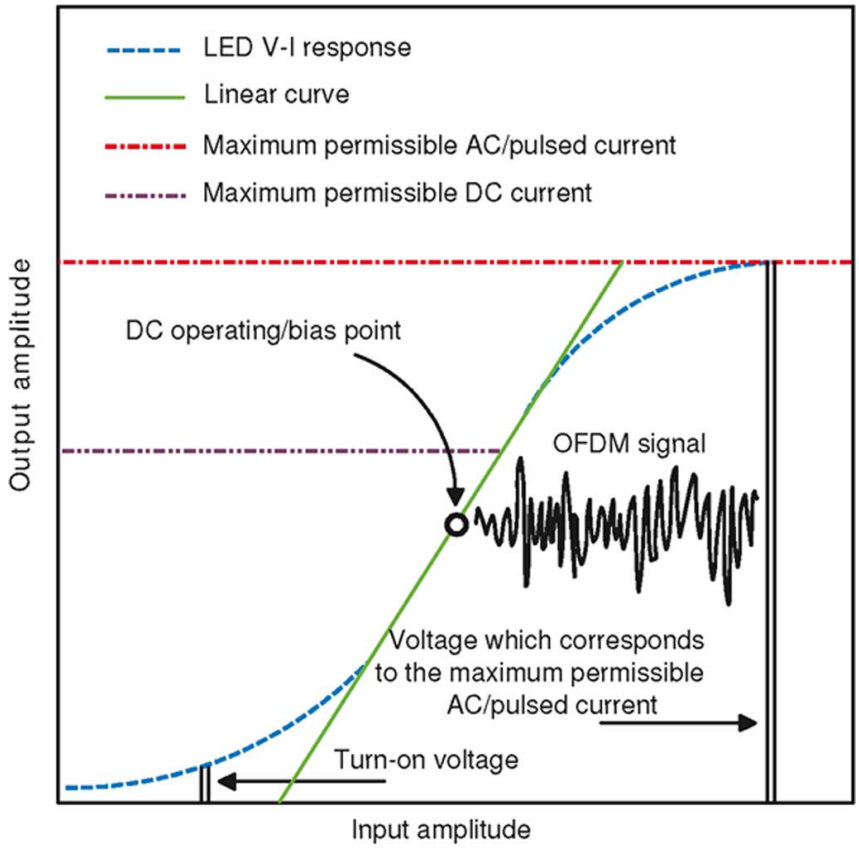

Figure 2.4: Illustration of nonlinear and linearised transfer characteristics of LEDs

of nonlinearity on the performance of DCO-OFDM-based systems under upper clipping. However, matching the desired LED's V-I characteristics to a mathematical polynomial introduces mathematical complexity and potential errors in the polynomial fitting.To overcome these limitations, a more accurate double-sided clipping model utilizing practical LED power parameters has been proposed in [46], with investigations conducted on the performance of basic variants of DCO-OFDM and ACO-OFDM. These studies highlight the necessity of evaluating performance under clipping distortion for any modulation scheme employed in VLC systems.

2.5 Introduction to Experimental Setup

Simultaneously, the attention surrounding the proof of concept for the hardware has sparked considerable interest in establishing the waveform within the research community. Numerous hardware implementations for wireless communication systems have been reported in the literature [47, 48]. However, the utilization of USRPs in wireless

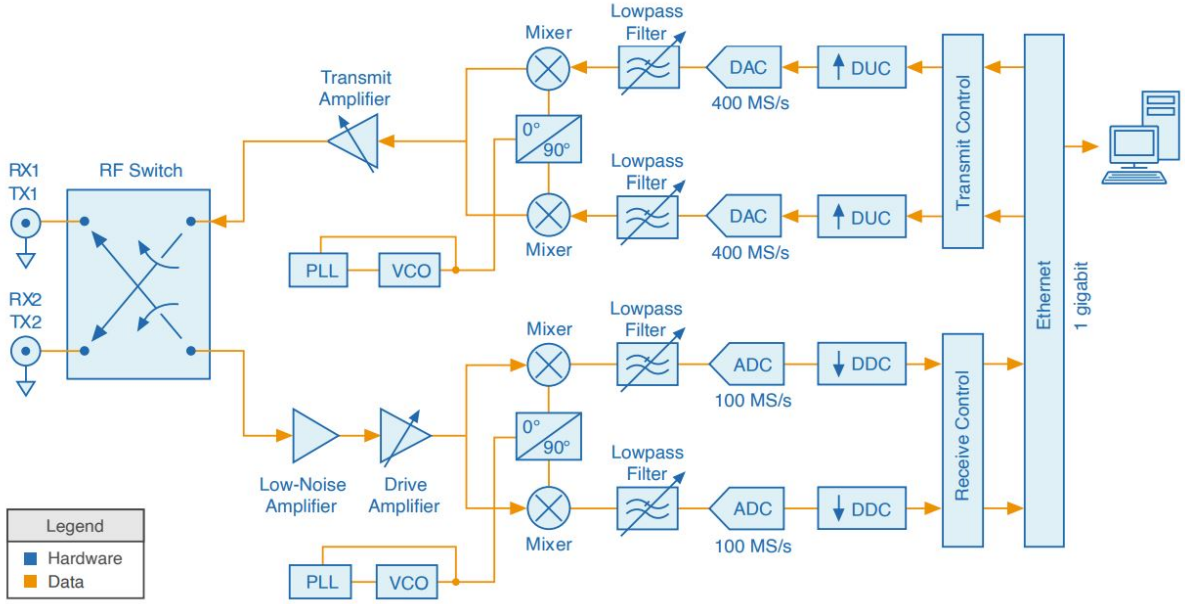

Figure 2.5: Block diagram showing the elements of USRP

system design has gained prominence due to their notable advantages [21, 49, 50]. The flexibility, user-friendly nature, and affordability of USRPs have made them invaluable for various applications. Unlike conventional waveform generators, USRPs offer convenient integration of components such as ADCs, DACs, FPGAs, and configurable daughterboards, allowing for tailored frequency requirements to suit specific applications [21, 49].

In modern wireless communication network designs, USRPs are extensively employed due to their ease of implementation and ability to address design challenges. On the other hand, LabVIEW, a graphical programming software, provides a user-friendly interface with external hardware. Thus, in this thesis, the experimental setup is designed by leveraging USRP hardware and National Instruments (NI) LabVIEW software. Figure 2.5 illustrates the elements of USRPs. The notable advantage of the USRP device lies in its configurability to any desired frequency through the use of configurable daughterboards. In this work, the transmitter and receiver USRPs used are the USRP X300 and USRP N210, respectively, with LFTx and LFRx boards occupying the daughterboard slots, offering a frequency range from 0 to 30MHz. The limited bandwidth of the LEDs and photodiodes restricts the frequency range. Commercially available white LEDs and the Thorlabs-PDA8A photodiode are employed. Furthermore, since LEDs require a unipo-

lar signal for intensity modulation, a Bias TEE ZFBT-6GW-FT+ from Mini-Circuits is incorporated to convert the bipolar RF electrical signal from the USRP into a unipolar signal. It is important to note that LabVIEW software handles the baseband processing of the modulating signal and cables such as PCIex4 and Ethernet cables are used to interface the USRPs with the LabVIEW operating system.

2.6 Summary

This chapter delves into the comprehensive background of OWC evolution and its significant advancements. It begins by providing a basic description of an OWC system within the context of real-time communication. The necessary functions and processing steps at various stages are then elaborated upon. Specifically, a detailed examination of crucial stages such as modulation, characteristics of front-end transmitters, key requirements of receiver processing steps, and hardware details are discussed.

This chapter extensively explores the available modulation techniques for optical systems based on Li-Fi, highlighting the benefits and areas where improvements are needed. In particular, it discusses the limitations of multi-carrier optical OFDM modulations in unipolar-constrained OWC systems, including their impact on SE, PE, OOB emissions, flexibility, and PAPR. The nonlinear characteristics of front-end transmitters are also addressed, along with their implications for system performance. Additionally, a brief overview of the hardware is provided to establish a preliminary understanding of the experimental testbed.

To overcome the aforementioned limitations associated with OFDM-based waveforms, the subsequent chapters of this thesis propose various novel waveforms that meet the requirements of OWC systems. The performance of these waveforms is analyzed considering the nonlinear clipping distortion introduced by front-end LED transmitters. Furthermore, experimental validation of all the waveforms is presented under different practical constraints. Finally, the chapter concludes with a summary of the findings and suggestions for future research, emphasizing the essential improvements and directions for further investigation.

Chapter 3

PAPR Reduction Technique for VLC Systems

3.1 Introduction

The Mobile data traffic has rapidly increased over the past few years due to rapid changes in the number of devices under usage. Wireless services like the Internet of Things (IoT), machine-to-machine (M2M) communications, and e-services like banking, health and learning require high data rates. The estimated data traffic for the future-generation wireless systems will rise to the order of hundreds (even thousands) compare to currently available systems [51]. In recent years, Visible Light Communication (VLC) allures the concentration of researchers, academicians and industries because of its eminent capabilities and advantages, such as electromagnetic wave-free transmission, untrammelled spectrum and endures to interference in radio frequency (RF) [52]. To ease the CC in implementation and to procure higher SE, DCO-OFDM has most widely opted for the VLC systems. However, the occurrence of a high PAPR has been leading to the dreadful nonlinear clipping distortion at light-emitting-diode (LED), which was recognized as a major problem in DCO-OFDM systems [14].

To solve this problem, distinct schemes are being employed to decrease the PAPR in DCO-OFDM systems. Authors in [53] and [54], proposed tone injection (TI) based techniques, by exercising semi-definite-programing (SDP) and branch-and-bound-technique (BBT) to find the optimal solution, which results in significant PAPR reduction. In [55], an enhanced active constellation adjunction algorithm was propounded to minimize the dimensions of DCO-OFDM-based systems rather than decreasing PAPR. Although these

methods can diminish the PAPR, they escalate the transmission power consumption and CC. Recently, certain reduction schemes of PAPR based on tone reservation (TR) were proposed to limit the transmission power consumption in DCO-OFDM-based systems [56]. The CC affiliated with the TR method is inflated in probing peak abandoned signals. The work in [57] initiated an algorithm for clipping to decrease the PAPR, simultaneously acquiring the advent in bit error rate (BER) performance. Moreover, to enhance the performance of PAPR reduction accompanied with pre-determined pilot sequences method was proposed for VLC systems in [58], in contrast, this introduction of pilot sequences has cost the SE. To diminish the PAPR, One more study in [59] introduced spatial multiplexing (SM) based technique, but, it necessitates multiple LEDs to transmit simultaneously, nothing but, each LED requires one driver circuit. Therefore, it involves multiple driver circuits, which increase the cost and CC of the system.

In RF OFDM systems, partial transmit sequence (PTS) and selected mapping (SLM) schemes have been observed as the most popular techniques for dwindling the PAPR. In OFDM systems, the least PAPR signal is found in PTS by merging the phase weighting vector with the OFDM signal sub-blocks [60], however, the CC is very high compares to conventional methods. In [61], the authors proposed a method which is the interleaved partitioned traditional PTS with low CC, but, the performance is very poor in terms of PAPR because of dependent candidate signals (CSs). Coming to SLM, to deploy this scheme in DCO-OFDM-based systems, diverse studies have been carried out in [62–65]. The strategy propounded in [62] is to merge chaos and the SLM technique to acquire control over phase rotation factors construction. To contrast, in [63] an investigation is carried out on SLM performance by employing five unique families of phase sequences, to be specific, pseudo-random interferometry code, chaotic, Walsh-Hadamard, Shapiro-Rudin, and random sequences and the culmination of these is a reduction of PAPR at different levels. The strategies adopted in [64, 65] are a special category of phase sequences of symmetric vectors and overlapped symbols to plummet the PAPR in DCO-OFDM signals respectively.

In addition to this, the difference in magnitudes of the signal obtained and predefined phase sequences in the frequency domain has been utilized in the blind detection of the side information (SI). Besides all the benefits, such methods result in high CC as

the construction of candidate signals demands carrying out multiple inverse fast Fourier transforms (IFFT) operations. Despite developing a wide range of PAPR reduction strategies with less CC, they may not be applicable for VLC systems for the reason of their nature i.e., real and positive [66–71]. To employ SLM and PTS methods, we require SI in addition to indicating the transmitted CSs but it leads to a consequence of a decrease in SE and increases the CC compares to conventional methods. As far as we are aware the design procedure for PAPR reduction schemes for VLC systems, has been still incorporated with some predominate issues such as high CC and SI transmission. In this thesis, to address this problem, we proposed a new PAPR reduction technique based on top samples detection and appending (TSDA), without using the side information. In the proposed technique, we first detect the top samples and then utilized them to reduce the PAPR. Since we are not using the multiple numbers of candidate signals in the proposed technique, the CC decreased by the number of candidate signals times, compared to SLM and PTS.

The rest of this chapter is structured as follows. Section 3.2 details the system model with the proposed PAPR reduction technique. Section 3.3 express the PAPR analysis of the resultant signal with appended samples. Section 3.4 illustrates the simulation results and compares the CC of SLM and PTS with the proposed one. Lastly, the conclusion is described in Section 3.5.

3.2 System Model

This section evokes the DCO-OFDM with the proposed scheme; TSDA for PAPR reduction. DCO-OFDM with TSDA technique is depicted in Fig. 3.1, which includes a transmitter, optical channel and receiver sections.

At the transmitting section, the input bit-stream sweeps through the serial-to-parallel converter which results in bit-chips based on the required modulation scheme which maps to complex signal, $X = [X(0), X(1), ..X(\frac{N}{2} - 1)]$. The complex data signal is going through the hermitian symmetry (HS) block and it is constrained to have HS, given as,

$$X(k) = X(N-k)^* \quad for \quad 0 < k < \frac{N}{2} \tag{3.1}$$

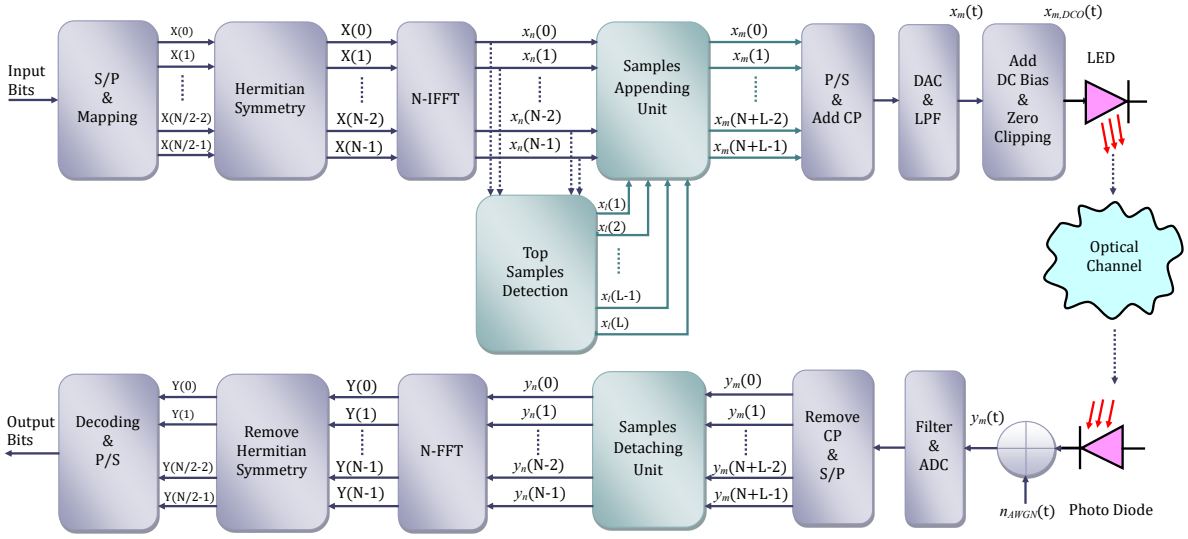

Figure 3.1: Block diagram of DCO-OFDM transceiver with TSDA Technique

and the two components $X(0)$ and $X(\frac{N}{2})$ are set to be zero, i.e $X(0) = X(\frac{N}{2}) = 0$. Because of the HS in the input, the output signal of the IFFT section, x_n is real, but not complex. The n^{th} time domain sample of x_n is $x_n(n)$ and it is given in [35] as

$$x_n(n) = \frac{1}{\sqrt{N}} \sum_{k=0}^{N-1} X(k) exp\left(\frac{j2\pi kn}{N}\right)_{n=0,1...N-1} \tag{3.2}$$

equation (3.2) can be written as

$$x_n(n) = \frac{1}{\sqrt{N}} \sum_{k=0}^{\frac{N}{2}-1} \left(X(k) exp\left(\frac{j2\pi kn}{N}\right) + X(N-k) exp\left(\frac{j2\pi(N-k)n}{N}\right)\right) \tag{3.3}$$

by substituting the equation (3.1) in (3.3) and putting $X(0) = X(\frac{N}{2}) = 0$

$$x_n(n) = \frac{1}{\sqrt{N}} \sum_{k=1}^{\frac{N}{2}-1} \left(X(k) exp\left(\frac{j2\pi kn}{N}\right) + X(k)^* exp\left(\frac{j2\pi kn}{N}\right)\right) \tag{3.4}$$

equation (3.4) can be written as

$$x_n(n) = \frac{2}{\sqrt{N}} \sum_{k=1}^{\frac{N}{2}-1} Re\left[X(k) exp\left(\frac{j2\pi kn}{N}\right)\right]_{n=0,1...N-1} \tag{3.5}$$

here, N is number of subcarriers which is even and the k^{th} subcarrier of X is represented as $X(k)$ in (3.5). Because of HS and $X(0) = X(\frac{N}{2}) = 0$, one can perceive that the number of unique-data symbols transmitted in each DCO-OFDM symbol is $\left(\frac{N}{2} - 1\right)$.

3.2.1 TSDA PAPR reduction technique

The proposed scheme consists of two blocks in the transmitter section. One is the top samples detector (TSD) and the second one is the samples appending unit (SAU). The TSD detect the top L samples from the actual sequence $\{x_n(n)\}_{n=0}^{N-1}$ and then fed to SAU. SAU appends the top L samples with N samples which are coming from the IFFT block which results in $N+L$ samples at the SAU output end.

TSD:- To find the top L samples, let x_i is a sample value of i^{th} maximum magnitude of $\{x_n(n)\}_{n=0}^{N-1}$ from $\left\{x_n^{(i)}(n)\right\}_{n=0}^{N-i}$. Then the top L samples are represented as $\{x_i\}_{i=1}^{L}$ and defined as,

$$\{x_i\}_{i=1}^{L} = \underset{x_n^{(i)}(n)}{\arg\ \max} \left(\left|\left\{x_n^{(i)}(n)\right\}_{n=0}^{N-i}\right|\right) \tag{3.6}$$

where $\left\{x_n^{(i)}(n)\right\}_{n=0}^{N-i} \subseteq \{x_n(n)\}_{n=0}^{N-1}$, and for $i=1$, $\left\{x_n^{(1)}(n)\right\}_{n=0}^{N-1}$ considered as $\{x_n(n)\}_{n=0}^{N-1}$ and for $i=2,3,..,L-1$the new data sets can be formed by [72] the eqauation given below,

$$\left\{x_n^{(i+1)}(n)\right\}_{n=0}^{N-1-i} = \left\{x_n^{(i)}(n)\right\}_{n=0}^{N-i} - \{x_i\} \tag{3.7}$$

Now we can find the top L samples by performing the iteration method with (3.6) and (3.7) and form the new sequence $< x_n >$ as,

$$< x_n > (i) \ = \ \{x_i\}_{i=1}^{L} \tag{3.8}$$

SAU:- SAU append the top L samples with N samples which are fed from the IFFT block. In (3.8), $< x_n >$ represents the top L samples of the actual sequence (3.5). To form the new sequence x_m, append the samples of (3.8) at the tail of the actual sequence (3.5), which results in x_m with $M = N + L$ samples.

$$x_m(m) = \{x_n, < x_n >\} \qquad \begin{matrix} n = 0,1,2,..N-1 \\ m = 0,1,...N+L-1 \end{matrix} \tag{3.9}$$

here, x_m is the result of the proposed technique and it is a modified version of DCO-OFDM symbol x_n with $N+L$ samples which need to be processed further. For eaxample, let us consider a OFDM symbol with 128 subcarriers, i.e., $N = 128$, and the appended top samples are 8, i.e., $L = 8$, then the resltant time domain signal $x_m(m)$ consists of 136 samples. The power components of time domain signal $x_m(m)$ is $x_m^2(m)$ and it is shown in Fig. 3.2. The succeeding process of the next SAU block is to convert the parallel signal

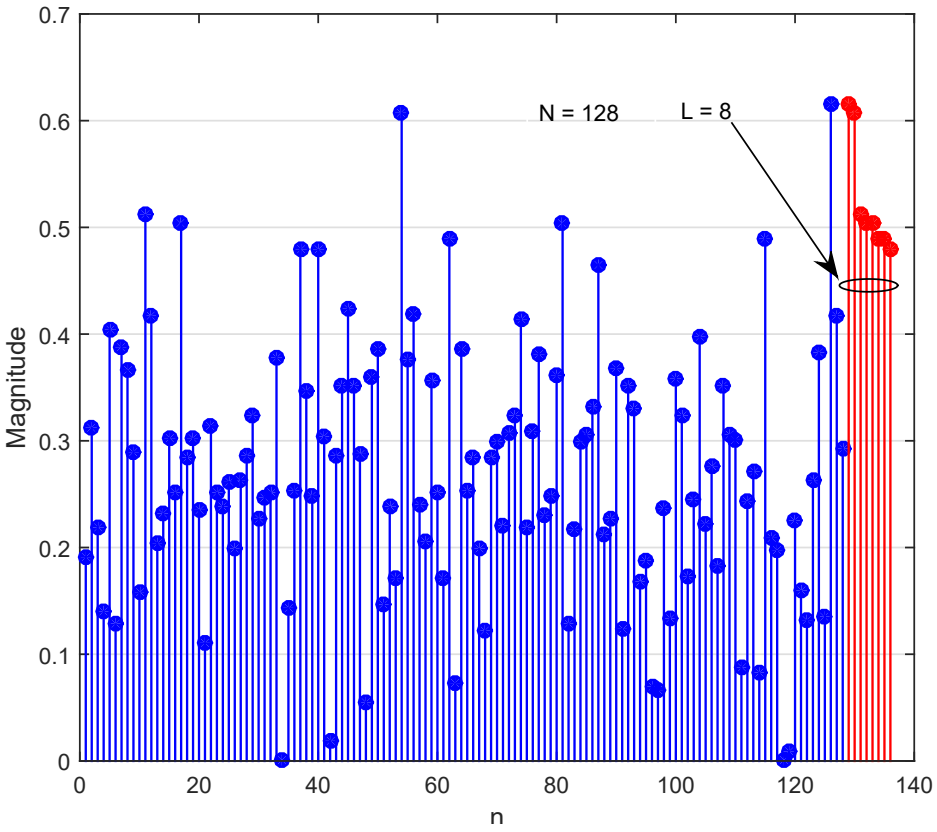

Figure 3.2: Power signal with N=128 after top samples (L=8) appended at the end.

$x_m(m)$ into serial data and then append the cyclic prefix (CP). Sequentially, the resultant signal is converted from digital to analogue and then passed through a low pass filter (LPF), which results in a bipolar signal $x_m(t)$.

For the large values of N, the continuous electrical signal $x_m(t)$ perhaps modelled as $X_m \sim \mathcal{N}(0, \sigma^2)$, which is Gaussian in nature with mean zero and variance $\sigma^2 = E\left[x_m^2(t)\right]$ is the electrical power which is considered as per the literature [14, 35]. Since high PAPR is the major problem in the DCO-OFDM signal, we need to add a huge DC bias to remove the negative peaks. Thus the huge DC bias leads to a deficiency in terms of optical power, we use it to add decent bias and clip the leftover negative portion. All the subcarriers would be affected by the clipping noise in standard DCO-OFDM systems because even and odd subcarriers carry the data symbols. The DC-bias level is relative to the standard deviation of the signal $x_m(t)$. If we denote the DC-biasing level as β_{DC}, then the β_{DC} is given in [73] as,

$$\beta_{DC} = k\sqrt{E\left[x_m^2(t)\right]} \tag{3.10}$$

where k is clipping factor and β_{DC} is represented as $10\log_{10}(k^2+1)$ dB. Since $x_m(t)$ is

bipolar, it needs to be converted into unipolar because IM/DD systems transmit only non-negative signals. Therefore, we added a sufficient DC-bias to $x_m(t)$ and clipped the leftover negative portion by taking into account the LED model which is considered in [44], which results in $x_{m,DCO}(t)$ and it is given in [74] as,

$$x_{m,DCO}(t) = \begin{cases} 0, & x_m(t) < -\beta_{DC} \\ x_m(t) + \beta_{DC}, & x_m(t) \geq -\beta_{DC} \end{cases} \tag{3.11}$$

Signal $x_{m,DCO}(t)$ is input to an ideal intensity modulator (IM), in which the output is directly proportional to the input electrical signal and then the output optical signal is transmitted over the VLC channel model as used in [75] by considering Line-of-Sight (LOS) path. Additive-white-Gaussian-noise (AWGN), $n_{AWGN}(t)$, which affects the signal is added in the electrical domain.

At the receiving section, we use to receive an optical signal with the help of a photodiode and then convert it into an electrical signal. The remaining process is the counterpart to the transmitter section which is the same as the traditional OFDM receiver [76] along with the samples detaching unit (SDU). The SDU section uses to allow $N + L$ samples at the input port and produces N samples at the output port, i.e., SDU detaches the bottom L samples from every OFDM symbol.

3.3 PAPR Analysis

PAPR is defined as the ratio of maximum peak power to the average power of the discrete OFDM signal [77]. Based on the definition of PAPR, we express the PAPR of (3.5) and (3.8) and denote them as $PAPR_A$ and $PAPR_L$, where $PAPR_A$ is actual and $PAPR_L$ is for appended top L samples.

$$PAPR_A = \frac{Max(|x_n|^2)}{\frac{1}{N}\sum_{n=0}^{N-1}|x_n|^2} \tag{3.12}$$

$$PAPR_L = \frac{Max(|<x_n>(i)|^2)}{\frac{1}{L}\sum_{i=1}^{L}|<x_n>(i)|^2} \tag{3.13}$$

After appending L samples to the actual sequence $x_n(n)$, the PAPR of the resulted signal $x_m(m)$ in (3.9) is defined as,

$$PAPR = \frac{Max(|x_m|^2)}{\frac{1}{M}\sum_{m=0}^{M-1}|x_m|^2} \tag{3.14}$$

Since the resultant sequence is the superset of actual and appended sequences in (3.9), we can represent the average power $\frac{1}{M}\sum_{m=0}^{M-1}|x_m|^2$ of the signal $x_m(m)$ as

$$\frac{1}{M}\sum_{m=0}^{M-1}|x_m|^2 = \frac{1}{N+L}\left(\sum_{n=0}^{N-1}|x_n|^2 + \sum_{i=1}^{L}|<x_n>(i)|^2\right) \tag{3.15}$$

by substituting the average power (3.15) in (3.14), the resultant expression can be computed as,

$$PAPR = \frac{Max(|x_m|^2)}{\frac{1}{N+L}\left(\sum_{n=0}^{N-1}|x_n|^2 + \sum_{i=1}^{L}|<x_n>(i)|^2\right)} \tag{3.16}$$

for further simplification, one can rewrite (3.16) as,

$$PAPR = \frac{N+L}{\sum_{n=0}^{N-1}|x_n|^2/Max(|x_m|^2) + \sum_{i=1}^{L}|<x_n>(i)|^2/Max(|x_m|^2)} \tag{3.17}$$

Since the resultant and appended sequences are formed from the actual sequence, the maximum energy of these three Eqs. (3.5) (3.8) (3.9) are the same and expressed as,

$$Max(|x_n|^2) = Max(|<x_n>(i)|^2) = Max(|x_m|^2) \tag{3.18}$$

from (3.18), substitute $Max(|x_n|^2$ and $Max(|<x_n>(i)|^2)$ instead of $Max(|x_m|^2)$ in (3.17), then the result can be expressed as,

$$PAPR = \frac{N+L}{\sum_{n=0}^{N-1}|x_n|^2/Max(|x_n|^2) + \sum_{i=1}^{L}|<x_n>(i)|^2/Max(|<x_n>(i)|^2)} \tag{3.19}$$

by substituting (3.12) and (3.13) in (3.19), it can be simplified as,

$$PAPR = \frac{(N+L).PAPR_A}{N+L\left(\frac{PAPR_A}{PAPR_L}\right)} \tag{3.20}$$

let's consider a variable $\gamma = PAPR_A/PAPR_L$ and put it in (3.20), which results in,

$$PAPR = \left(\frac{N+L}{N+L\gamma}\right).PAPR_A \tag{3.21}$$

for $L = 1$, the $PAPR_L = 1$, which implies $\gamma = PAPR_A$ and it is the upper limit of γ, and for $L = N$, the $PAPR_L = PAPR_A$, which implies $\gamma = 1$ and it is the lower limit of γ. Therefore the range of γ is

$$1 \leq \gamma \leq PAPR_A \tag{3.22}$$

as L increases from 1 to N, eventually γ converges to unity and it is shown in Fig. 3.3, which increse the $N + L\gamma$ value compares to $N + L$. Consequently, the resultant PAPR will decreases to $\left[\frac{N+L}{N+L\gamma}\right]$ times of actual $PAPR_A$.

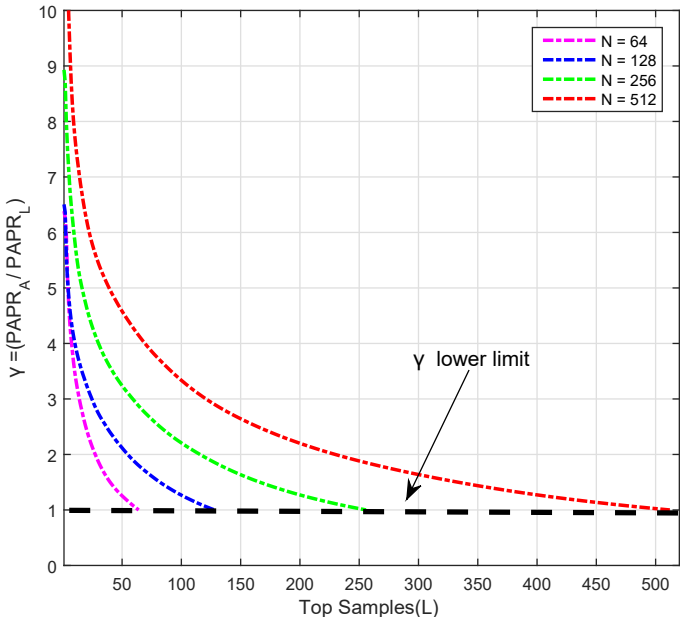

Figure 3.3: Lower limit or Converges of γ in TSDA technique using the different number of subcarriers with respect to the appended samples (top L samples).

3.4 Results and Discussion

In this section, we evaluated the TSDA technique for the DCO-OFDM system by considering the PAPR reduction, BER performance and CC as the evaluation metrics. We used a complementary cumulative distribution function (CCDF) to compute the PAPR (at $CCDF = 10^{-3}$) of the DCO-OFDM system and it's defined as the probability of PAPR which exceeds the threshold value, $PAPR_o$ [78]. Then, we compared the simulation results of the proposed technique with the conventional reduction techniques such as SLM and PTS. We used MATLAB software to simulate the system model, and the simulation

parameters are tabularized in Table 3.1.

Table 3.1: Simulation parameters

Parameter	**DCO-OFDM**
Mapping	4-QAM, 16-QAM and 64-QAM
Number of Sub Carriers(N)	128, 256 and 512
OFDM Symbols	10^4
β_{DC}	7 dB
Clipping factor (k)	2
CCDF	10^{-3}

The theoretical PAPR performance of the proposed TSDA technique (3.21) for DCO-OFDM with the different number of subcarriers (for N=128 and 256) for different modulation orders (4QAM, 16QAM, and 64QAM) are shown in Fig. 3.4. As the number of appended samples (L) increased, the resultant PAPR decreased significantly, and always there is a quid-pro-quo relation between L and PAPR reduction.

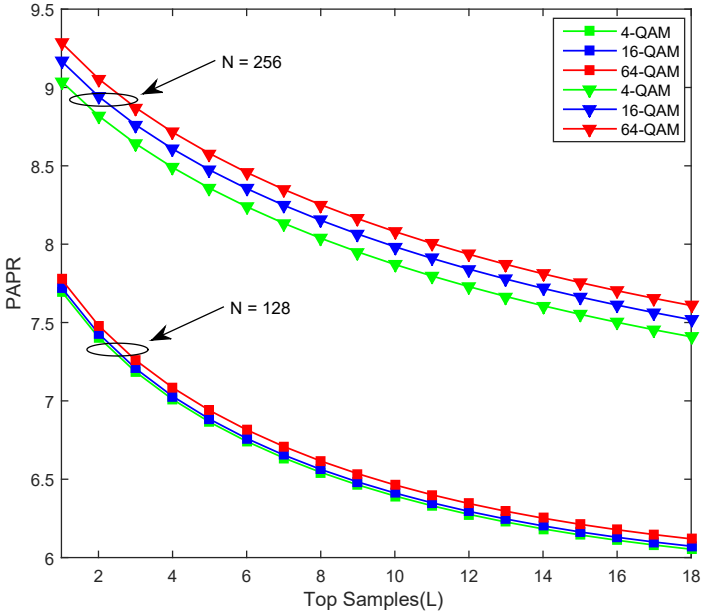

Figure 3.4: Theoretical PAPR performance of TSDA technique for N=128 and 256.

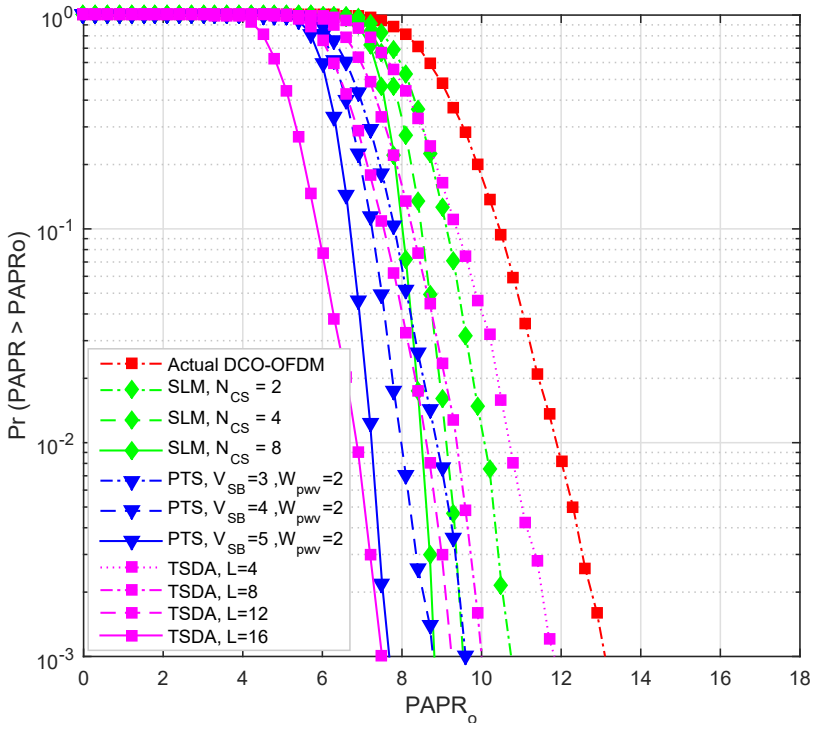

Figure 3.5: PAPR comparison of TSDA with SLM and PTS techniques for N=128 with 4-QAM modulation.

3.4.1 Simulation Results

The PAPR comparison of the proposed TSDA technique with SLM and PTS at CCDF of 10^{-3} is depicted in Fig. 3.5, 3.6, 3.7. To evaluate the PAPR performance, we simulated the DCO-OFDM system with a different number of subcarriers (for N=128, 256, and 512) for different modulation orders as tabularized in Table 3.1.

In Fig. 3.5, the depicted simulation result shows the PAPR of the DCO-OFDM system with different reduction techniques using 128 subcarriers and a 4-QAM modulation scheme. Further, it is observed that the TSDA technique obtains 11.9 dB, 10.0 dB, 9.2 dB, and 7.4 dB for the different numbers of top samples (L), 4, 8, 12, and 16 respectively. Firstly, compared to the PAPR of the DCO-OFDM system (13 dB, without any technique), the PAPR of the TSDA technique reduced by 1.1 dB, 3.0 dB, 3.8 dB, 5.6 dB with the number of top samples 4, 8, 12, 16 respectively. We have also observed that the SLM technique obtains 10.9 dB, 9.5 dB, and 8.9 dB for the different number of CSs (N_{CS}), 2, 4, 8 respectively. Secondly, compared to the PAPR of SLM with two CSs (10.9 dB), the PAPR of the TSDA technique reduced by 0.9 dB, 1.7 dB, and 3.5 dB with the

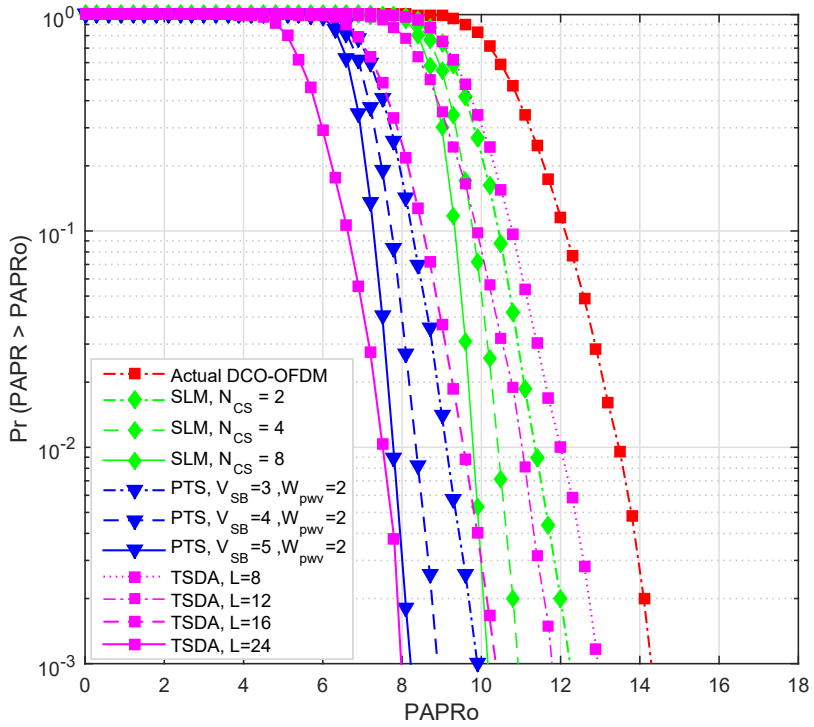

Figure 3.6: PAPR comparison of TSDA with SLM and PTS techniques for N=256 with 16-QAM modulation.

number of top samples 8, 12, and 16 respectively. Similarly, compared to the PAPR of SLM with four CSs (9.5 dB), the PAPR of TSDA reduced by 0.3 dB, and 2.1 dB with the number of top samples 12, 16 respectively. Sequentially, compared to the PAPR of SLM with eight CSs (8.9 dB), the PAPR of TSDA was reduced by 1.5dB with 16 top samples. Therefore, the TSDA technique with $L = 16$ gives better performance than the SLM technique with the different number of CSs 2, 4 and 8. We have also observed that the PTS technique obtains 9.6 dB, 8.8 dB, and 7.6 dB for the different number of CSs ($W_{pwf}^{V_{sb}-1}$), 4, 8, 16 respectively. Here, W_{pwf} and V_{sb} are the number of phase weighting factors and disjoint sub-blocks respectively, and we considered $W_{pwf} = 2$ and V_{sb} is equal to 3, 4, and 5 in simulation results. Thirdly, compared to the PAPR of PTS with four CSs (9.6 dB), the PAPR of the TSDA technique reduced by 0.4 dB, and 2.2 dB with the number of top samples 12, and 16 respectively. Similarly, compared to the PAPR of PTS with eight and sixteen CSs (8.8 dB, 7.6 dB), the PAPR of TSDA reduced by 1.4dB and 0.2 dB with 16 top samples respectively. Therefore, the TSDA technique with $L = 16$ gives a better performance than the PTS technique with a different number of CSs, 4, 8 and 16.

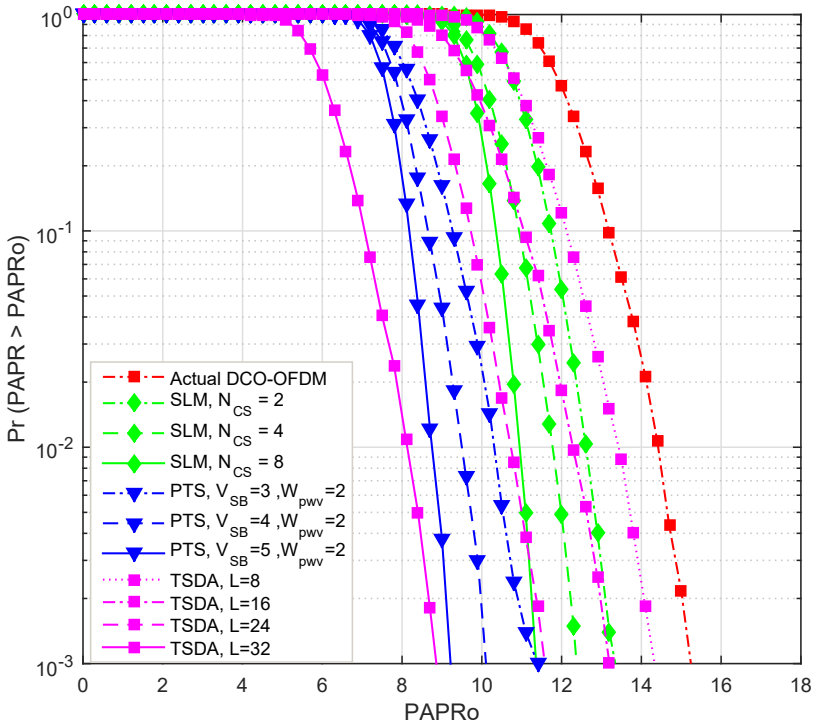

Figure 3.7: PAPR comparison of TSDA with SLM and PTS techniques for N=512 with 64-QAM modulation.

In Fig. 3.6, the depicted simulation result shows the PAPR of the DCO-OFDM system with different reduction techniques using 256 subcarriers and 16-QAM modulation order. We have also observed that the TSDA technique obtains 13 dB, 11.8 dB, 10.2 dB, and 8.0 dB for the different number of top samples (L), 8, 12, 16, and 24 correspondingly. Initially, compared to the PAPR of the DCO-OFDM system (14.2 dB, without any technique), the PAPR of the TSDA technique reduced by 1.2 dB, 2.4 dB, 4.0 dB, 6.2 dB with the number of top samples 8, 12, 16, 24 correspondingly. We have also observed that the SLM technique obtains 12.2 dB, 11.0 dB, and 10.2 dB for the different numbers of CSs, 2, 4, 8 correspondingly. Then, compared to the PAPR of SLM with two candidate signals (12.2 dB), the PAPR of the TSDA technique reduced by 0.4 dB, 2.0 dB, and 4.2 dB with the number of top samples 12, 16, and 24 correspondingly. Likewise, compared to the PAPR of SLM with four candidate signals (11.0 dB), the PAPR of TSDA reduced by 0.8 dB, 3.0 dB with the number of top samples 16, 24 correspondingly. Likewise compared to the PAPR of SLM with eight candidate signals (10.2 dB), the PAPR of TSDA reduced by 2.2 dB with 24 top samples. Therefore, the TSDA technique with $L = 24$ gives better performance than the SLM technique with the different number of CSs 2, 4 and 8. We

Table 3.2: PAPR comparison of TSDA technique with SLM and PTS

Reduction Technique	***Parameters*** ***Ncs, Vsb, Wpws and L***	PAPR in dB at $CCDF = 10^{-3}$		
		N=128	***N=256***	***N=512***
Actual	*L=0*	13.0	14.2	15.2
SLM	*Ncs=2*	10.9	12.2	13.3
	Ncs=4	9.5	11.0	12.3
	Ncs=8	8.9	10.1	11.5
PTS	*Wpwf=2, Vsb=3*	9.6	9.9	11.6
	Wpwf=2, Vsb=4	8.8	8.9	10.1
	Wpwf=2, Vsb=5	7.6	8.2	9.2
TSDA (proposed)	*L=4*	11.9	-	-
	L=8	10.0	13	14.2
	L=12	9.2	11.8	-
	L=16	7.4	10.2	13.2
	L=24	-	8.0	11.7
	L=32	-	-	8.9

have also observed that the PTS technique obtains 9.9 dB, 8.9 dB, and 8.2 dB for the different numbers of CSs 4, 8, and 16 correspondingly. Then, compared to the PAPR of PTS with 4, 8, and 16 CSs (9.9 dB, 8.9 dB, 8.2 dB), the PAPR of the TSDA technique reduced by 1.9 dB, 0.9 dB, and 0.2 dB correspondingly with 24 top samples. Therefore, the TSDA technique with $L = 24$ gives a better performance than the PTS technique with the different number of CSs 4, 8 and 16. Similarly in Fig. 3.7, the portrayed simulation result illustrates the PAPR of the DCO-OFDM system with diverse reduction techniques using 512 subcarriers and 64-QAM modulation scheme. We have also observed that the TSDA technique with $L = 32$ gives an improved performance than the PTS technique with the different number of CSs 4, 8 and 16 as tabularized in Table. 3.2.

The second metric we used to evaluate the proposed technique is the BER performance of the DCO-OFDM system. In Fig. 3.8, and Fig. 3.9, the depicted simulation result shows the BER performance of DCO-OFDM system with and without TSDA reduction technique using 256 and 512 subcarriers with different modulation orders (4-QAM, 16-QAM, and 64-QAM). From Fig. 3.8, we observed that the BER performance of the

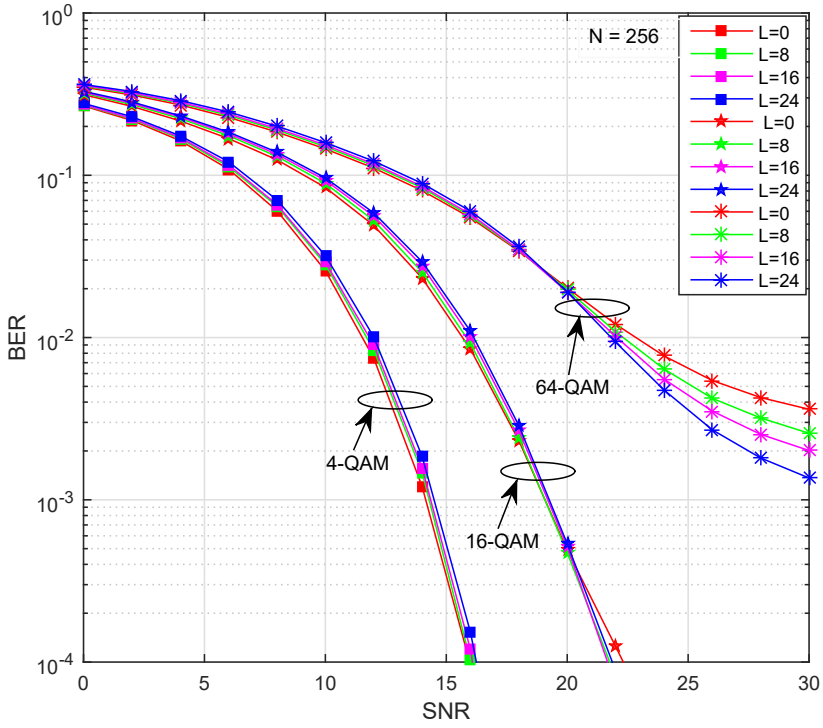

Figure 3.8: BER performance of TSDA technique for N=256 with different modulation order.

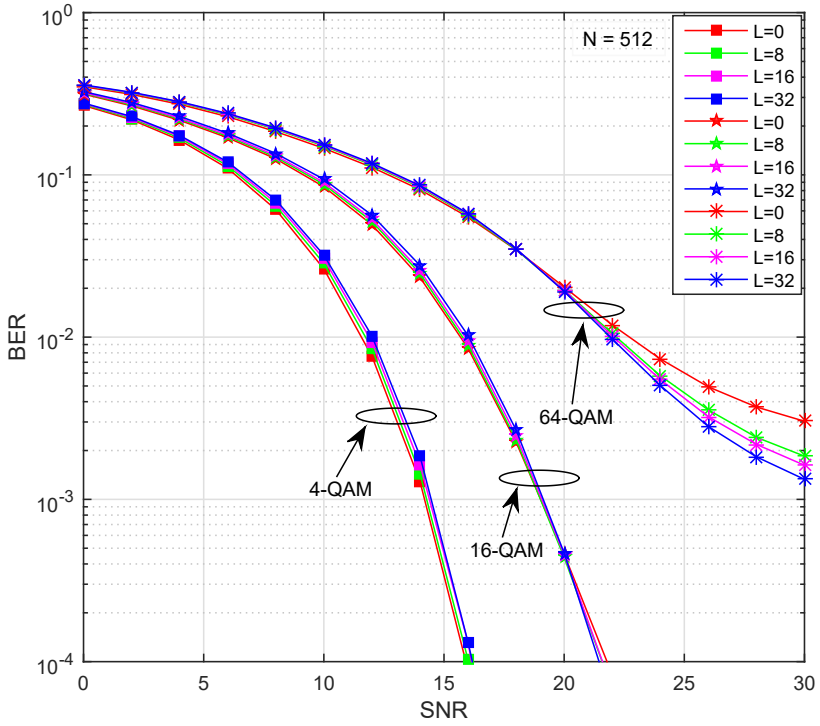

Figure 3.9: BER performance of TSDA technique for N=512 with different modulation order.

Table 3.3: CC comparison of TSDA technique with SLM and PTS in terms of CMs and CAs

Reduction Technique	**CMs**	**CAs**
SLM	$N_{cs}\left(\frac{N_{osf}N}{2}\right)\log_2\left(N_{osf}N\right)$	$N_{cs}\left(N_{osf}N\right)\log_2\left(N_{osf}N\right)$
PTS	$W_{pwf}^{V_{sb}-1}\left(\frac{N_{osf}N}{2}\right)\log_2\left(N_{osf}N\right)$	$W_{pwf}^{V_{sb}-1}\left(N_{osf}N\right)\log_2\left(N_{osf}N\right)$
TSDA (Proposed)	$\left(\frac{N_{osf}N}{2}\right)\log_2\left(N_{osf}N\right)$	$\left(N_{osf}N\right)\log_2\left(N_{osf}N\right)$

DCO-OFDM system with TSDA, using 256 subcarriers and different modulation order, is increased by less than 1dB ($< 1dB$) as increasing the top samples 8, 16, and 24 correspondingly. Likewise, from Fig. 3.9, we also perceived that the BER performance of DCO-OFDM system with TSDA, using 512 subcarriers and different modulation order, is increased by less than 1dB ($< 1dB$) as increasing the top samples 8, 16, and 32 respectively. We have also noticed that the BER performance of the DCO-OFDM system with N=512 and 64-QAM at low SNR almost coincides with the original one (without any technique). Therefore, we can put forward the proposed TSDA technique for a system with higher-order, modulations and subcarriers.

3.4.2 Computational Complexity analysis

CC is the third metric which we used in evaluating the TSDA technique by accounting for the real-time implementation. However, it can be computed by the number of subcarriers N and oversampling factor N_{osf} used in one IFFT computation. Generally, to compute the IFFT $(N_{osf}N/2)\log_2(N_{osf}N)$ number of Complex Multiplications (CMs) and $(N_{osf}N)\log_2(N_{osf}N)$ number of Complex Additions (CAs) are required. SLM and PTS reduction techniques require the N_{CS} and $W_{pwf}^{V_{sb}-1}$ number of IFFT computations needs to be computed correspondingly. Whereas, the proposed TSDA technique requires only one IFFT computation. This thing put forward the proposed technique as substantially very simple to implement in real-time compared to SLM and PTS. The comparison of the CC of proposed and traditional reduction techniques are tabularized in Table. 3.3 in terms of CMs and CAs.

Table 3.4: CC comparison of TSDA technique with SLM and PTS

Reduction Technique	*Parameters* *Ncs, Vsb, Wpws and L*	CMs			CAs		
		N=128	*N=256*	*N=512*	*N=128*	*N=256*	*N=512*
SLM	*Ncs=2*	896	2048	4608	1792	4096	9216
	Ncs=4	1792	4096	9216	3584	8192	18432
	Ncs=8	3584	8192	18432	7168	16384	36864
PTS	*Wpwf=2, Vsb=3*	1792	4096	9216	3584	8192	18432
	Wpwf=2, Vsb=4	3584	8192	18432	7168	16384	36864
	Wpwf=2, Vsb=5	7168	16384	36864	14336	32768	73728
TSDA (proposed)	$\forall L$	448	1024	2304	896	2048	4608

3.4.3 CCRR

The CCRR is defined in [78] as,

$$CCRR = \left(1 - \frac{Complexity\ of\ proposed\ technique}{Complexity\ of\ conventional\ technique}\right) \times 100\% \tag{3.23}$$

To compute the CCRR, we computed the computations in terms of CMs and CAs of the proposed technique, SLM, and PTS techniques for the different number of subcarriers 128, 258, and 512 with the oversampling factor one, and tabularized in Table. 3.4.

Table 3.5: CCRR of TSDA technique Compares to SLM and PTS Reduction Techniques

Reduction Technique	***Parameters Ncs, Vsb and Wpwf***	**CCRR in CM**	**CCRR in CA**
		$\forall N$	$\forall N$
SLM	*Ncs=2*	50.00	50.00
	Ncs=4	75.00	75.00
	Ncs=8	87.50	87.50
PTS	*Wpwf=2, Vsb=3*	75.00	75.00
	Wpwf=2, Vsb=4	87.50	87.50
	Wpwf=2, Vsb=5	93.75	93.75

We noticed that the CCRR of TSDA ($\forall L$) with SLM using CSs 2, 4, 8 are computed as 50.00, 75.00, and 87.50 correspondingly. We have also perceived that the CCRR of

the proposed technique ($\forall L$) with PTS using CSs 4, 8, 16 are computed as 75.00, 87.50, 93.75 correspondingly. CCRR of the TSDA technique in terms of CMs and CAs with SLM and PTS is tabularized in Table 3.5. Consequently, we can state that the CCRR of the proposed technique with SLM and PTS is increased to 87.50 and 93.75 as increasing the candidate signals 8 and 16 correspondingly.

3.5 Summary

In this chapter, we introduced a novel technique called Top Sample Detection and Appending (TSDA) for reducing PAPR in DCO-OFDM systems. The effectiveness of the proposed technique was validated through theoretical analysis and simulation results. One notable advantage of the TSDA scheme is that it does not require any side information, unlike existing techniques such as Selected Mapping (SLM) and Partial Transmit Sequence (PTS). Side information refers to additional data or signals needed for PAPR reduction, which can increase CC and overhead. By eliminating the need for side information, the TSDA technique simplifies the implementation process.

Furthermore, the TSDA technique not only enhances PAPR reduction performance but also reduces the CC compared to conventional SLM and PTS techniques. The lower CC of the TSDA scheme makes it more efficient in terms of resource utilization. An implicit advantage of the reduced CC is a decrease in processing delay. This aspect is particularly beneficial in real-time implementations where timely signal transmission is crucial.

Chapter 4

Low-complex ADO-OFDM for VLC Systems

4.1 Introduction

Visible Light Communication (VLC) systems make use of pre-installed white light-emitting diodes (LEDs) for data transmission in the visible light range of 400nm to 900nm for indoor wireless communication systems. White LEDs are preferably used in VLC systems, because of their advantages such as efficient power consumption with a longer lifespan when compared to other LED sources. Moreover, the low cost of LEDs makes them a dominant source for data transmission as well as illumination. White LEDs can offer modulation bandwidths reaching 20 MHz [79] in the modulation process, where the electrical signal is converted into an optical signal. For acquiring improved transmission capacity and maximizing the usable bandwidth, high SE modulation orders are used with basic equalization techniques. Therefore, optical wireless communications (OWC) using white LEDs have attained very good attention to increasing data transmission in indoor wireless communication systems.

Since the multipath reflections present in the VLC system [80], the channel response produces low pass filter (LPF) characteristics and its 3dB bandwidth is highly affected [81]. However, the interference among the symbols called inter-symbol interference (ISI) can occur due to multipath reflections present in the optical systems and it also causes degradation in link performance. Orthogonal frequency division multiplexing (OFDM) being an emerging technology has been used in the VLC system to encounter the result of the multipath reflection to increase the SE using adaptive modulation techniques like

power and bit loading [82]. OFDM scheme segregates the available spectrum into the required number of subcarriers which are flat and have sufficient frequency spacing such that the orthogonality among the succeeding subcarriers can be achieved.

It should be noted that the OFDM requires to support the VLC environment which makes use of the IM/DD for signal transmission and receptions respectively. The message signal which is used to transmit over the LED needs to be modulated from an electrical to an optical signal in terms of light intensity whereas, the photo-diode (PD) can counter the transmitter process at the receiver section. Since the LEDs allow only unipolar signals, the transmitting message signal must be real and non-negative. Thus, the OFDM needs to constrain the input signal under hermitian symmetry (HS) [83] to attain the real signal at the front-end LED of OWC systems. Henceforth, the required non-negative real signal can be achieved by adding DC bias or clipping the complete negative part of the real signals. These two techniques are mentioned as DCO-OFDM [84–88] and ACO-OFDM respectively [75, 89, 90].

The ACO-OFDM and DCO-OFDM schemes have some inbuilt drawbacks based on the efficiency paradigm. However, the DCO-OFDM achieves the unipolar signal by adding the DC-bias which will decrease the PE of the optical signal [14] whereas, ACO-OFDM utilizes only the odd subcarriers for symbol transmission, which results in a reduction in SE [91]. To overcome these problems, an efficient modulation scheme called ADO-OFDM was presented in [1]. In ADO-OFDM, even subcarriers are used in the ACO-OFDM and the odd subcarriers are used in the DCO-OFDM. However, ADO-OFDM combines the advantages of DCO-OFDM and ACO-OFDM, where all subcarriers are used to carry the data, the overall SE is better than ACO-OFDM and due to half of the subcarriers are used in ACO-OFDM which is more PE, the overall optical PE is better than DCO-OFDM. However, due to asymmetrically clipping noise falls on the even subcarriers of DCO-OFDM, the ACO-OFDM signal should be retrieved first and then make use of it to generate the DCO-OFDM signal, which increases the latency and computational complexity. Therefore, traditional ADO-OFDM does not gratify the specifications of fifth-generation (5G) and beyond communication systems.

Nevertheless, an LED is a non-ohmic device that is distinguished by its non-linear characteristics in terms of current and voltage. Additionally, the optical radiated power

and the driving current of an LED are related non-linearly. Thus, the non-linear phenomenon produces the harmonics at high frequencies, which can affect the predetermined signal and lead to intermodulation products over the distinct subcarriers. Likewise, both the lower and upper clippings are the main sources of signal distortion, in which the lower clipping distortion takes place below the LED turn-on-voltage (TOV) and the upper clipping distortion takes place at the maximum allowable current of the LED. Particularly in OFDM, these distortions are represented in terms of a high PAPR arising from the superimposition of independent subcarriers which are inputs to the inverse fast Fourier transform (IFFT) and results in large peaks in time domain signal [77, 92, 93]. Thus, the non-linear effects of LED on the performance of optical-OFDM need to be observed to counter it in real-time implementation. The performance of ACO-OFDM and DCO-OFDM under the nonlinear effect of LED was deliberated in [94].

In this chapter, to address the issues mentioned in the literature, we proposed a new modulation technique called a nonlinear modelled Low-complex ADO-OFDM (LADO-OFDM) for VLC systems, which utilizes the pre-distortion technique to mitigate the mutual-interference occurring in DCO-OFDM and ACO-OFDM. Due to the eradication of mutual interference, the DCO-OFDM and ACO-OFDM demodulation process can be done parallelly at the receiver section unlike in traditional ADO-OFDM, which results in substantially decreased computing complexity and latency. The performance of the proposed LADO-OFDM under the nonlinear effect of two LED models is studied and compared with the traditional ADO-OFDM in terms of bit error rate (BER) and computing complexity. The effect of clipping distortion of LED has been examined concerning the dynamic range of LED and DC-bias point. In addition to this, LADO-OFDM is also compared with the pulse-amplitude-modulated discrete multitone modulation (PAM-DMT) [36] in terms of BER.

The rest of this chapter is structured as follows. Section 4.2 describes the two LED models opted to study the effect of LED nonlinearity on the performance of the proposed system. The system model of the proposed LADO-OFDM is presented in Section 4.3. Signal analysis is briefly presented in Section 4.4 and followed by Section 4.5 describes the simulation results and discussions. The summary of this chapter is finally described in Section 4.6.

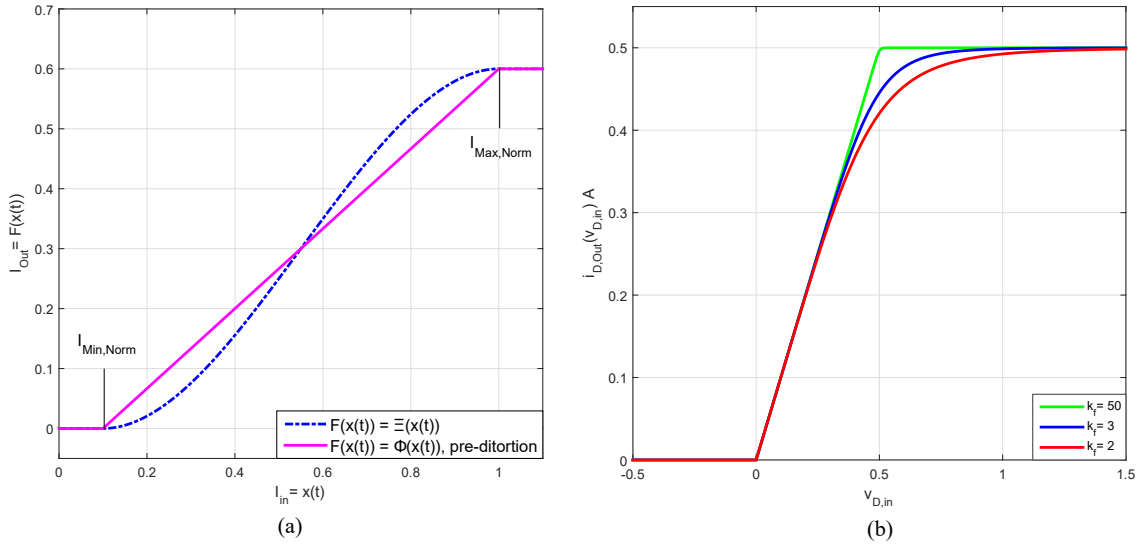

Figure 4.1: Nonlinear-characteristics of an LED under (a) Model-I: LED characteristic of the adopted optical front-end $\Xi(x(t))$ along with linearized characteristic after pre-distorting with the inverse polynomial function $\phi(x(t))$, (b) Model-II: LED characteristics for distinct knee factors using $f(v_{\mathrm{D,in}}) = v_{\mathrm{D,in}}/R$ with a maximum permissible AC current, $i_{\mathrm{D,max}} = 0.5A$ and the normalized resistance, $R = 1\Omega$.

4.2 LED models

For every individual waveform designed for VLC, it is the non-linear behaviour of the LEDs that essentially inflicts the challenge which has led to producing the distortion and finally resulting in the degradation of performance. LEDs are to be maintained at a minimum TOV below which are said to be in zero current conduction and cut-off state. The time-domain real-valued bipolar modulating signal is transmitted through the LED restricting to its linear portion which is part of exponential characteristics. So, before applying the modulating signal distinguished by high peak power, the LEDs must be biased. By clipping lower peaks at the TOV, the restricted linear portion of the LED curve deteriorates the signal by amplitude distortion. Later, the upper peaks at their maximum permissible current are intentionally clipped in their time domain before having given out the light signal by the LED. These non-linear characteristics which clip both the upper and lower peaks of the modulated signal should have a mathematical polynomial fitting which is needed in the Monte Carlo simulations. Therefore, the sophisticated generalized LED models which are used in this work were considered in [44, 45]. An

LED model based on a piecewise polynomial which reflects the non-linear behaviour of an LED for a VLC system was proposed in [45]. In this model, the LED dynamic range was conditioned to linearise the signal from a minimum to a maximum optical power to recompense the non-linear behaviour of the LED by pre-distorting the inverse polynomial function. In the analogue circuitry, the bipolar signal is dc-biased by β_{DC} and clipped at zero levels to obtain the unipolar signal $x(t)$ to be transmitted by the front-end LED. The nonlinear characteristics of the LED are generalized as a relation between the input current, $I_{\text{in}} = x(t)$, proportional to the square root of the electrical power, and the output current, $I_{\text{out}} = F(x(t))$, proportional to the optical power. Consequently, the current signal, $x(t)$, is subjected to a nonlinear distortion function, $F(x(t))$, as it is passed through the front-end LED. We have considered two examples as given in [45], one is the generalized non-linear sigmoid function $F\left(x(t)\right) = \Xi\left(x(t)\right)$, and another one is a linearized function, $F\left(x(t)\right) = \phi\left(x(t)\right)$ which can be attained from the inverse polynomial function, $\Xi^{-1}\left(x(t)\right)$. The example of non-linear sigmoid function $\Xi\left(x(t)\right)$ with increased precision of the polynomial coefficients are given in [45] as,

$$\Xi\left(x(t)\right) = \begin{cases} 0, & \text{if } x(t) \leq 0.1 \\ \alpha_1 x^3(t) + \alpha_2 x^2(t) + \alpha_3 x(t) + \alpha_4, & \text{if } 0.1 < x(t) \leq 1 \\ 0.6, & \text{if } x(t) > 1 \end{cases} \tag{4.1}$$

where, $\alpha_1 = -1.6461$, $\alpha_2 = 2.7160$, $\alpha_3 = -0.4938$ and $\alpha_4 = 0.0239$ respectively. The polynomial function having its pre-distortion function is depicted in Fig. 4.1(a). In the same figure, the $I_{\text{Min,Norm}}$ and $I_{\text{Max,Norm}}$ are the normalized minimum and maximum input currents respectively, and $I_{\text{Max,Norm}} = 1$.

On the other hand, an LED model with a linear increase was proposed in [44] and is popularly known as the Rapps model. This LED model incorporates the optical OFDM signal onto the V-I characteristics of the front-end LED. The Rapps model describes that the amplitude distortion arises in the portion of nonlinear characteristics of the LED and is used in optimizing the system constraints like constellation order, signal power and bias point to attain better performance. Therefore, the Rapps model also has been integrated with the proposed LADO-OFDM modulation for optical wireless communication systems to limit the signal level to V-I characteristics of the front-end LED. From Rapp's model [44], the nonlinear characteristics of the front-end LED are modelled as a relation between the input voltage, $v_{D,in} = x(t)$, and the output current, $i_{D,Out}(v_{D,in}) = F(x(t))$.

Consequently, the signal, $x(t)$, is subjected to a nonlinear distortion function, $F(x(t))$, as it is passed through the front-end LED. The considered nonlinear model of the LED can be expressed as

$$i_{D,Out}(v_{D,in}) = \begin{cases} h(v_{D,in}), \text{ if } v_{D,in} \geq 0 \\ 0, \text{ if } v_{D,in} < 0 \end{cases} \tag{4.2}$$

here, $i_{D,Out}$ and $v_{D,in}$ are the current and voltage of the front-end LED, and $h(v_{D,in})$ is given as,

$$h(v_{D,in}) = \frac{f(v_{D,in})}{\left(1 + \left(\frac{f(v_{D,in})}{i_{D,\max}}\right)^{2k_f}\right)^{\frac{1}{2k_f}}} \tag{4.3}$$

here, the maximum permissible alternative current pulses pass through an LED is $i_{\mathrm{D,Max}}$ and the data-sheet/measured V-I characteristics of the LED describing function is $f(v_{\mathrm{D,in}})$. Using the knee factor k_f, the hard and smooth clippings are used to clip the lower and upper peaks of the signal respectively and the corresponding characteristics are depicted in Fig.4.1(b).

4.3 System Model

In this section, we address the transceiver structure of LADO-OFDM for VLC systems under nonlinear distortion.

4.3.1 Transmitter

In Fig.4.2, the top portion of the schematic diagram depicts the transmitter section of LADO-OFDM. The transmitter does have distinct paths to generate ACO-OFDM and DCO-OFDM signals correspondingly. Besides these parts, the processing of the signal seems to be very close to the traditional ACO-OFDM transmitter [14]. The given input bit-streams are converted from serial to parallel data and then mapped to the corresponding QAM order symbols. The corresponding input symbol vectors of the bitstream-I and II, $\mathbf{S}_1$ and $\mathbf{S}_2$ are shown in Fig. 4.3. Fig. 4.3(a) illustrates that the QAM symbols corresponding to bitstream-I which can be assigned to the odd subcarriers of the ACO-OFDM signal modulation and Fig. 4.3(b)illustrates that the QAM symbols corresponding to bitstream-II which can be assigned to the even subcarriers of the DCO-OFDM signal

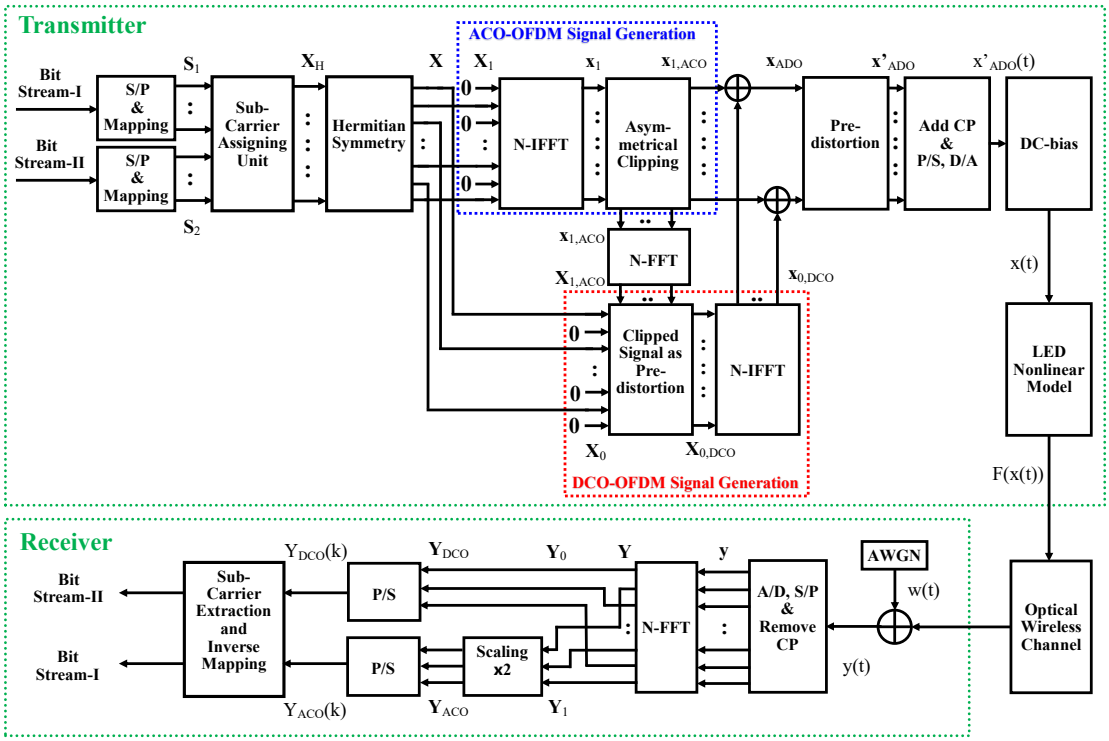

Figure 4.2: Block diagram of proposed LADO-OFDM transmitter and receiver with non-linear LED models.

modulation. Successively, the subcarrier assignment takes place to form the message symbol vector $\mathbf{X}_H$. Fig. 4.3(c) represents the subcarrier assignment for the mapped QAM symbols such that the bitstream-I symbols can be loaded onto the odd subcarriers of the ACO-OFDM signal modulation and the bitstream-II symbols can be loaded onto the even subcarriers of the DCO-OFDM signal modulation. However, the information vector $\mathbf{X}$ is compelled to have hermitian symmetry to guarantee the IFFT yields real values only and it is represented in terms of message symbol vector as $\mathbf{X} = [0, \mathbf{X}_H(k), 0, \mathbf{X}_H^*(\frac{N}{2} - k)]$, where, $k = 1, 2, .., (\frac{N}{2} - 1)$ and N is the number of subcarriers in the OFDM symbol. Furthermore, the input data vector $\mathbf{X}$ is divided into even and odd components, where, $\mathbf{X}_0$ comprises the symbols reflecting the QAM constellation points upon even subcarriers, which is represented as $\mathbf{X}_0 = [X(0), 0, X(2), ..., X(N-2), 0]$, and $\mathbf{X}_1$ comprises the symbols reflecting the QAM constellation points upon odd subcarriers and it is given as $\mathbf{X}_1 = [0, X(1), 0, X(3), ..., X(N-1)]$. Since the $\mathbf{X}$ elements have hermitian symmetry, the $\mathbf{X}_0$ and $\mathbf{X}_1$ elements would have hermitian symmetry too. Firstly, the signals $\mathbf{x}_{1,ACO}$

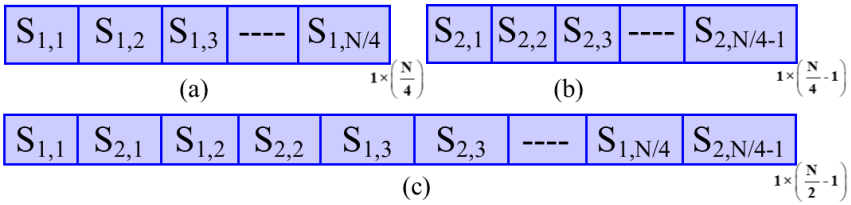

Figure 4.3: Subcarrier assignment. (a) $\mathbf{S}_1$: message symbol vector corresponding to the bitstream-I, (b) $\mathbf{S}_2$: message symbol vector corresponding to the bitstream-II, (c) $\mathbf{X}_H$: subcarrier assignment for the mapped symbols of bitstream-I and II

and $\mathbf{x}_{0,DCO}$ are generated and then combined to generate the new signal $\mathbf{x}_{ADO}$. Since we endorse the nonlinear LED models (I and II), the nonlinear characteristic of LED model-I transmitter can be compensated by pre-distortion with the corresponding inverse nonlinear-function of LED model-I [45] and there is no pre-distortion block for LED model-II [44] because of the knee factor, which can linearize the nonlinear characteristics of LED model-II. The signal $\mathbf{x}_{ADO}$ inputs to the pre-distortion block to generates $\mathbf{x}'_{ADO}$ for LED model-I, whereas both $\mathbf{x}_{ADO}$ and $\mathbf{x}'_{ADO}$ are same for the LED model-II. In general, a cyclic prefix (CP) is added at the starting point of every OFDM symbol to diminish the inter-carrier-interference (ICI) and inter-symbol-interference (ISI). Therefore, we added a CP to the pre-distorted signal $\mathbf{x}'_{ADO}$, and then converted from parallel-to-serial (P/S) data and the resultant signal is converted from digital-to-analogue (D/A) signal, $\mathbf{x}'_{ADO}(t)$. Since the signal $\mathbf{x}'_{ADO}(t)$ is bipolar, we need to add an appropriate DC-bias accordingly in [35] to make the signal $\mathbf{x}'_{ADO}(t)$ into the unipolar signal, $x(t)$. Finally, the signal $x(t)$, is passed through a nonlinear LED model to output the signal, $F(x(t))$, and it is transmitted through an optical wireless channel [95].

4.3.2 Receiver

In Fig.4.2, the bottom portion of the block diagram depicts the receiver section of the proposed LADO-OFDM system. The receiver does have distinct paths to demodulate the ACO-OFDM and the DCO-OFDM signals respectively. At the receiver section, we assumed a flat channel with AWGN $w(t)$ and perfect equalization to attain $y(t)$. Then, we engaged a matched filter to detect the received signal, and the detected signal is passed through an analogue-to-digital converter (ADC) to produce the digital signal. Next, the

resultant signal is subjected to a serial-to-parallel (S/P) converter to obtain the parallel data, and we removed the CP to generate the actual time-domain signal, $\mathbf{y}$. Next, we passed the time-domain signal, $\mathbf{y}$, through the FFT block to convert into frequency-domain to acquire the received subcarriers, $\mathbf{Y}$. However, the received subcarriers are divided into even subcarriers $\mathbf{Y}_0 = [Y(0), 0, Y(2), ..., Y(N-2), 0]$ and odd subcarriers $\mathbf{Y}_1 = [0, Y(1), 0, Y(3), ..., Y(N-1)]$ to recover the symbols transmitted over the corresponding subcarriers. Since the DCO-OFDM signal is transmitted over the even subcarriers, the received DCO-OFDM signal, $\mathbf{Y}_{DCO}$, is directly obtained from the received even subcarriers, $\mathbf{Y}_0$. On the other hand, because the ACO-OFDM signal is transmitted over the odd subcarriers, the ACO-OFDM signal, $\mathbf{Y}_{ACO}$, is obtained from the received odd subcarriers, $\mathbf{Y}_1$, by scaling with a factor of two [89]. Sequentially, $\mathbf{Y}_{DCO}$ and $\mathbf{Y}_{ACO}$ are subjected into parallel-to-serial converters to outputs $Y_{DCO}(k)$ and $Y_{ACO}(k)$ respectively. Next, the subcarrier extraction and inverse mapping take place after parallel-to-serial conversion, which produces the transmitted bitstream I and II respectively.

4.4 Signal Representation

In this section, we provided the representation of a new LADO-OFDM system with an LED model and illustrated how message symbols are transmitted over the odd and even subcarriers and how they can be retrieved at the receiver section independently. Initially, it was used in [89], that the ACO clipping noise just alters the even subcarriers and doesn't make any clipping effects to the odd subcarriers. Later in [35], it was shown that if we use only the even subcarriers for DCO-OFDM signal transmission, the corresponding clipping noise alters only the even subcarriers. Therefore, from both the clipping noises, neither of the clipping noise alters the odd subcarriers.

4.4.1 Transmitter Signal Representation

Firstly, the signal $\mathbf{X}_1$ is fed to the IFFT block to generate $\mathbf{x}_1$, which is bipolar and real. Successively, the ACO-OFDM signal, $\mathbf{x}_{1,ACO} = [x_{1,ACO}(0), x_{1,ACO}(1), x_{1,ACO}(2), ..., x_{1,ACO}(N-1)]$ is generated by clipping the signal $\mathbf{x}_1$ at zero level. As given in [89], the magnitude of the required signal gets halved due to clipping noise in the ACO-OFDM

signal transmission, and it's get added to the even subcarriers. Therefore, the ACO-OFDM signal, $\mathbf{x}_{1,ACO}$, is given as,

$$\mathbf{x}_{1,ACO} = \frac{1}{2}\mathbf{x}_1 + \mathbf{n}_{1,ACO} \tag{4.4}$$

where $\mathbf{n}_{1,ACO}$ is the ACO-OFDM clipping noise and its FFT encompasses the only even subcarriers while $\mathbf{x}_1$ encompasses the odd subcarriers of the optical OFDM system. However, the clipped signal $\mathbf{x}_{1,ACO}$ is transformed into the frequency domain to attain the $\mathbf{X}_{1,ACO}$, which is used to obtain the clipping noise on the even subcarriers, so that, it can be utilized in pre-distorting the signals in DCO-OFDM generation. The frequency domain signal can be expressed as,

$$\mathbf{X}_{1,ACO} = \underbrace{\frac{1}{2}\mathbf{X}_1}_{\substack{\text{on odd} \\ \text{subcarriers}}} + \underbrace{\mathbf{N}_{1,ACO}}_{\substack{\text{on even} \\ \text{subcarriers}}} \tag{4.5}$$

where, the signals $\frac{1}{2}\mathbf{X}_1$ and $\mathbf{N}_{1,ACO}$ are the ACO-OFDM clipped signals over the odd and even subcarriers correspondingly, and they can be represented as,

$$\frac{1}{2}\mathbf{X}_1 = \begin{cases} 0, & \text{for even SCs} \\ \mathbf{X}_{1,ACO}, & \text{for odd SCs} \end{cases} \tag{4.6}$$

$$\mathbf{N}_{1,\text{ACO}} = \begin{cases} \mathbf{X}_{1,ACO}, & \text{for even SCs} \\ 0, & \text{for odd SCs} \end{cases} \tag{4.7}$$

unlike the signal generation in the traditional system [1], the proposed system generates DCO-OFDM signal by pre-distorting the signal $\mathbf{X}_0$ with the frequency domain transformed clipped ACO-OFDM signals over the even subcarriers, i. e., the clipping noise corresponding to even subcarriers of $\mathbf{X}_{1,ACO}$ is subtracted from the even subcarriers of the signal $\mathbf{X}_0$, which produces the clipping noise pre-eliminated signal $\mathbf{X}_{0,DCO}$ as shown in Fig. 4.4, and it is expressed as,

$$\mathbf{X}_{0,\text{DCO}} = \begin{cases} \mathbf{X}_0 - \mathbf{X}_{1,ACO}, & \text{for even SCs} \\ \mathbf{X}_0, & \text{for odd SCs} \end{cases} \tag{4.8}$$

sequentially, subjecting the signal $\mathbf{X}_{0,\text{DCO}}$ into the IFFT block, the frequency domain signal is converted into the time domain signal, $\mathbf{x}_{0,DCO}$, and it is given in [89] as $\mathbf{x}_{1,DCO} =$

$[x_{1,DCO}(0), x_{1,DCO}(1), x_{1,DCO}(2), ..., x_{1,DCO}(N-1)]$. Then, add the ACO-OFDM signal $\mathbf{x}_{1,ACO}$ with the DCO-OFDM signal $\mathbf{x}_{0,DCO}$ to obtain the LADO-OFDM signal, $\mathbf{x}_{ADO}$ as,

$$\mathbf{x}_{\mathrm{ADO}} = \mathbf{x}_{0,\mathrm{DCO}} + \mathbf{x}_{1,\mathrm{ACO}} \tag{4.9}$$

from the eqn. (4.7) and eqn. (4.8), one can obtain the pre-distorted frequency domain DCO-OFDM signal $\mathbf{X}_{0,DCO}$ as,

$$\mathbf{X}_{0,\mathrm{DCO}} = \mathbf{X}_0 - \mathbf{N}_{1,\mathrm{ACO}}, \qquad \text{for all SCs} \tag{4.10}$$

for the perception of the frequency domain, we can transform the eqn. (4.9) into the frequency domain, and it can be expressed as,

$$\mathbf{X}_{\mathrm{ADO}} = \mathbf{X}_{0,\mathrm{DCO}} + \mathbf{X}_{1,\mathrm{ACO}}, \qquad \text{for all SCs} \tag{4.11}$$

substituting the eqn. (4.5) and the eqn. (4.10) in eqn. (4.11), one can obtain the LADO-OFDM signal, $\mathbf{X}_{ADO}$ as,

$$\mathbf{X}_{\mathrm{ADO}} = \mathbf{X}_0 + \frac{1}{2}\mathbf{X}_1, \qquad \text{for all SCs} \tag{4.12}$$

here, when the signals DCO-OFDM and ACO-OFDM are added, ACO-clipping noise can be recompensed, i.e., in eqn. (4.12), $\mathbf{X}_{ADO}$ represents the mutual interference free signal as shown in Fig. 4.4. From the eqn. (4.9), the signal $\mathbf{x}_{ADO}$ is optionally subjected to a pre-distortion function to linearise the signal from a minimum to a maximum optical power to recompense the LED non-linear distortion. Then, we use to add the CP and convert it into P/S first and then D/A next, which results in $x^{'}_{ADO}(t)$. Since the signal $x^{'}_{ADO}(t)$ is bipolar, we need to add an appropriate DC-bias, $\beta_{DC} = \mu\sqrt{E[(x^{'}_{ADO}(t))^2]}$ accordingly in [35] to make the signal $x^{'}_{ADO}(t)$ unipolar, and it can be given as

$$x(t) = \begin{cases} x^{'}_{ADO} + \beta_{DC}, & \text{if } \; x^{'}_{ADO} + \beta_{DC} > 0 \\ 0, & \text{if } \; x^{'}_{ADO} + \beta_{DC} \leq 0 \end{cases} \tag{4.13}$$

here, β_{DC} defined as $10\log_{10}(\mu^2+1)$ dB and μ is a clipping factor. Finally, the signal $x(t)$ is subjected to an LED non-linear model (Model-I or II) to generate $F(x(t))$, which needs to be transmitted over the optical channel.

4.4.2 Receiver Signal Representation

Let the signal $y(t)$ be the received signal corresponding to the transmitted signal $x(t)$ subjected to the non-linear transmitter (LED) after transmitting over the optical

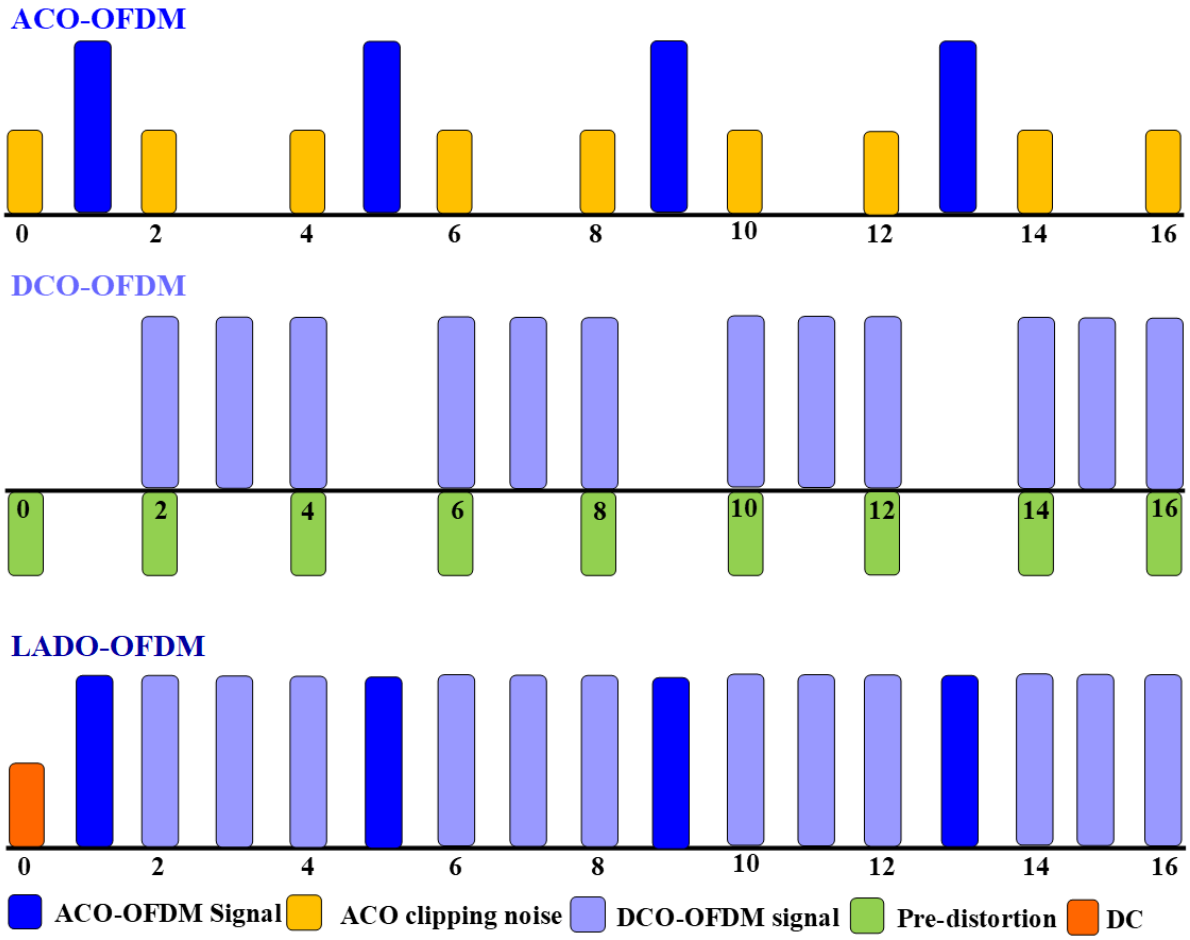

Figure 4.4: Subcarrier structure in LADO-OFDM

channel. By assuming that there is a perfect reception at the photodiode, the received signal $y(t)$ is modelled in [95, 96] as,

$$y(t) = R * h(t) * x(t) + w(t) \tag{4.14}$$

here, R is the photodiode responsivity, which is taken as unity in the simulations.

At the receiver, we assumed a flat channel with AWGN $w(t)$ and perfect equalization to attain $y(t)$. Then, it is passed through ADC, S/P converter and sequentially, generated the signal $\mathbf{y}$ by removing the CP. Next, we subject the signal $\mathbf{y}$ into the FFT block to output the received sub-carriers, $\mathbf{Y}$. Since the mutual interference between DCO-OFDM and ACO-OFDM signals is mitigated, we can directly retrieve both the signals independently from the even and odd sub-carriers of $\mathbf{Y}$ respectively. Then $\mathbf{Y}$ is divided into two sub-carrier sections, i.e., even subcarriers, $\mathbf{Y}_0$, and odd sub-carriers, $\mathbf{Y}_1$. Therefore, the

resultant sub-carrier sets $\mathbf{Y}_0$ and $\mathbf{Y}_1$ are defined as,

$$\mathbf{Y}_0 = \begin{cases} \mathbf{Y}, & \text{for even SCs} \\ 0, & \text{for odd SCs} \end{cases} \tag{4.15}$$

$$\mathbf{Y}_1 = \begin{cases} 0, & \text{for even SCs} \\ \mathbf{Y}, & \text{for odd SCs} \end{cases} \tag{4.16}$$

In the DCO-OFDM demodulation process, $\mathbf{Y}_0$ is directly considered as $\mathbf{Y}_{DCO}$ whereas, in the ACO-OFDM demodulation process, $\mathbf{Y}_1$ is scaled by a factor of two, and then it is considered as $\mathbf{Y}_{ACO}$. The signals, $\mathbf{Y}_{DCO}$ and $\mathbf{Y}_{ACO}$ are given as,

$$\mathbf{Y}_{\text{DCO}} = \mathbf{Y}_0, \qquad \text{for all SCs} \tag{4.17}$$

$$\mathbf{Y}_{\text{ACO}} = 2\mathbf{Y}_1, \qquad \text{for all SCs} \tag{4.18}$$

Then the signals $\mathbf{Y}_{DCO}$ and $\mathbf{Y}_{ACO}$ are converted into P/S to produce $\mathrm{Y}_{DCO}(k)$, $\mathrm{Y}_{ACO}(k)$ signals respectively. Finally, the signals $\mathrm{Y}_{DCO}(k)$ and $\mathrm{Y}_{ACO}(k)$ are subjected to sub-carriers extraction and inverse mapping to produce actual bitstream-I and II.

4.4.3 Computational complexity

Even though the proposed LADO-OFDM signal can mitigate the mutual interference between DCO-OFDM and ACO-OFDM, it can also decrease the receiver latency and slightly increases the transmitter complexity because of pre-distorting the ACO clipped signal in DCO-OFDM generation at the transmitter. However, the computational complexity of the proposed LADO-OFDM and traditional ADO-OFDM signals are examined in terms of CAs and CMs and is tabularized in Table. 4.1. In the traditional ADO-OFDM

Table 4.1: Computational Complexity comparison

	Transmitter		Receiver		Overall	
	CMs	CAs	CMs	CAs	CMs	CAs
ADO-OFDM [1]	$N\log_2 N$	$2N\log_2 N$	$2N\log_2 N$	$4N\log_2 N$	$3N\log_2 N$	$6N\log_2 N$
LADO-OFDM (Proposed)	$\frac{3}{2}N\log_2 N$	$3N\log_2 N$	$\frac{1}{2}N\log_2 N$	$N\log_2 N$	$2N\log_2 N$	$4N\log_2 N$

scheme, the IFFT with N points is performed two times at the transmitter section and

two times at the receiver section. In addition to this, FFT with N points is performed two times at the receiver section. Thus, the computational complexity of the traditional ADO-OFDM scheme with N subcarriers is given in [35] as the overall performed CMs and CAs are $3N\log_2 N$ and $6N\log_2 N$ respectively. However, in the proposed LADO-OFDM scheme, the IFFT with N points is performed two times and the N point FFT is performed only once at the transmitter and receiver sections. Thus, the computational complexity of the proposed LADO-OFDM scheme with N subcarriers is evaluated as the overall performed CMs and CAs are $2N\log_2 N$ and $4N\log_2 N$ respectively. Therefore, the computational complexity of the proposed LADO-OFDM is decreased by 33% when compare to ADO-OFDM in terms of CMs and CAs and it is shown in Fig. 4.5 for a different number of subcarriers.

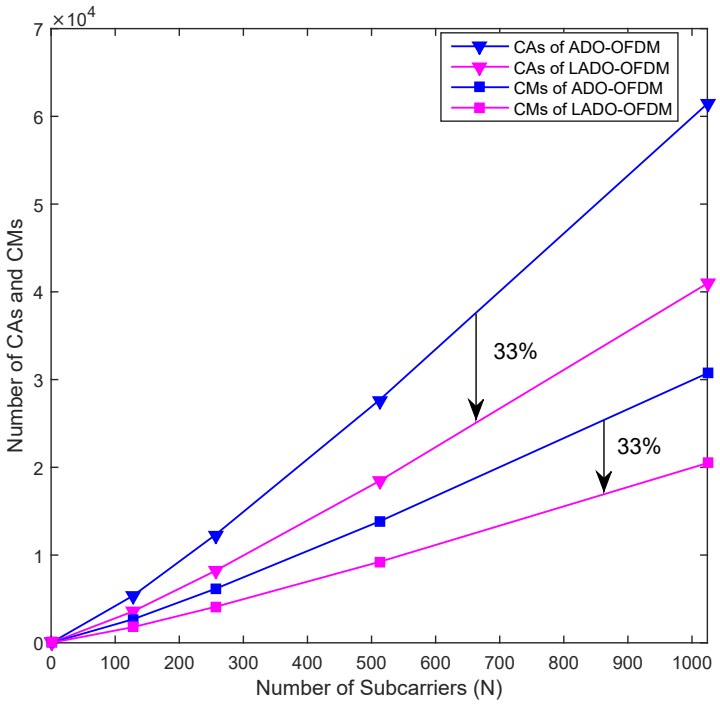

Figure 4.5: Comparision of the computational complexity of LADO-OFDM and ADO-OFDM

Table 4.2: Simmulation Parameters

Parameter	**Specification**
Modulation orders	16-QAM and 64-QAM
Sub-carriers per OFDM symbol	128
Number of OFDM symbols	10^4
Cyclic prefix	10
ADC sampling rate (f_s)	8M symbols per sec
Oversampling factor	1.0
Transmission distance (m)	2.0
Photo diode responsivity	0.8 and 1.0 A/W

Table 4.3: Condition for QAM orders of DCO-OFDM and ACO-OFDM

Case No.	**Condition for QAM orders**
Case-I	$M_{\text{QAM,ACO}} > M_{\text{QAM,DCO}}$
Case-II	$M_{\text{QAM,ACO}} = M_{\text{QAM,DCO}}$
Case-III	$M_{\text{QAM,ACO}} < M_{\text{QAM,DCO}}$

4.5 Results and Discussion

In the results section, we presented the simulation results of the proposed LADO-OFDM system under the optical wireless channel. The simulation results are obtained employing Monte Carlo bit-error-rate (BER) simulations. The key thing that impacts the performance of any signal under the VLC system could be the nonlinearity of the front-end LED transmitter. To analyse the LADO-OFDM along with the standard ADO-OFDM scheme that is used for comparative study, two simplified LED nonlinear models presented in section 4.2 are used. Thus, we considered the equivalent simulation parameters for LADO-OFDM and ADO-OFDM for a good comparison. The simulation parameters are tabulated in Table 4.2 and the conditions for QAM orders of three different cases are tabulated in Table 4.3. The IQ sampling rate nothing but the ADC sampling rate, was set at 8 million symbols per second. In real-time scenarios, this rate might be lower due to the LED's limited modulation bandwidth. Additionally, the oversampling factor is

considered as one, and in practical situations, it could be higher.

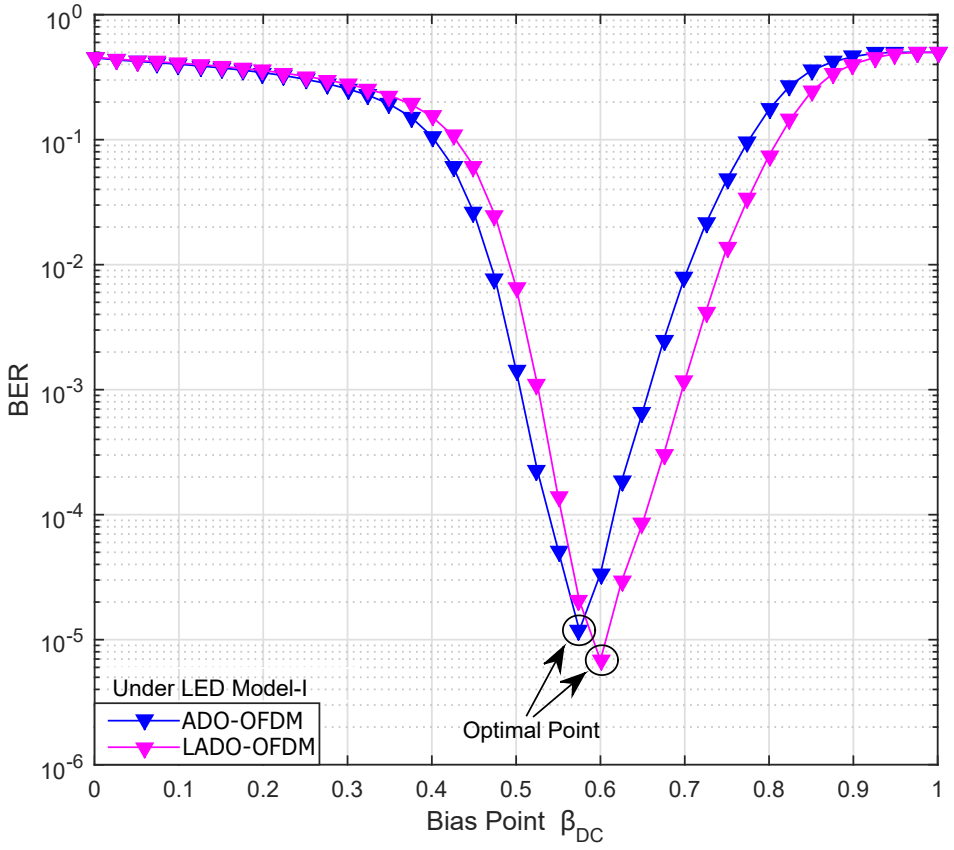

Figure 4.6: BER performance of the proposed LADO-OFDM and ADO-OFDM with respect to bias point under LED nonlinear clipping using QAM orders $M_{\text{QAM,ACO}} = M_{\text{QAM,DCO}} = 16$ with a fixed $SNR = 28dB$.

4.5.1 Simulation Results

Under LED Model-I

Imposed an LED nonlinearity over the proposed LADO-OFDM and traditional ADO-OFDM signals with piecewise polynomial function (4.1), which is linearised by pre-distorting with the inverse polynomial function. The signal under examination needs to be controlled in terms of an optimum biasing level to achieve better performance by eliminating the clipping distortion caused by LED nonlinearity. However, it is key thing to find a minimal bias point to limit the nonlinear clipping distortion. Therefore, for the

proposed LADO-OFDM and conventional ADO-OFDM signals under LED model-I, the Mount-Carlo simulations have been performed using modulation order of 16-QAM over the DC bias-point at an SNR of $28dB$ and are shown in Fig. 4.6. The BER performance of the proposed LADO-OFDM and conventional ADO-OFDM signals under three distinct cases are simulated and are shown in Fig. 4.7, 4.9, 4.10. From the depicted Fig. 4.6, it can be observed that the optimal bias point of conventional and proposed signals are giving the optimal BER performance at DC-bias of $0.575V$ and $0.600V$ respectively. Thus, the lower clipping noise degraded the BER performance below the optimal bias point and the upper clipping noise degraded the BER performance above the optimal bias point in both signals as shown in Fig. 4.6. It is also observed that the optimal bias point of the proposed one is shifted from $0.575V$ to $0.600V$ in comparison with the conventional one, which can increase the intensity level of an LED. At the optimal bias point $0.6V$, the proposed LADO-OFDM outperforms the ADO-OFDM in terms of BER as shown in Fig. 4.6. As per the procedure shown in Fig. 4.6, we found the optimal bias points of the LADO-OFDM for different combinations of QAM orders considered in three cases and is tabularized in Table 4.4.

Table 4.4: Bias point of LADO-OFDM and ADO-OFDM under different cases

Case No.	$M_{\mathbf{QAM,ACO}}$	$M_{\mathbf{QAM,DCO}}$	**Bias Point**
Case-II	16	16	0.60V
Case-I	64	16	0.65V
Case-III	16	64	0.65V
Case-II	64	64	0.70V

From the depicted Fig. 4.7, the BER performance of the LADO-OFDM outperforms the traditional ADO-OFDM under nonlinear clipping distortion introduced by the LED model-I in case-I with a bias point of 0.65V for 128 subcarriers. The proposed LADO-OFDM obtained a considerable $BER = 10^{-3}$ at an SNR of $27dB$, and $26dB$ with nonlinear clipping distortion and pre-distortion respectively, whereas ADO-OFDM obtained at an SNR of $31dB$, $29dB$. BER performance gains $4dB$ and $3dB$ power due to recompensed ACO clipping noise on even subcarriers in LADO-OFDM compares to ADO-OFDM with nonlinear clipping distortion and pre-distortion respectively. Since the

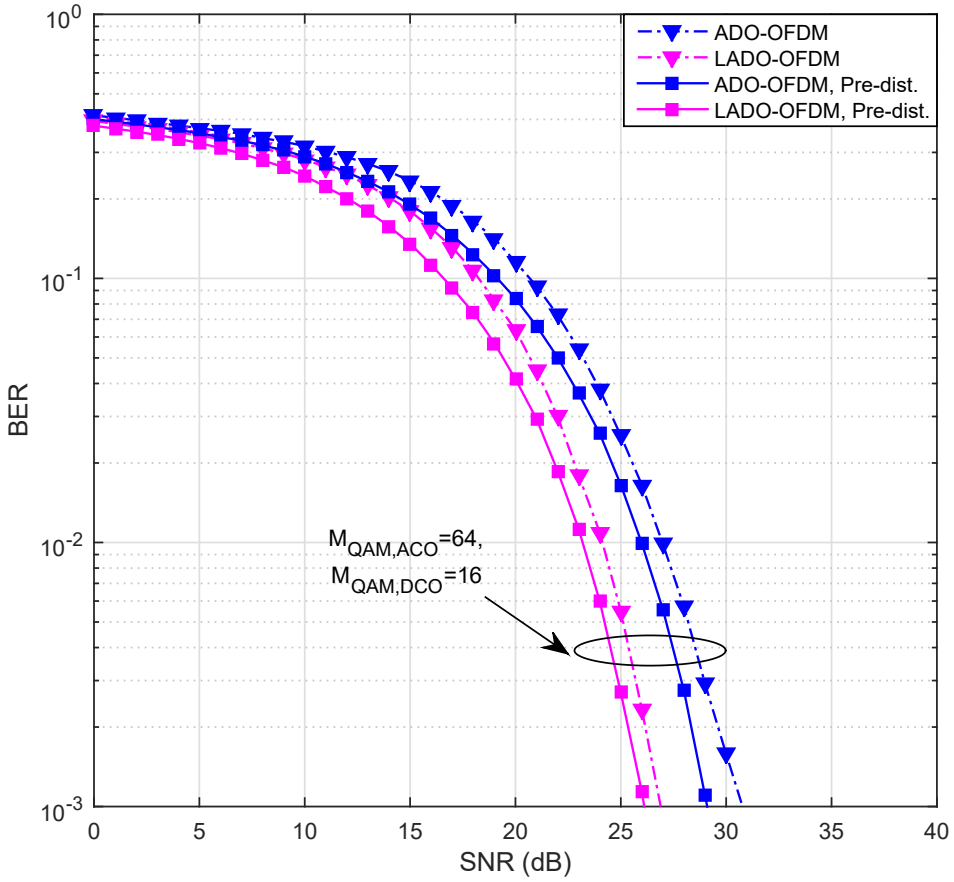

Figure 4.7: BER performance of LADO-OFDM and ADO-OFDM under LED model-I in case-I with 128 subcarriers.

QAM order condition is taken as case-I, the lower QAM order symbols are assigned to DCO-OFDM which results in a higher Euclidian distance among the QAM symbols compares to higher QAM order symbols which are assigned to ACO-OFDM. Thus, the BER performance of LADO-OFDM gains only $1dB$ power with pre-distortion compared to nonlinear clipping distortion introduced by the LED model-I. Thus, the nonlinear clipping noise slightly affects the BER performance of LADO-OFDM in case-I.

From the depicted Fig. 4.8, the BER performance of the LADO-OFDM outperforms the traditional ADO-OFDM under nonlinear clipping distortion introduced by the LED model-I in case-I with a bias point of 0.65V for 128 subcarriers with the photodiode responsivities 1.0 A/W and 0.8 A/W respectively. However, The BER performance of both systems is degraded by decreasing the photodiode responsivity. With the photodiode

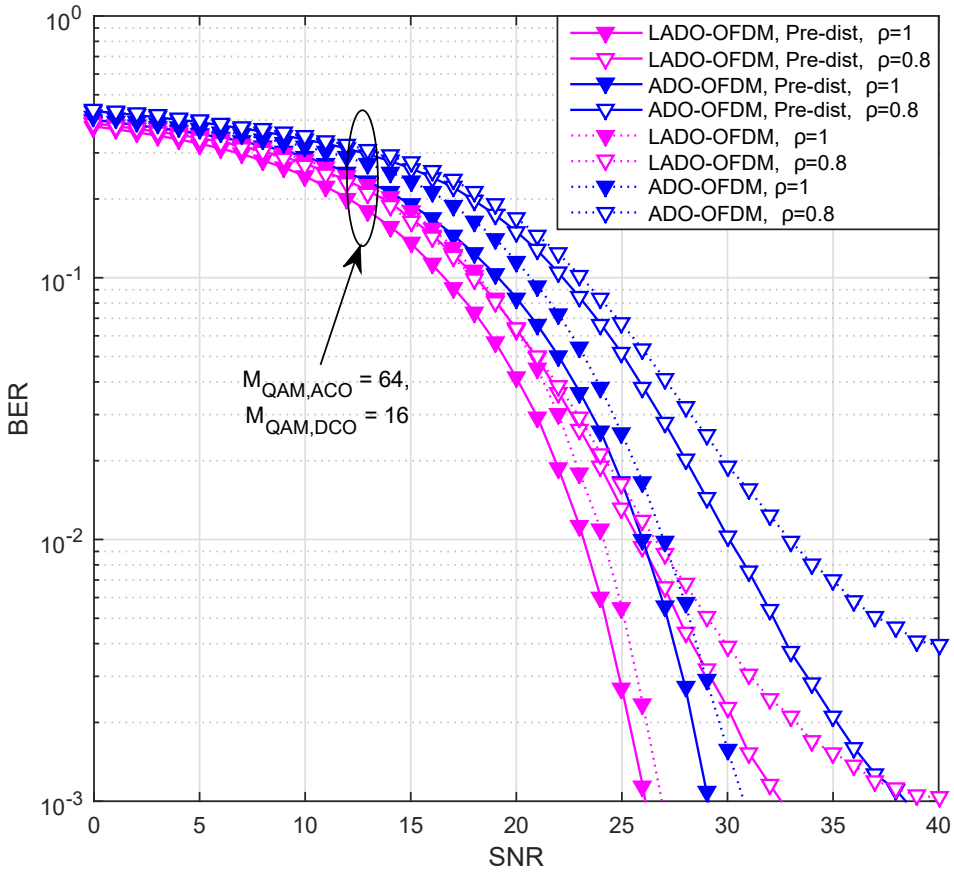

Figure 4.8: BER performance of LADO-OFDM and ADO-OFDM under LED model-I in case-I with 128 subcarriers for different photodiode responsivities (i.e., 0.8 and 1.0 A/W).

responsivity of 0.8 A/W, the proposed LADO-OFDM obtained a required $BER = 10^{-3}$ at an SNR of 40.0 dB, 32.5 dB with nonlinear clipping distortion and pre-distortion respectively, whereas ADO-OFDM obtained at an SNR of 38dB with pre-distortion, and did not obtain the required BER under nonlinear clipping distortion. therefore, the BER performance gains huge power due to recompensed ACO clipping noise on even subcarriers in LADO-OFDM compares to ADO-OFDM. From the results, it is observed that the BER performance degraded as the photodiode responsivity decreased from 1.0 A/W to 0.8 A/W under nonlinear clipping distortion as well as pre-distortion.

From the illustrated Fig. 4.9, LADO-OFDM under LED model-I outperforms the ADO-OFDM in terms of BER in case-II with a bias point of 0.60V for 16QAM and 0.70V for 64QAM using 128 subcarriers. The proposed LADO-OFDM with 16QAM achieved a considerable $BER = 10^{-3}$ at an SNR of $26.5dB$, and $24.5dB$ with a clipping distortion and

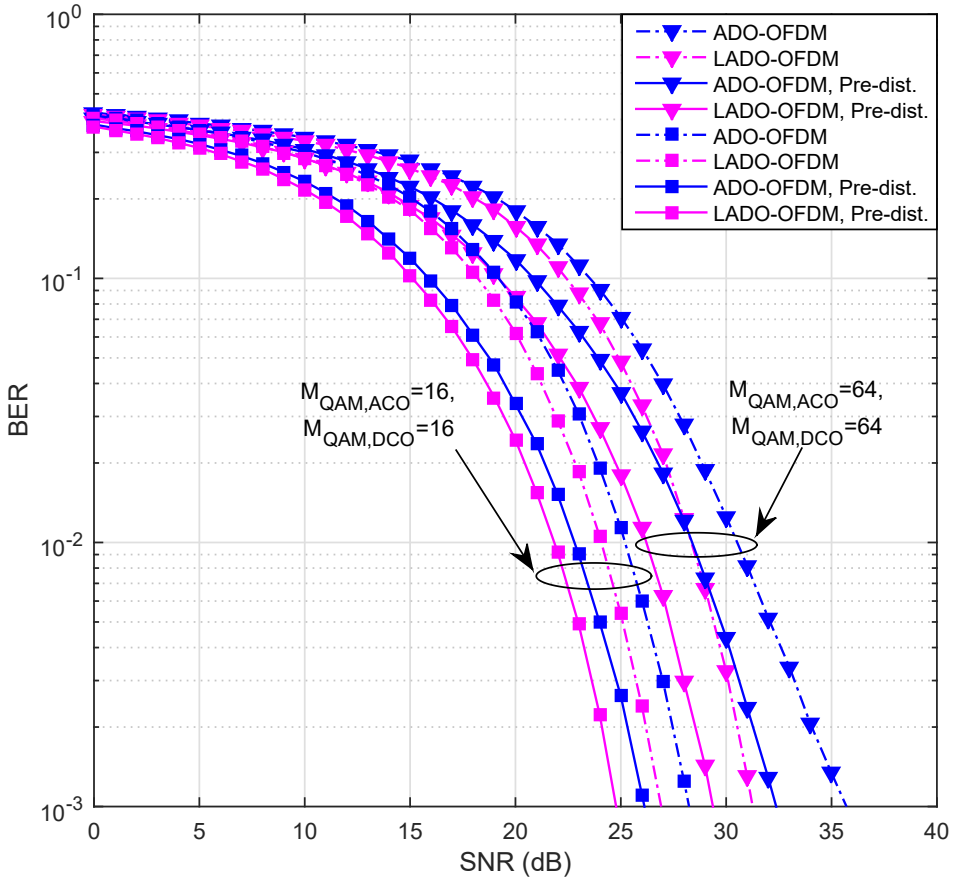

Figure 4.9: BER performance of LADO-OFDM and ADO-OFDM under LED model-I in case-II with 128 subcarriers.

pre-distortion respectively, whereas ADO-OFDM obtained at an SNR of 28.0dB, 26.0dB. Thus, the BER performance gains 1.5dB, 1.5dB power due to recompensed ACO clipping noise over the even subcarriers in LADO-OFDM compares to ADO-OFDM. However, LADO-OFDM with 64QAM attained a substantial $BER = 10^{-3}$ at an SNR of 31.5dB, 29.5dB with an LED nonlinear distortion and pre-distortion individually, whereas ADO-OFDM achieved at an SNR of 35.5dB, 32.5dB. Thus, the BER performance gains 4.0dB, 3.0dB power in LADO-OFDM compared to ADO-OFDM. Since the QAM order condition is taken as case-II, the BER performance of LADO-OFDM gains 2dB power with pre-distortion compares to nonlinear clipping distortion induced by the LED model-I. Thus, the nonlinear clipping noise moderately affects the BER performance of LADO-OFDM in case II compares to case-I.

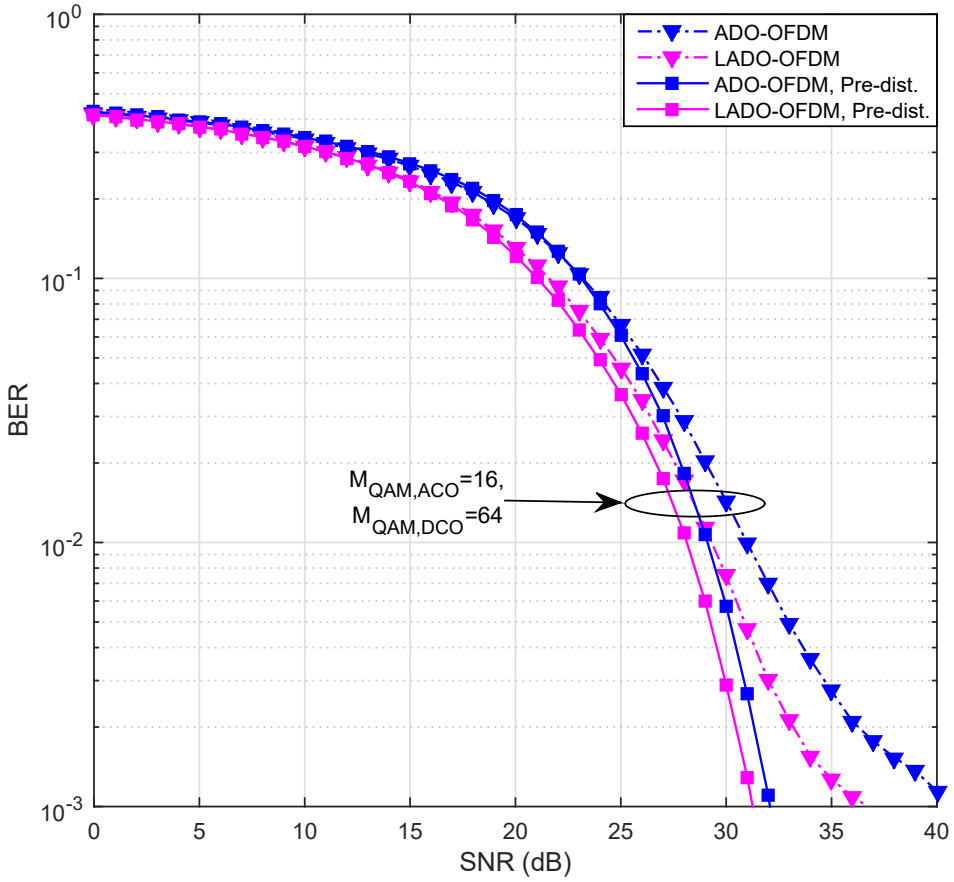

Figure 4.10: BER performance of LADO-OFDM and ADO-OFDM under LED model-I in case-III with 128 subcarriers.

From the portrayed Fig. 4.10, the new LADO-OFDM under LED model-I outperforms the ADO-OFDM in terms of BER in case-III with a bias point of 0.65V using 128 subcarriers. The proposed LADO-OFDM achieved a considerable $BER = 10^{-3}$ at an SNR of 37.0dB, and 31.0dB with a clipping distortion and pre-distortion respectively, whereas ADO-OFDM obtained at an SNR of 41.0dB, 32.0dB. Thus, the BER performance gains 4.0dB, 1.0dB power due to recompensed ACO clipping noise over the even subcarriers in LADO-OFDM compares to ADO-OFDM. Since the QAM order condition is taken as case-III, the BER performance of LADO-OFDM gains 6dB power with pre-distortion compares to nonlinear clipping distortion introduced by the LED model-I in case-III. Thus, the nonlinear clipping noise highly affects the BER performance of LADO-OFDM in case III when compare to case-I and II. Among the three cases, case-I outperforms case II and III in terms of BER in both the signals under LED model-I. However, the proposed

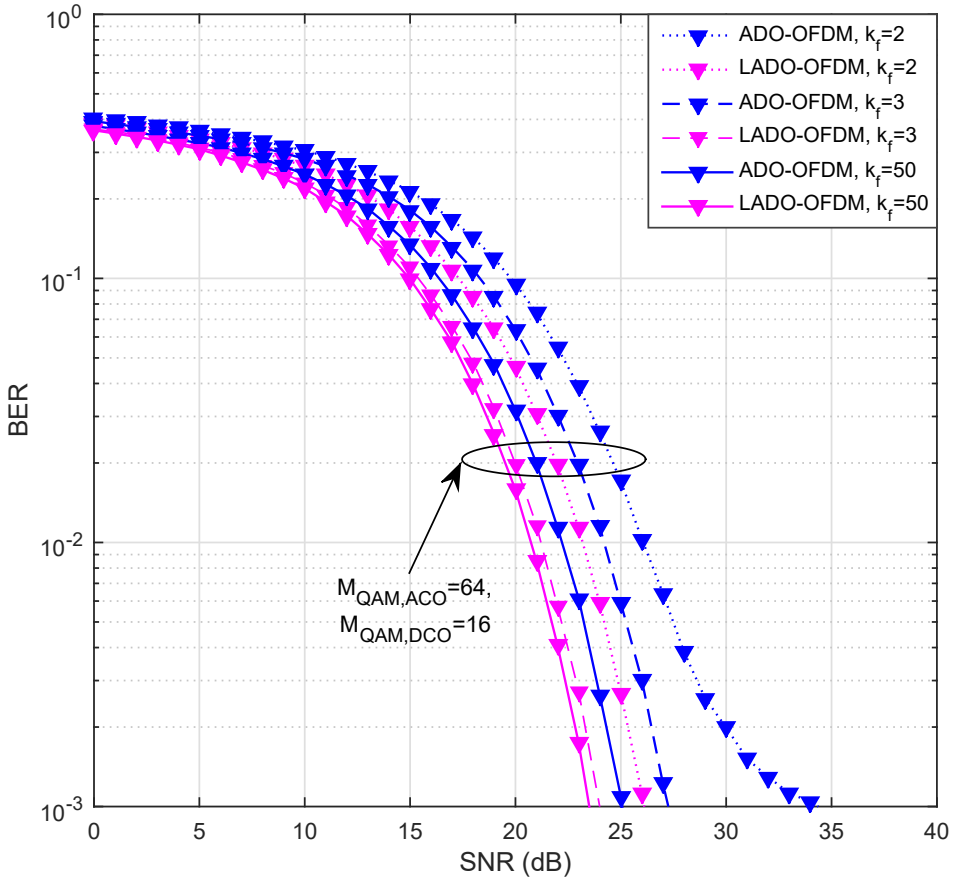

Figure 4.11: BER performance of LADO-OFDM and ADO-OFDM under LED model-II in case-I with 128 subcarriers.

LADO-OFDM outperforms the traditional ADO-OFDM in terms of BER.

Under LED Model-II

Integrated a signal paradigm k_f to smooth clip the upper peaks of the signal by imposing the LED nonlinearity over the proposed LADO-OFDM, ADO-OFDM and PAM-DMT with an LED model-II rather than utilizing a separate nonlinear polynomial function. The soft clipping which is used in this model has enhanced the BER performance by linearizing the nonlinear effect by conditioning the knee factor, k_f. This LED model appropriately incorporates distinct paradigms like maximum acceptable alternative current, a suitable extent of upper clipping level and bias point. Therefore, for the proposed LADO-OFDM, ADO-OFDM and PAM-DMT signals under LED model-II, the Mount-

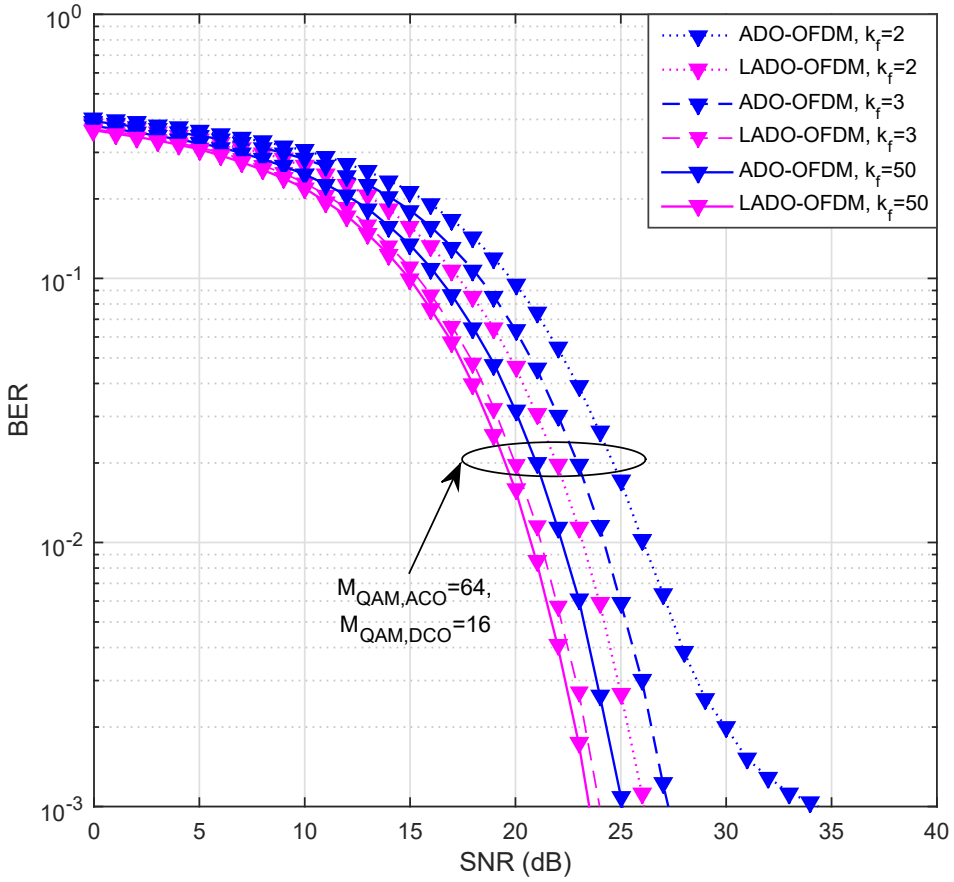

Figure 4.12: BER performance of LADO-OFDM and ADO-OFDM under LED model-II in case-I with 128 subcarriers.

Carlo simulations have been performed to distinguish the feasible BER performance of an LED so that the LED selection process becomes easier in real-time. Therefore, we considered an LED as given in [13] and biased at $\beta_{DC} = 0.6V$ with a maximum allowable AC $i_{\mathrm{D,max}} = 0.5A$ and the normalized resistance $R = 1\Omega$ with an optimal slope characteristic $f(v_{\mathrm{D,in}}) = v_{\mathrm{D,in}}/R$. The BER performance of the proposed LADO-OFDM and ADO-OFDM signals under three distinct cases I, II and III and also LADO-OFDM and PAM-DMT signals under case II are simulated by varying the knee factor and are shown in Fig. 4.11, 4.13, 4.14 and 4.15.

From the depicted Fig. 4.12, the new LADO-OFDM under LED model-II outperforms the ADO-OFDM in terms of BER in case-I with a bias point of 0.6V using 128 subcarriers by varying the knee factor. The proposed LADO-OFDM achieved a consider-

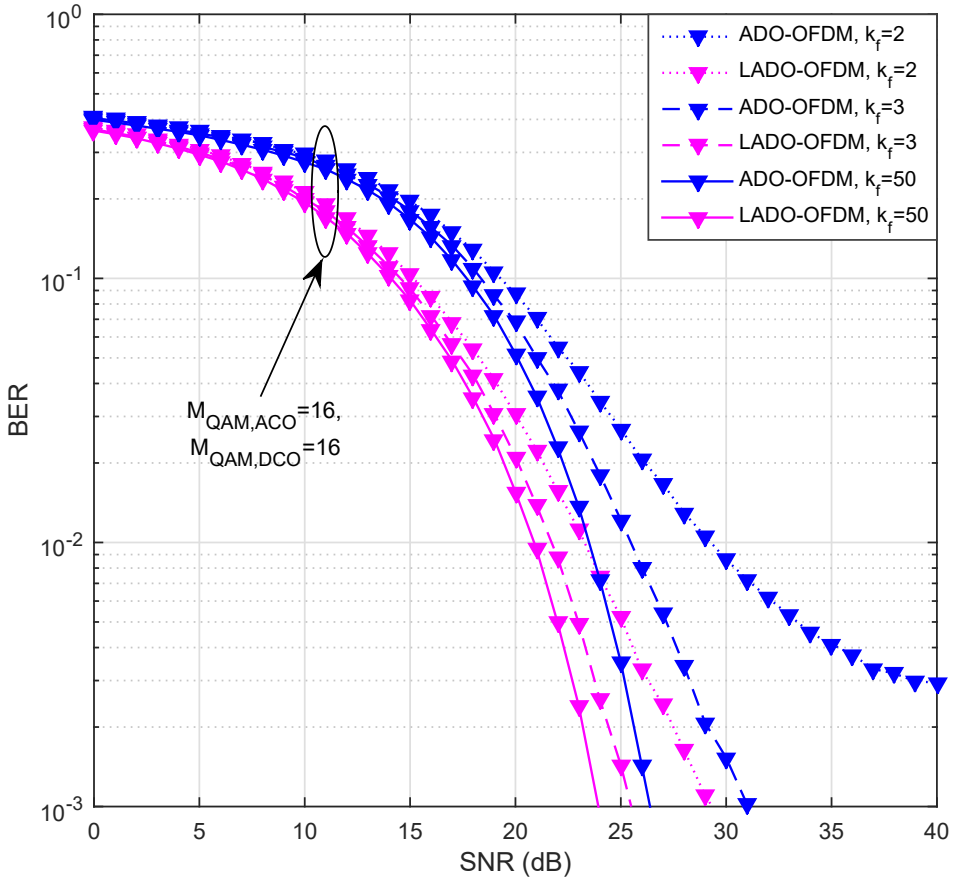

Figure 4.13: BER performance of LADO-OFDM and ADO-OFDM under LED model-II in case-II with 128 subcarriers.

able $BER = 10^{-3}$ at an SNR of $26.0dB$, $24.0dB$ and $23.5dB$ with knee factors of 2, 3 and 50 respectively, whereas ADO-OFDM obtained at an SNR of $34.0dB$, $27.0dB$ and $25.0dB$ with knee factor of 2, 3 and 50 respectively. Thus, the BER performance gains $8.0dB$, $4.0dB$ and $1.5dB$ power due to recompensed ACO clipping noise over the even subcarriers in LADO-OFDM compares to ADO-OFDM. Thus, the LED nonlinear distortion highly impacts the BER performance at $k_f = 2$ in both signals. However, this nonlinear distortion impact is very low at $k_f = 50$ which is nothing but the nonlinear characteristics of LED can be linearized at a higher knee factor, $k_f > 50$.

From the portrayed Fig. 4.13, 4.15 the LADO-OFDM under LED model-II outperforms the ADO-OFDM in terms of BER in case-II and case-III with a bias point of 0.6V using 128 subcarriers by varying the knee factor. Thus, the LED nonlinear effect can be

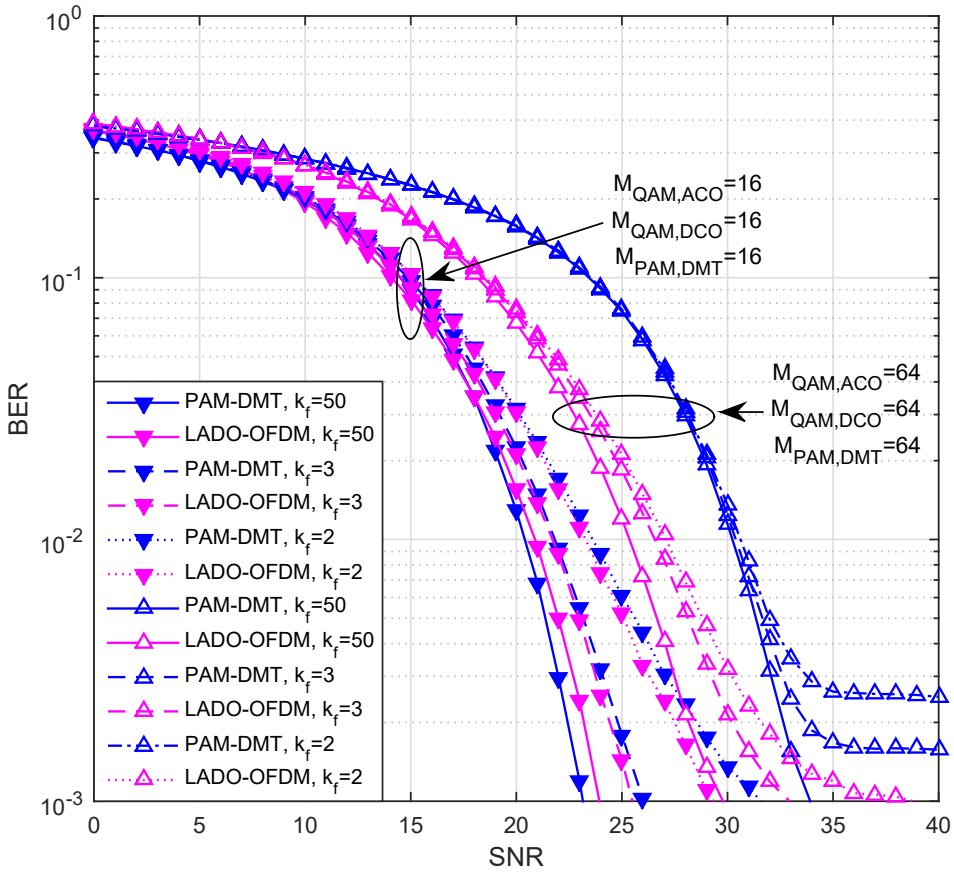

Figure 4.14: BER performance of LADO-OFDM and PAM-DMT under LED model-II in case-II with 128 subcarriers.

present at the lower values of k_f and it can be eliminated by increasing the knee factor, k_f.

From the depicted Fig. 4.14, we observed that the BER performance of the proposed LADO-OFDM outperformed the PAM-DMT performance with the increase in the nonlinear effect of the LED which will be present in the real-time scenario. It is also observed that the BER performance of the proposed LADO-OFDM is slightly low at the lower QAM orders whereas a good performance can be found at the higher QAM orders when compared to PAM-DMT. Therefore, the proposed LADO-OFDM is more suitable for higher QAM orders compared to PAM-DMT.

From the Fig. 4.12, 4.13, 4.14 and 4.15, we observed that the knee factor k_f does not affect the BER performance considerably at lower SNR, which is nothing but the

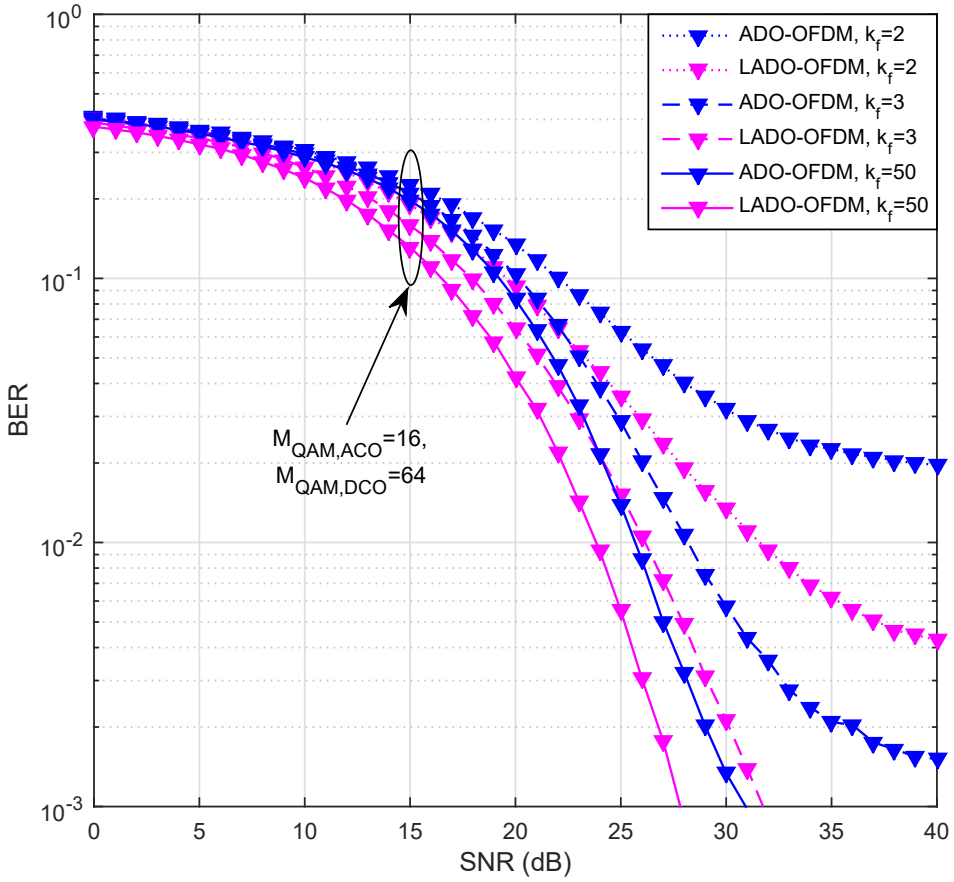

Figure 4.15: BER performance of LADO-OFDM and ADO-OFDM under LED model-II in case-III with 128 subcarriers.

upper clipping peaks are very less at lower signal power. However, increasing the signal power results in affecting the BER performance considerably at lower k_f values. Among these three cases, case-I outperforms case-II and III in terms of BER in both the signals under LED model II. However, the proposed LADO-OFDM outperforms the traditional ADO-OFDM in terms of BER.

4.6 Summary

In this chapter, a new modulation technique called LADO-OFDM for VLC systems to meet the specifications of 5G networks, including low computing complexity and latency. The main objective of the LADO-OFDM scheme is to address the issue of

mutual interference between two existing modulation techniques used in VLC systems, namely, DCO-OFDM and ACO-OFDM. By employing a pre-distortion technique, the LADO-OFDM scheme aims to mitigate this mutual interference. One advantage of the LADO-OFDM scheme is that it enables parallel demodulation processes for DCO-OFDM and ACO-OFDM at the receiver side, eliminating the need for sequential processing as required in ADO-OFDM. This parallel demodulation approach reduces computing complexity and latency compared to ADO-OFDM.

The chapter also investigated the performance of the proposed LADO-OFDM scheme under two generalized LED (Light Emitting Diode) models. Specifically, the study examines the effects of nonlinear clipping distortion on the LED's dynamic range and bias point. It is observed that a larger dynamic range of LEDs leads to better performance. To achieve a linearized LED dynamic range, the transmitted signal is pre-distorted using a piecewise polynomial model or by increasing the knee factor in Rapp's model. Monte-Carlo simulations are conducted to evaluate the Bit Error Rate (BER) performance of the LADO-OFDM scheme compared to ADO-OFDM and PAM-DMT schemes under the effect of LED nonlinearity. The results show that the proposed LADO-OFDM scheme outperformed the traditional ADO-OFDM and PAM-DMT schemes in terms of BER, computing complexity, and latency in the presence of LED nonlinearity.

Chapter 5

Variably Biased Asymmetrically Clipped Optical OFDM for VLC Systems

5.1 Introduction

In the context of Visible Light Communications (VLC), a new waveform called LADO-OFDM has been initiated in the previous chapter, by pre-distorting with the asymmetrically clipping noise to eliminate the mutual interference. Moreover, the LADO-OFDM enables parallel demodulation processes for DCO-OFDM and ACO-OFDM at the receiver side by eliminating the need for sequential processing as required in ADO-OFDM. This parallel demodulation approach reduces CC compared to ADO-OFDM. However, in both modulation schemes, a constant high DC bias has been used to attain the unipolar signal, which can decrease the PE. Therefore, a new bias design is required to address the PE problems.

In this chapter, a novel modulation scheme called Variably-biased Asymmetrically-clipped Optical-OFDM (VAO-OFDM) with pre-distortion for Visible Light Communication systems is conceived to improve PE. In VAO-OFDM, ACO-OFDM is modulated on the upper layer and a new modulation called variably Biased Optical-OFDM (VBO-OFDM) is performed on the lower layer to improve PE. Apart from this, the VBO-OFDM is also proposed and utilized in the VAO-OFDM to improve PE. In ADO-OFDM, a constant high DC bias has been used which is not required for all the samples whereas, in the VAO-OFDM, a variably bias is designed based on the set of specific samples of the Time

Domain (TD) signal. However, variably bias does not impose any interference on the originally transmitted symbols due to its frequency components falling on the pre-defined subcarriers. Due to the pre-distortion process, the CC of the VAO-OFDM is decreased significantly compares to ADO-OFDM. The simulation results show that the VAO-OFDM outperforms the ADO-OFM in terms of PE. Further, the VAO-OFDM is also validated on the experimental Testbed with LabView software and the Universal Software-defined Radio Pheriparals (USRPs).

The rest of this chapter is structured as follows for the remaining sections: The system model is explained in Section 5.2, and simulation and experiment outcomes are discussed in Section 5.3. Last but not least, section 5.4 provides the summary.

5.2 VAO-OFDM System Model

In this section, we described the VAO-OFDM with pre-distortion, which consists of two layered modulation processes as done in ADO-OFDM [1].

5.2.1 Transmitter

In traditional ADO-OFDM [35], the ACO-OFDM modulation is performed on upper layer whereas the DCO-OFDM was performed on lower layer with a constant DC-bias. However, in the proposed VAO-OFDM modulation scheme, upper layer functions as similar to the ACO-OFDM in ADO-OFDM, and a variably bias-based (VB) optical OFDM (VBO-OFDM) modulation can be performed on lower layer as shown in Fig.5.1. Apart from this, the VBO-OFDM scheme is also proposed in this chapter to improve the PE using the variable bias unlike the constant DC-bias in the DCO-OFDM.

Let $\mathbf{S} = \{S_0, S_1, S_2, ..., S_{3M/8\,-1}\} \in \mathbb{C}^{\left(\frac{3M}{8}\right)\times 1}$ be a QAM symbol vector obtained from the input bitstream based on the required QAM order [97], while M denotes the number of subcarriers in a single OFDM symbol, and $\mathbb{C}$ represents the set of complex numbers. To obtain the required subcarrier structure, the QAM symbols need to be framed in a specific arrangement denoted as $\mathbf{Q} = \{Q_0, Q_1, Q_2, ..., S_{M/2-2}\} \in \mathbb{C}^{\left(\frac{M}{2}-1\right)\times 1}$, and defined

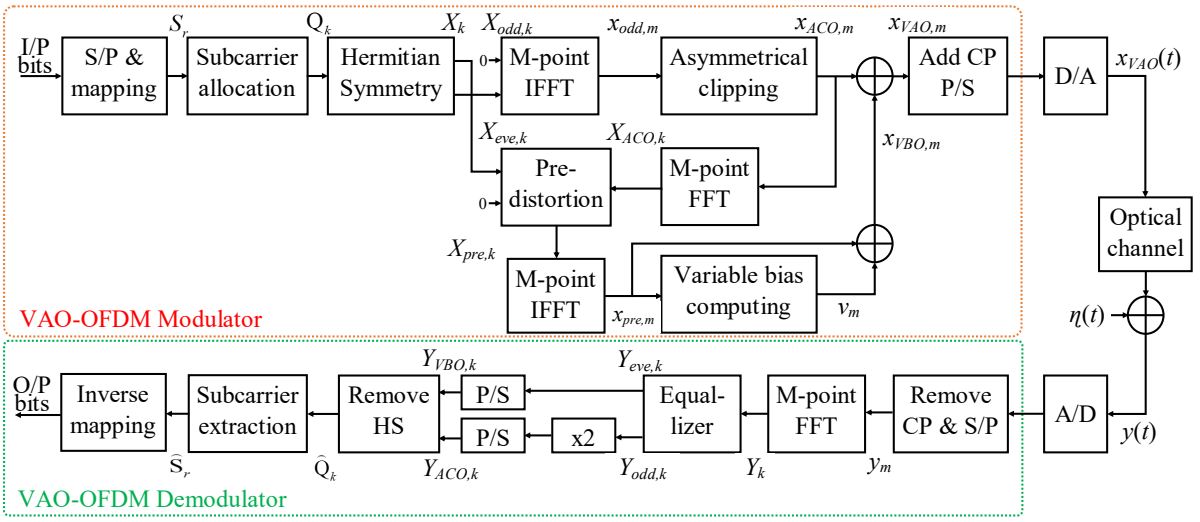

Figure 5.1: Block diagram of VAO-OFDM scheme

as,

$$Q_r = \begin{cases} S_{r-\lfloor \frac{r}{4} \rfloor}, \ r = 2(2\ell+2)+\eta, \ \ell = 0,1,2,...,\frac{M}{8}-1 \\ \\ 0, \qquad r = 2(2\mu+1)+1, \ \mu = 0,1,2,...,\frac{M}{8}-2 \end{cases} \tag{5.1}$$

where, $\eta = 0, 1, 2$. For these optical OFDM systems, to ensure the real signal in TD, we imposed HS on frequency domain (FD) signal, and it can be defined as

$$X_k = \begin{cases} 0, & k = 0, \frac{M}{2} \\ \\ Q_\Gamma, & k = \Gamma+1 \\ \\ Q^*_{\frac{M}{2}-(\Gamma+2)}, & k = \frac{M}{2}+\Gamma+1 \end{cases} \tag{5.2}$$

where, $\Gamma = 0, 1, 2, ..., \frac{M}{2}-2$. To assign the layered wise QAM symbols to the VAO-OFDM modulation scheme, the QAM symbols vector $\mathbf{X}$ shown in Fig. 5.2 (a) is divided into the even components $X_{eve,k}$ and the odd components $X_{odd,k}$. Further, the odd components in $X_{eve,k}$ and the even components in $X_{odd,k}$ are fixed to zero such that the HS can not be affected, where the resulted QAM symbol vector $X_{odd,k}$ is input to the upper layer for ACO-OFDM and $X_{eve,k}$ is input to the lower layer for VBO-OFDM are shown in Fig. 5.2 (b) and Fig. 5.2 (c) respectively.

In the first layer, ACO-OFDM is performed with $X_{odd,k}$ signal, which results in

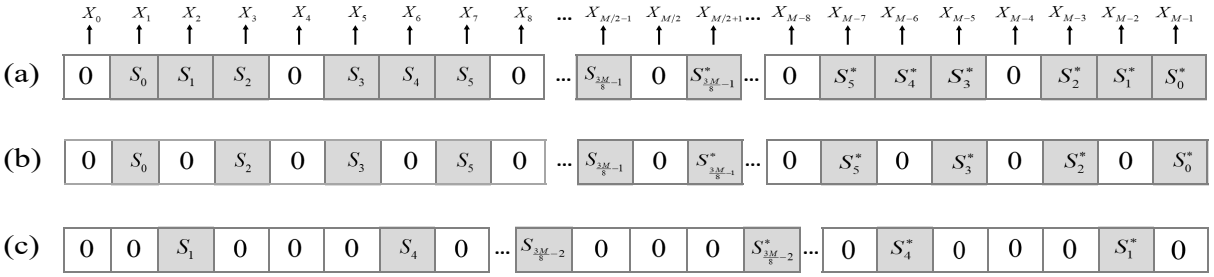

Figure 5.2: Frequency-domain demonstration of the proposed VAO-OFDM: (a) Actual QAM symbol vector $\mathbf{X}$, (b) input symbol vector $X_{odd,k}$ to the ACO-OFDM, (c) input symbol vector $X_{eve,k}$ to the VBO-OFDM.

$x_{odd,m}$, and it is given in [1] as,

$$x_{odd,m} = \frac{1}{M}\sum_{k=0}^{M-1} X_{odd,k} \exp\left(\frac{j2\pi km}{M}\right), m = 0, 1, ..., M-1 \tag{5.3}$$

where, $x_{odd,m}$ follows a half-wave symmetry as $x_{odd,m} = -x_{odd,m+M/2}$ for $0 < m < M/2$. Therefore, without any loss of information, the negative part can be clipped to guaranty the positivity of the signal. The asymmetrically clipping (AC) operation is given in [89] as,

$$\lfloor x_{odd,m} \rfloor_{clip} = \begin{cases} x_{odd,m}, & x_{odd,m} > 0 \\ 0, & x_{odd,m} < 0 \end{cases}, \tag{5.4}$$

where $\lfloor . \rfloor_{clip}$ represents the zero clipping operator. Therefore, the ACO-OFDM TD signal, $x_{ACO,m}$ can be expressed as,

$$x_{ACO,m} = \lfloor x_{odd,m} \rfloor_{clip} \tag{5.5}$$

However, amplitude of resultant ACO-OFDM TD signal $x_{ACO,m}$ is reduced by a factor of two due to asymmetrical clipping noise and it can be added to even subcarriers [89]. Then the ACO-OFDM signal $x_{ACO,m}$ can be represented as [1],

$$x_{ACO,m} = \frac{1}{2} x_{odd,m} + \lambda_{odd,m} \tag{5.6}$$

where $\lambda_{odd,m}$ represents the asymmetrical clipping noise, and its FD signal can occupy even subcarriers whereas signal $x_{odd,m}$ occupy the odd ones only [89]. Further, ACO-OFDM signal can be converted into the FD signal such that it can be used in the clipping noise-obtaining process, which can be used in the pre-distortion process of lower layer

modulation. Thus the resultant FD signal is represented in [1] as,

$$X_{ACO,k} = \overbrace{\frac{1}{2}X_{odd,k}}^{\text{odd subcarriers}} + \overbrace{\Lambda_{odd,k}}^{\text{even subcarriers}} \tag{5.7}$$

here $\frac{1}{2}X_{odd,k}$ is ACO-OFDM signal over odd subcarriers and $\Lambda_{odd,k}$ is clipping noise over even subcarriers, and they can also redefined as,

$$\frac{1}{2}X_{odd,k} = \begin{cases} 0, & k = 2b \\ X_{ACO,k}, & k = 2b+1 \end{cases} \tag{5.8}$$

and,

$$\Lambda_{odd,k} = \begin{cases} X_{ACO,k}, & k = 2b \\ 0, & k = 2b+1 \end{cases} \tag{5.9}$$

where $b = 0, 1, 2, ..., \frac{M}{2} - 1$. However, the second layer is modulated with the new modulation called VBO-OFDM where the bias depends on the specific sample amplitudes unlike the DCO-OFDM in traditional ADO-OFDM system which is fixed bias for all the samples [1]. Therefore, the VBO-OFDM signal can be generated by pre-distorting FD signal $X_{eve,k}$ with the $X_{ACO,k}$ signals where the clipping noise of $X_{ACO,k}$ is subtracted from the $X_{eve,k}$ over even subcarriers only, and the signals over odd subcarriers remains same. Therefore, the pre-distorted signal $X_{pre,k}$ which is a noise-free signal, and it is defined as,

$$X_{pre,k} = \begin{cases} X_{eve,k} - X_{ACO,k}, & k = 2b \\ X_{eve,k}, & k = 2b+1 \end{cases} \tag{5.10}$$

Further, one can employ an IFFT operator to perform the OFDM modulation on $X_{pre,k}$ signal to obtain the TD signal $x_{pre,m}$, and it can be expressed as,

$$x_{pre,m} = \frac{1}{M}\sum_{k=0}^{M-1} X_{pre,k} \exp\left(\frac{j2\pi km}{M}\right), m = 0, 1, ..., M-1 \tag{5.11}$$

here, $x_{pre,m}$ represents the TD version of the signal $X_{pre,k}$, and it is a bipolar signal which cannot be transmitted through the LED directly due to nonlinear clipping distortion. Therefore, to transmit through the LED, the signal must be unipolar such that the signal can not be affected by the LED nonlinear effect. To obtain the unipolar and non-negative signal, we employed a variably bias which depends on the amplitudes of the specific samples of the signal $x_{pre,m}$, unlike the constant DC-bias for all the samples.

Algorithm 1 Variably-bias Computing Algorithm

Input: TD signal $x_{pre,m}$, for $m = 0, 1, 2, ..., M-1$

Output: variably-bias signal v_m, for $m = 0, 1, 2, ..., M-1$

Initialization: $a_m = \{0\}_{m=0}^{\frac{M}{4}-1}$, for M subcarriers

procedure

    find the minimum value of four specific samples $x_{pre,m}$, $x_{pre,m+\frac{M}{4}}$, $x_{pre,m+\frac{M}{2}}$, and $x_{pre,m+\frac{3M}{4}}$ of the signal $x_{pre,m}$

    for $m = 0$ to $\frac{M}{4} - 1$ **do**

        $a_m = \min\left\{x_{pre,m}, x_{pre,m+\frac{M}{4}}, x_{pre,m+\frac{M}{2}}, x_{pre,m+\frac{3M}{4}}\right\}$

    end for

    for $m = 0$ to $\frac{M}{4} - 1$ **do**

        $a_m \leftarrow -a_m$

    end for

    for $l = 0$ to 3 **do**

        for $m = 0$ to $\frac{M}{4} - 1$ **do**

            $v_{m+\frac{lM}{4}} = a_m$

        end for

    end for

end procedure

However, a poorly designed bias might interfere with the originally transmitted signal which can decrease the system performence. To address this issue, we first propose Theorem 1 as follows:

Theorem-1: The fast Fourier transform (FFT) of a discrete sequence v_m occupies only the $4p$-th ($p = 0, 1, ..., M/8 - 1$) located subcarriers if the structure of v_m is designed as

$$v_m = v_{m+\frac{M}{4}} = v_{m+\frac{M}{2}} = v_{m+\frac{3M}{4}}, m = 0, 1, ..., M/4 - 1 \tag{5.12}$$

Proof: Kindly refer the Appendix.

According to Theorem 1, when the proposed variably bias satisfies (5.12), the interference caused by the variably bias is imposed on just the $4p$-*th* positioned subcarriers, which are orthogonal to the information data symbols in the corresponding modulation

scheme. Therefore, to induce interference into the reserved subcarriers that do not carry significant data symbols, we propose to add the same variably bias for the four samples $\left\{x_{pre,m+nM/4}\right\}_{n=0}^{3}$ respectively.

Then we compute the variably bias using the pseudocode given in Algorithm 1, which can be added to the corresponding four samples $x_{pre,m}, x_{pre,m+\frac{M}{4}}, x_{pre,m+\frac{M}{2}}$, and $x_{pre,m+\frac{3M}{4}}$ respectively. In which, if one of the four sample is negative then the least value can be considered as minimum bias and is added to the same samples $\left\{x_{pre,m+nN/4}\right\}_{n=0}^{3}$ by reversing the polarity to attain the nonnegative signal. In case the four samples are positive then the bias is not required, but the least value can be subtracted from the four samples to increase the PE, while the non-negativity is retained. Therefore, we add a bias which depends on signal samples value as,

$$\begin{aligned} v_m &= v_{m+\frac{M}{4}} = v_{m+\frac{M}{2}} = v_{m+\frac{3M}{4}} \\ &= -\min\left\{x_{pre,m}, x_{pre,m+\frac{M}{4}}, x_{pre,m+\frac{M}{2}}, x_{pre,m+\frac{3M}{4}}\right\} \\ & m = 0, 1, ..., M/4 \ - 1 \end{aligned} \tag{5.13}$$

From (5.13), it can be noticed that the proposed bias depends on the specific samples of the TD signal unlike the constant DC-bias as shown in Fig. 5.3. By adding the bias signal v_m to the TD signal $x_{pre,m}$, the modulated signal, $x_{VBO,m}$ can be defined as,

$$x_{VBO,m} = x_{pre,m} + v_m, m = 0, 1, ..., M-1 \tag{5.14}$$

From Fig. 5.1, the final modulated signal can be represented as,

$$x_{VAO,m} = x_{ACO,m} + x_{VBO,m}, m = 0, 1, ..., M-1 \tag{5.15}$$

where, $x_{VAO,m}$ is the real and non-negative signal.

Transform (5.14) and (5.15) into the FD to better understand the interference and clipping noise cancellation, which results in

$$X_{VBO,k} = X_{pre,k} + V_k, k = 0, 1, ..., K-1 \tag{5.16}$$

and

$$X_{VAO,k} = X_{ACO,k} + X_{VBO,k}, k = 0, 1, ..., K-1 \tag{5.17}$$

further, substituting (5.9) in (5.10) results in

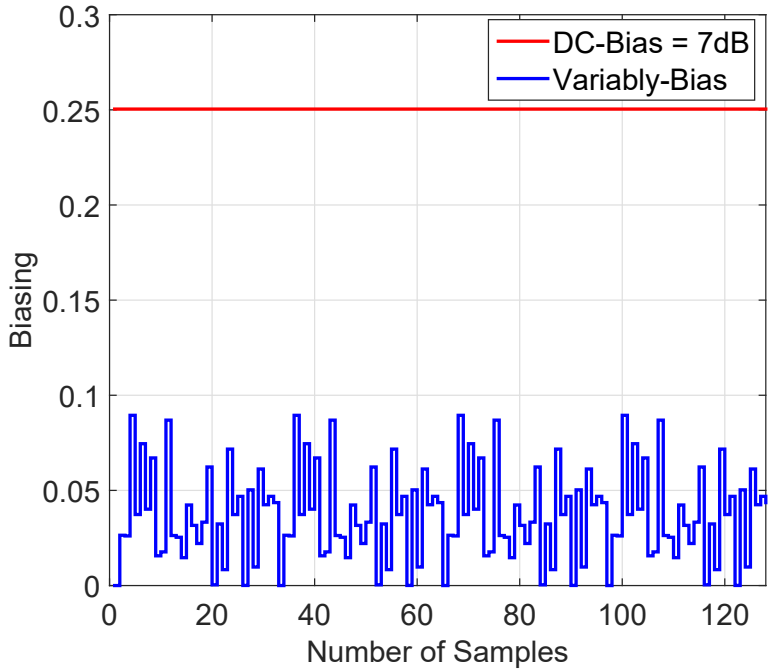

Figure 5.3: Simulation: Illustration of variably bias and DC-bias with 4-QAM, M=128 subcarriers

$$X_{pre,k} = X_{eve,k} - \Lambda_{odd,k}, k = 0, 1, ..., K-1 \tag{5.18}$$

To obtain the $X_{VBO,k}$, put (5.18) in (5.16). Then, the resulting variably biased signal in the FD can be expressed as,

$$X_{VBO,k} = X_{eve,k} - \Lambda_{odd,k} + V_k, k = 0, 1, ..., K-1 \tag{5.19}$$

By substituting the (5.7) and (5.19) in (5.17), we can obtain the pre-distorted variably biased asymmetrically clipped signal without any asymmetrically clipping noise. Therefore, the final modulated signal in the FD can be defined as,

$$X_{VAO,k} = X_{eve,k} + \frac{1}{2}X_{odd,k} + V_k, k = 0, 1, ..., K-1 \tag{5.20}$$

where V_k represents the FD version of the TD sequence v_m. According to Theorem 1, the signal V_k contains only the $4p$-th located subcarriers, which means the interference caused by the sequence v_m on the remaining subcarriers is successfully eliminated by following the v_m structure as in (5.12).

Next to (5.15), the addition of Cyclic Prefix (CP) and then the parallel to serial

(P/S), digital to anolog (D/A) conversions are done sequentially to obtain the continuous signal $x_{VAO}(t)$.

5.2.2 Channel

The signal which is obtained through the unipolar conversion can be transmitted over the optical channel, which consists of both the line-of-sight (LOS), and the non-line-of-sight (NLOS) components respectively. In [95], the optical channels for the VLC system are modelled with short-distance LOS links in terms of delay and linear attenuation. The path loss in LOS links are expressed in [95] as,

$$h_{LOS} = \frac{A_{PD}\,(w+1)}{2\pi D^2}\cos^{w}(\psi)\, g_{opf}(\varphi)\, g_{con}(\varphi)\cos(\varphi) \tag{5.21}$$

where, A_{PD} is area of the photodiode, D represents the LOS distance between LED and the photodiode, and ψ, φ represents the irradiance and incidence angle to the receiver respectively. Further, the function $g_{opf}(\varphi)$ describes the gain of the optical-filter and $g_{con}(\varphi)$ describes the gain of the optical-concentrator. The order of Lambertian emission is represented as w and it is defined as,

$$w = \frac{-\ln 2}{\ln\left[\cos\left(\psi_{1/2}\right)\right]} \tag{5.22}$$

where, $\psi_{1/2}$ represents the semi-angle at half-power of the transmitter. Likewise, in NLOS, the path-loss after the first bounce can be expressed as [95],

$$h_{NLOS} = \frac{(w+1)\,A_{PD}\Delta A}{2\pi D_{Si}^2 D_{iR}^2}\rho\cos^{w}(\psi_{Si})\cos(\varphi_{Si})\cos(\varphi_{iR}) \tag{5.23}$$

where, ΔA represents the reflecting surface and D_{Si} is the distance of source to Reflection Point (RP) and D_{iR} is the distance of RP to receiver. Further, the angles ψ_{Si}, φ_{Si}, φ_{iR} represent irradiance, and incidence angles at the transmitter, and receiver, RP respectively. The parameters are integrated similarly to the [95]. By considering the LOS, and NLOS path-losses, the multipath optical channel is given in the succeeding paragraphs. Let the impulse response of the multipath optical channel in discrete TD is represented as $h(m)$, then the ES $y_{ele}(m)$ at the photodiode can be given in [81] as,

$$y_{ele}(m) = R * x_{VAO}(m) * h(m) + \eta(m) \tag{5.24}$$

where, R represents responsivity of photodiode in A/W, and $\eta(m)$ is the total noise. The considered channel model is defined in [81] and it is given as,

$$y_{ele}\,(m) = \sum_{l=0}^{L-1} h(l) x_{VAO}(m-l) + \eta(m) \tag{5.25}$$

here, L path optical-channel is considered and the responsivity R of the photodiode is deliberated as unity.

5.2.3 Receiver

The receiver part of the VAO-OFDM system is shown in the block diagram at the bottom of Fig.5.1. The receiver contains only a single demodulation route for the ACO-OFDM and VBO-OFDM signals, unlike the traditional ADO-OFDM demodulation scheme , which results in CC reduction compared to ADO-OFDM [1]. Let the received signal be $y(t)$ with the transmitted signal $x_{VAO}(t)$ over the optical channel, which is described deliberately in the channel section [81] . Thereafter, in order to detect the received signal $y(t)$, we applied a matching filter. Further, an analogue-to-digital converter (A/D), serial to parallel (S/P) converter, and a CP remover are then applied to the received signal to produce the discrete TD signal y_m [1]. Thereafter, the received FD signal Y_k can be obtained by performing an FFT operation on the time-domain signal y_m [1]. Due to the mutual interference between ACO-OFDM and VBO-OFDM signals being eliminated at the transmitter with the pre-distortion process, we can directly recover each signal from the even and odd sub-carriers of Y_k separately. Further, the signal Y_k can be divided into odd subcarriers $Y_{odd,k}$ and even subcarriers $Y_{eve,k}$ after the equalization processes respectively.

Therefore, the ACO-OFDM signal $Y_{ACO,k}$ can be obtained directly from the $Y_{odd,k}$ by multiplying with a factor of two to compensate for the asymmetrical clipping noise, and it is given in [89] as $Y_{\mathrm{ACO,k}} = 2Y_{odd,k}, \forall k$ which is equivalent to,

$$Y_{\mathrm{ACO,k}} = X_{odd,k}, \forall k \tag{5.26}$$

Further, the VBO-OFDM signal $Y_{VBO,k}$ can be obtained directly from the $Y_{eve,k}$ and it can be represented as $Y_{VBO,k} = Y_{eve,k}$. According to *Theorem 1*, since the variably biased sequence has the structure as shown in (5.12), the resulted signal occupies only the $4p$-th

located subcarriers and hence the resulting signal $Y_{VBO,k}$ can be expressed as,

$$Y_{VBO,k} = \begin{cases} X_{eve,k}, & k = 2p+1 \\ X_{eve,k}, & k = 2(2p+1) \\ V_k, & k = 4p \end{cases} \tag{5.27}$$

where, $p = 0, 1, ..., M/8 - 1$ and V_k represents the IFFT of variably biased sequence v_m. From the symbol structure shown in Fig. 5.2 (c), the odd components of signal $X_{eve,k}$ for $k = 2p + 1$ are set to zero before the transmission taken palce. Therefore, the effective $Y_{VBO,k}$ signal can be directly obtained from the $k = 2(2p + 1)$-th positioned subcarriers which are interference-free caused by the variably biased sequence.

Thereafter, by reframing the $Y_{ACO,k}$ and $Y_{VBO,k}$ and removing the HS, extracting subcarriers, one can obtain the corresponding QAM symbols which can be inversely mapped and further processed for S/P conversion to attain the actual output bit stream.

5.2.4 CC

Although the VAO-OFDM can reduce the interference between VBO-OFDM and ACO-OFDM and hence improve the PE, the CC of the transmitter section is slightly increased due to the pre-distortion process whereas the receiver CC decreased significantly when compared to ADO-OFDM. Further, the CC of both modulation schemes is evaluated in terms of CAs and CMs. The VAO-OFDM requires $4M \log_2^M$ CAs and $2M \log_2^M$ CMs respectively, whereas the traditional ADO-OFDM requires $6M \log_2^M$ CAs and $3M \log_2^M$ CMs respectively. Therefore, the overall CC of the proposed VAO-OFDM is significantly decreased when compared to traditional ADO-OFDM.

5.3 Results and Discussion

This section describes the discussions on the simulation results of the VAO-OFDM modulation in comparison with the ADO-OFDM, ACO-OFDM and DCO-OFDM, and the experimental results of the VAO-OFDM are compared with the ADO-OFDM. The simulation parameters we considered in this test are tabularized in Table 5.1.

Table 5.1: Simulation parameters

Parameter	**Values**
QAM orders	4, 8, 16, 32, 64, 128, 256
Sub-carriers (M)	128
OFDM Symbols	10^5
CP length	8
DC bias for ADO-OFDM and DCO-OFDM	7 dB

5.3.1 Simulation Results

In the simulation process, we used 10^5 OFDM symbols with each OFDM symbol consisting of 128 subcarriers and loaded with the different QAM orders of 4, 8, 16, 32, 64, 128 and 256 symbols respectively. Then the Monte-Carlo simulations are performed on the modulation schemes such as DCO-OFDM, ACO-OFDM, and ADO-OFDM including the proposed VAO-OFDM for a fair comparison. In the simulation, we used a CP with a length of 8, and $7dB$ DC- bias is used for the DCO-OFDM and ADO-OFDM respectively. In adition to this, we used a normalized $E_{b(opt)}/N_0$ which can be obtained by making the optical power to be unity. Furthermore, the required normalized $E_{b(opt)}/N_0$ for the acceptable $BER = 10^{-3}$ is defined as $< E_{b(opt)}/N_0 >_{BER}$. Firstly, The performance is evaluated in terms of bit error rate (BER) against the ratio of normalized optical-bit-energy $E_{b(opt)}$ to the noise power N_0, $E_{b(opt)}/N_0$. Secondly, the performance of the used modulation schemes are evaluated in terms of $< E_{b(opt)}/N_0 >_{BER}$ against the constellation orders at an acceptable BER of 10^{-3}.

Finally, the performance of the VAO-OFDM modulation scheme is evaluated in terms of $< E_{b(opt)}/N_0 >_{BER}$ against the bitrate/ normalized bandwidth. Whereas the modulation bandwidths of the modulation schemes are considered from [1, 35]. However, due to the effective subcarriers utilized in ACO-OFDM being $\frac{M}{4}$, the bitrate/ normalized bandwidth of the ACO-OFDM is obtained as $\log_2 N_{ACO}/2\left(1+\frac{2}{M}\right)$. Similarly, $\frac{M}{2}-1$ number of effective subcarriers are used in DCO-OFDM, and hence the bitrate/normalized

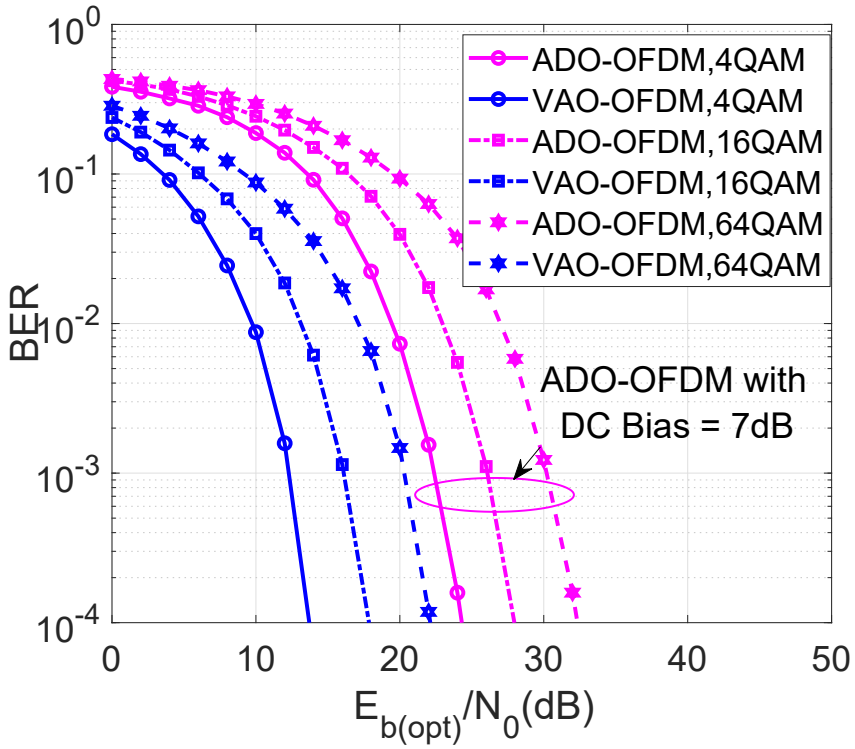

Figure 5.4: Simulation: BER performance of the VAO-OFDM with QAM orders of 4, 16, 64 in comparison with the ADO-OFDM with QAM orders of 4, 16, 64 with a DC-bias of $7dB$

bandwidth of the DCO-OFDM is obtained as $\log_2 N_{ACO}/2\left(1+\frac{2}{M}\right)$ where the N_{ACO} and N_{DCO} represents the QAM constellation orders of the ACO-OFDM and DCO-OFDM respectively. From both the layers in ADO-OFDM, each layer utilize $\frac{M}{4}$ effective subcarriers, and hence the bitrate/ normalized bandwidth of the ADO-OFDM is obtained as $(\log_2 N_{ACO}+\log_2 N_{DCO})/2\left(1+\frac{2}{M}\right)$. However, in the VAO-OFDM, the upper and lower layers utilize the $\frac{M}{4}$ and $\frac{M}{8}$ effective subcarriers respectively. Therefore, the bitrate/ normalized bandwidth of the VAO-OFDM is obtained as $\left(2\log_2 N_{ACO}+\log_2 N_{VBO}\right)/4\left(1+\frac{2}{M}\right)$ where the N_{VBO} represents the QAM constellation order of the VBO-OFDM.

Fig. 5.4 illustrates the simulation results of the ADO-OFDM with a constant DC bias of $7dB$ and the VAO-OFDM in terms of BER against the $E_{b(opt)}/N_0$ with the three QAM orders of 4, 16, 64 constellations. However, the VAO-OFDM outperformed than the ADO-OFDM in terms of BER. From Fig. 5.4, we perceived that the VAO-OFDM gain SNR of $10dB$, $10dB$, and $10dB$ at a BER value of 10^{-3} over the traditional ADO-OFDM with 4-QAM, 16-QAM, and 64-QAM respectively. Unlike in ADO-OFDM, we

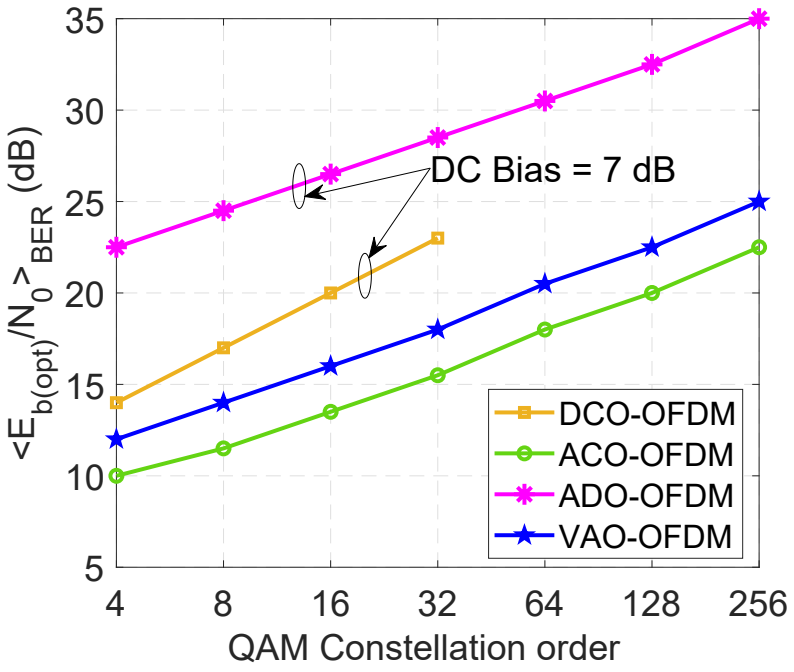

Figure 5.5: Simulation: $< E_{b(opt)}/N_0 >_{BER}$ against distinct constellations for DCO-OFDM, ADO-OFDM with 7dB, ACO-OFDM, and VAO-OFDM.

are not doing the error propagation in the VAO-OFDM, and this error propagation can be perfectly mitigated by the pre-distortion process where the asymmetrical clipping noise can be subtracted from the VBO-OFDM signal in the FD. Therefore, this mutual interference mitigation results in better performance in VAO-OFDM compared to ADO-OFDM in terms of BER.

Fig. 5.5 depicts the plots between the $< E_{b(opt)}/N_0 >_{BER}$ and the constellation orders at an acceptable BER of 10^{-3}, for DCO-OFDM and ADO-OFDM a DC-bias of $7dB$ is added to make the signal real and non-negative. From Fig. 5.5, we can observe that the VAO-OFDM requires lower $< E_{b(opt)}/N_0 >_{BER}$ for the QAM orders of 4, 8, 16, 32, 64, 128 and 256 constellations whereas the ADO-OFDM requires higher $< E_{b(opt)}/N_0 >_{BER}$ because of its additional DC-bias. For instant, the VAO-OFDM 4-QAM gained $10dB$ of power when compared to the ADO-OFDM 4-QAM. However, it is also observed that the ACO-OFDM outperforms the DCO-OFDM, ADO-OFDM and VAO-OFDM with the cost of SE. Furthermore, it is also perceived that the plots in the Fig. 5.5 are linear and parallel to each other, which infers that the rate of change of $< E_{b(opt)}/N_0 >_{BER}$ is similar for the DCO-OFDM, ACO-OFDM, ADO-OFDM and VAO-OFDM respectively.

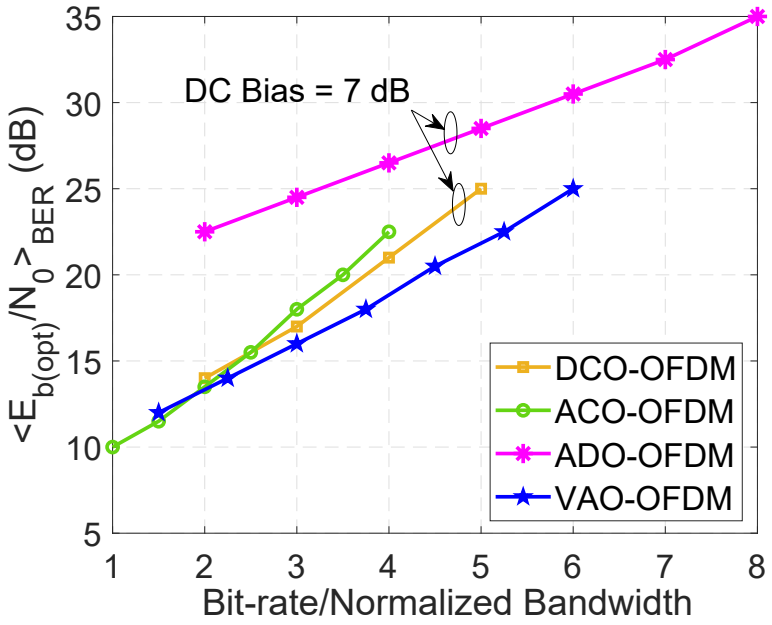

Figure 5.6: Simulation: $< E_{b(opt)}/N_0 >_{BER}$ against bitrate/ normalized bandwidth for DCO-OFDM with QAM orders of 4, 8, 16, 32 with a DC-bias of 7dB, and ADO-OFDM with a DC-bias of 7dB, ACO-OFDM and VAO-OFDM modulation schemes with QAM orders of 4, 8, 16, 32, 64, 128 and 256.

Fig. 5.6 portrays the plots of $< E_{b(opt)}/N_0 >_{BER}$ versus the bitrate/normalized bandwidth of DCO-OFDM, ACO-OFDM, ADO-OFDM and VAO-OFDM respectively. However, for DCO-OFDM and ADO-OFDM a DC bias of $7dB$ is added to make the signal real and non-negative to eliminate the nonlinear clipping distortion. From Fig. 5.6, one can observe that the VAO-OFDM outperforms the ADO-OFDM in terms of $< E_{b(opt)}/N_0 >_{BER}$. In a detailed manner, to achieve the bitrate/normalized bandwidth of 3 and 6 bit/s/Hz, the VAO-OFDM requires lower $< E_{b(opt)}/N_0 >_{BER}$ which are $16dB$ and $25dB$ for the 16-QAM and 256-QAM constellations respectively whereas the ADO-OFDM requires higher $< E_{b(opt)}/N_0 >_{BER}$ which are $24dB$ and $32dB$ for the 8-QAM and 64-QAM constellations respectively. Compare to ADO-OFDM, the VAO-OFDM gains $8dB$ and $7dB$ power at the bitrate/normalized bandwidth of 3 and 6 bit/s/Hz respectively. From Fig. 5.6, it is also perceived that the VAO-OFDM outperforms the ACO-OFDM and DCO-OFDM with a DC bias of $7dB$. For example, to achieve the bitrate/normalized bandwidth of 3 bit/s/Hz, VAO-OFDM requires lower $< E_{b(opt)}/N_0 >_{BER}$ which is $16dB$ for the 16-QAM constellation whereas the DCO-OFDM requires higher $< E_{b(opt)}/N_0 >_{BER}$

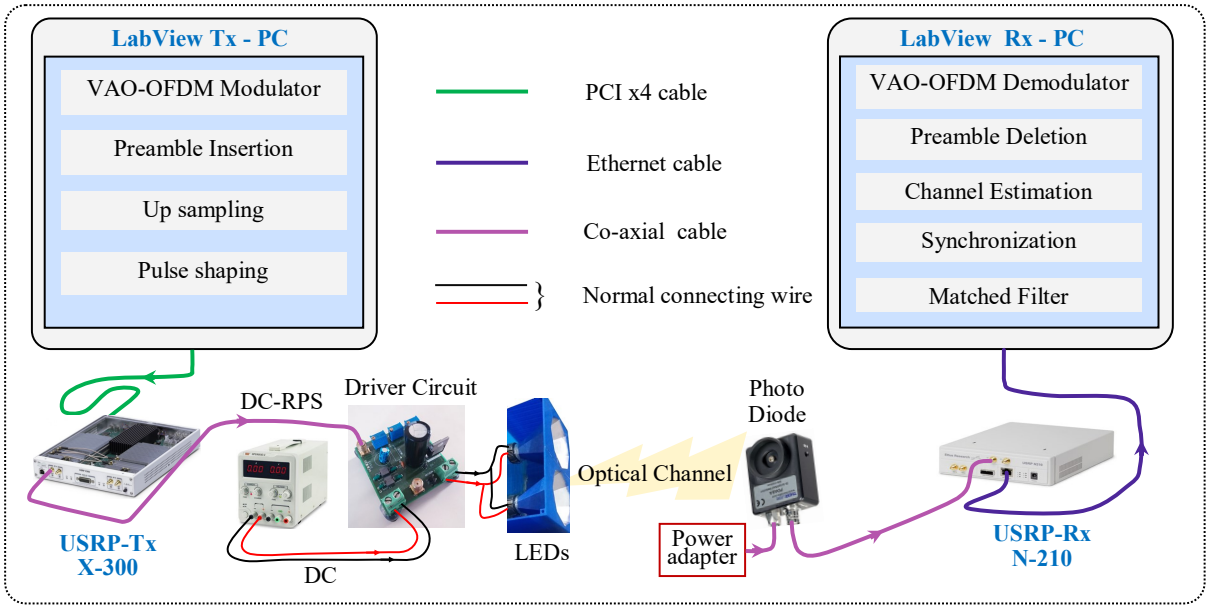

Figure 5.7: Block diagram of the experimental illustration procedure for the VAO-OFDM and ADO-OFDM (for ADO-OFDM, we used ADO-OFDM modulator and demodulator [1] instead of VAO-OFDM modulator and demodulator respectively)

which is $17dB$ for the 8-QAM constellations, and hence VAO-OFDM gains $1dB$ power than DCO-OFDM. However, to achieve the bitrate/normalized bandwidth of 3 bit/s/Hz, ACO-OFDM requires higher $< E_{b(opt)}/N_0 >_{BER}$ which is $18dB$ for the 64-QAM constellations, and hence VAO-OFDM gains $2dB$ power than the ACO-OFDM. Based on this information, the VAO-OFDM outperforms the DCO-OFDM and ADO-OFDM in terms of PE and ACO-OFDM in terms of SE. Though there is a trade-off between SE and PE, the proposed VAO-OFDM achieved higher bit-rate/normalized bandwidth at lower $< E_{b(opt)}/N_0 >_{BER}$ when compared with ADO-OFDM, ACO-OFDM and DDO-OFDM.

5.3.2 Experimental Results

This subsection presents the details of experiments along with the results that validate the VAO-OFDM and ADO-OFDM modulations on a practical test bed for a fair comparison. Fig. 5.7 depicts the block diagram of the experimental procedure for the VAO-OFDM and ADO-OFDM (for ADO-OFDM, we used ADO-OFDM modulator and demodulator [1] instead of VAO-OFDM modulator and demodulator respectively). The illustration of the practical test bed used in this work is shown in Fig. 5.8. The transmit-

Table 5.2: Experimental Parameters

Parameter	**Specification**	**Parameter**	**Specification**
Modulation order	4 QAM	Link Distance	102 to 114 cm
Number of subcarriers	128	Frank sequence length	16
Cyclic Prefix length	8	LED	OSRAM HL (25W, 12V)
Null carriers	4	Frame duration	2.21 ms
Oversampling factors	4, 2	Photodiode	PD-TarLabs, PDA8A (DC-50 MHz), 0.56 A/W @ 820 nm
USRP IQ sampling rate	4M	USRP with LFTx and LFRx Daughter boards	Ettus X300 and N210
Samples in one Frame	8840	Carrier Frequency f_c	3 MHz
Pulse Shaping Filter	Raised Cosine a length of 8	Bandwidth	1 MHz, 2 MHz

ter PC (Tx-PC) and receiver PC (Rx-PC) are equipped with Lab-view software which is used to carry out the baseband modulation. Using LFTx and LFRx daughter boards, the Ettus USRP x300 (USRP-Rx) and USRP N210 (USRP-Tx) is used as a transmitter and receiver USRPs respectively. The experimental parameters we have considered in this experiments are given in Table 5.2.

The proposed VAO-OFDM and ADO-OFDM systems are deliberated with $M = 128$ subcarriers along with 4-QAM symbols for a fair comparison. In each data frame, 16 OFDM symbols are loaded along with the pre-amble length (modified Frank Sequence) of 16, and zero padding from the two sides of the OFDM symbol, which constitutes together 2202 samples. Further, these 2202 samples are over-sampled with a factor of 4 (4 and 2 are for bandwidth of 1MHz and 2 MHz respectively) resulting in 8808 samples. Sequentially, these samples are pulse-shaped with a filter length of 8 resulting in 8840 samples. These generated samples in PC-Tx are processed by the transmitter USRP-Tx, in which, the Digital to Analog Conversion (DAC) with In-phase (I)/ Quad-phase (Q) (IQ) sampling rate of 4M samples/second and up-conversion can be performed. Since we are inputting the real signal to the USRP, one can be perceived that the component Q in the signal

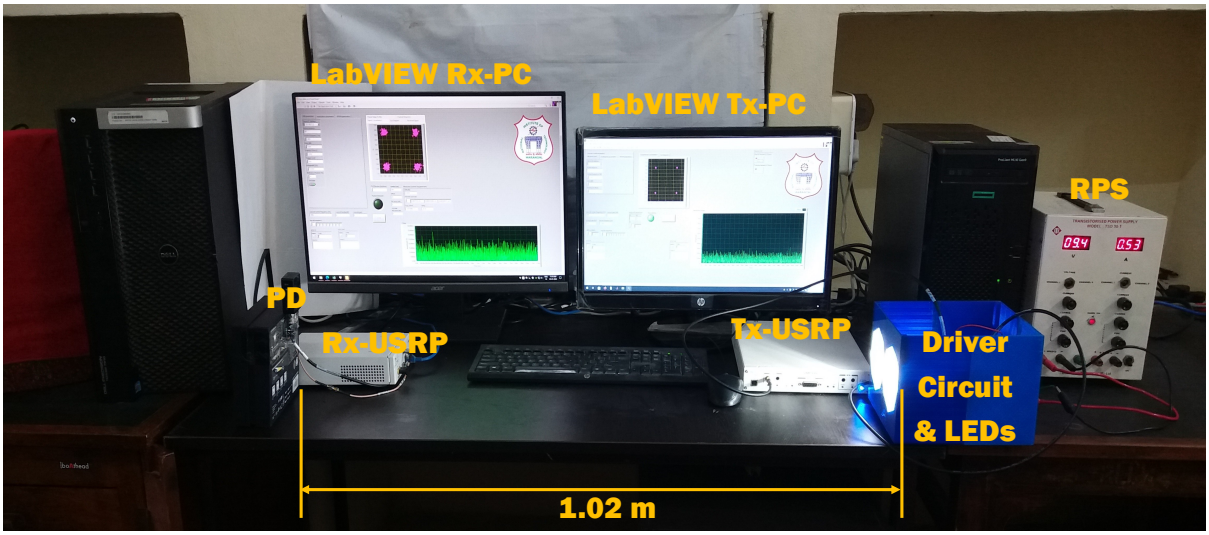

Figure 5.8: Experimental set-up utilized for the implementation of VAO-OFDM and ADO-OFDM

is zero. The I component of the transmitted data frame with a duration of 2.21ms is resoluted by dividing the length of frame by IQ rate, which is shown in Fig. 5.9 (a) with a preamble at the beginning of the data frame. Subsequently, the frequency up-conversion can be done by using the USRP-Tx which results in a desired RF frequency signal, given as input to the LED driver circuit resulting in a unipolar signal which drives the LEDs. Given that the USRP can only provide voltage signals and that a current mode driver must be used to drive LEDs linearly, proper LED biassing is also essential for optimal performance. Therefore, a DC bias current source is implemented by using a current feedback amplifier, the LT1206, which is mounted in a transconductance amplifier (TCA) configuration as implemented in [98].

On other hand, in the receiver section, without any focusing lens from the transmitter to the receiver, the photodiode (Thorlabs-PDA8A) receives the intensity-modulated light signal by varying the distance from 102 cm to 110 cm. Subsequently, the ES can be obtained by the photodiode from the received optical signal. After the amplification processes, the USRP-Rx down-converts and generates the data frame which is delayed and attenuatedas shown in Fig. 5.9(b), but the duration has remained unchanged. Therefore, the capture duration needs to be at least tenfold longer than the data frame's duration in order to retrieve it. The received data frame is subsequently processed by the Rx-PC where it goes through matched filtering, synchronising processes, and channel estimation

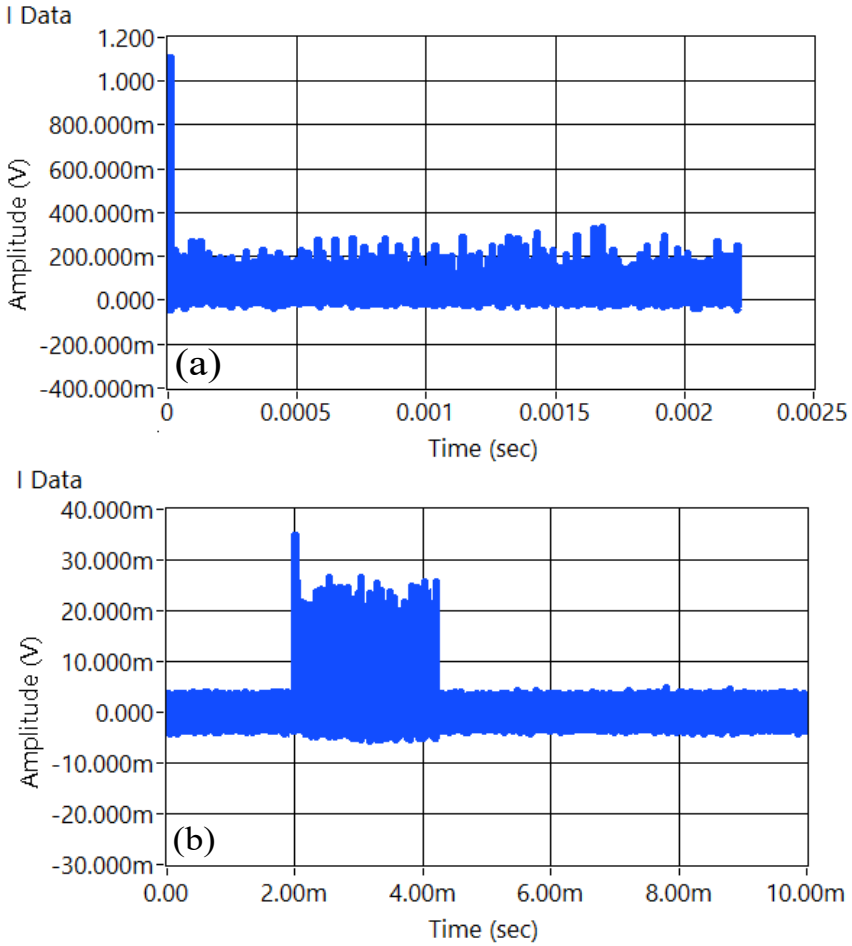

Figure 5.9: A plot of TD signals. (a) the transmitted data Frame, and (b) the received data Frame

processes as shown in Fig. 5.7. In the current work, minimum mean square error (MMSE) estimation for the channel and conventional synchronisation methods such as the Schmidl and Cox methods are used [99,100]. As soon as the data frame is demodulated, the VAO-OFDM and ADO-OFDM demodulators recover an estimated number of QAM symbols respectively. The de-mapper eventually extracts the data bits from the estimated QAM symbols.

Fig. 5.10 (a) and Fig. 5.10 (b) illustrate the experimentally obtained BER performance comparison against the transmitter's and receiver's separation in cm for the signal bandwidth of 1 MHz and 2MHz respectively. Performing 1000 iterations, the average BER is obtained by varying the distance from 102 cm to 110 cm. Further, the constellations of both the modulation schemes at a distance of 102 cm are also incorporated in Fig. 5.10 (a) and Fig. 5.10 (b) correspondingly. From Fig. 5.10 (a) and Fig. 5.10 (b), it is observed

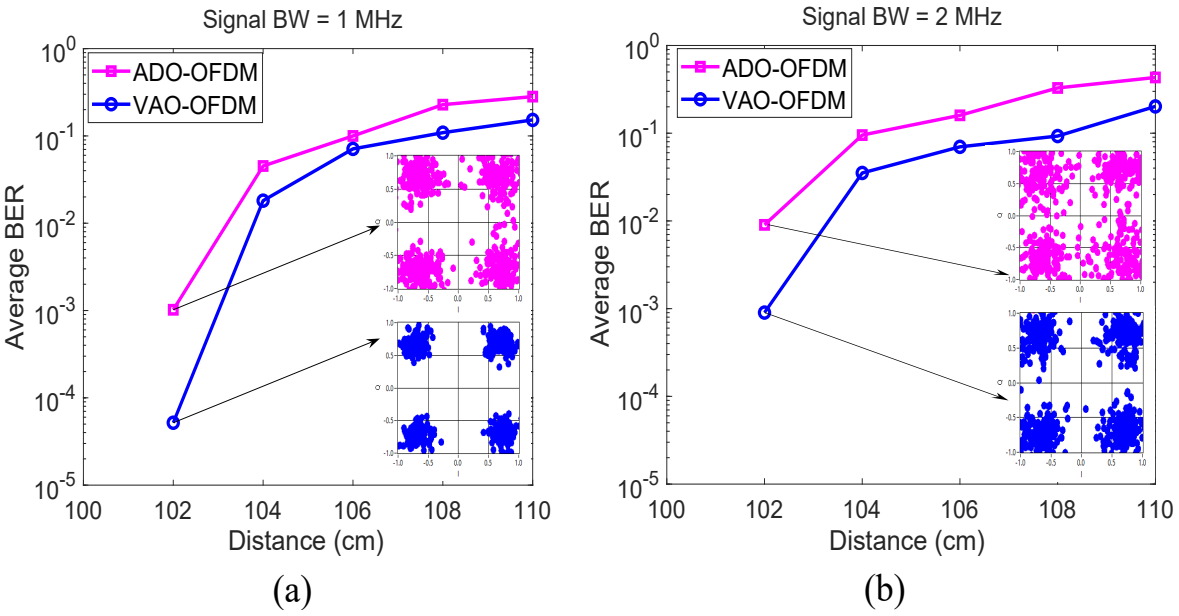

Figure 5.10: Experimentally obtained BER performance against the transmitter's and receiver's separation in cm, and incorporated with the constellation diagrams at a separation of 102 cm between transmitter and receiver at a signal bandwidth of (a) $1MHz$ and (b) $2MHz$

that the BER performance of ADO-OFDM and VAO-OFDM is obtained as 1.02×10^{-3} and 5.18×10^{-5} at a signal bandwidth of 1 MHz and 8.98×10^{-3} and 9.04×10^{-4} at a signal bandwidth of 2 MHz respectively. Therefore, the VAO-OFDM BER performance is enhanced substantially when compare to ADO-OFDM. Also, it can be noted that the BER performance of both schemes are substantially good at lower distances, whereas increasing distance degraded the BER performance. Therefore, the VAO-OFDM outperformed the ADO-OFDM in terms of BER against the transmitter's and receiver's separation in cm. It is also perceived that both the modulation schemes with a signal bandwidth of 1 MHz outperformed the signal bandwidth of 2 MHz. However, in terms of BER performance, the VAO-OFDM outperformed the ADO-OFDM in both cases with a signal bandwidth of 1 MHz and 2 MHz respectively.

5.4 Summary

In this chapter, a novel modulation scheme called Variably-biased Asymmetrically-clipped Optical-OFDM (VAO-OFDM) for VLC systems is proposed. The main goal of

this modulation scheme is to improve PE in VLC systems. In VAO-OFDM, a specific bias is introduced in such a way that it depends on specific sample amplitudes. The frequency domain signals with this bias are placed on specific subcarriers that are located at regular intervals of $4pth$. This design ensures that the biased signals do not interfere with the originally transmitted symbols, resulting in improved PE.

Simulation results show that VAO-OFDM with different QAM orders (4, 16, and 64) outperform the existing ADO-OFDM scheme with 4-QAM at a Bit Error Rate (BER) of 10^{-3}. This implies that VAO-OFDM 64-QAM requires lower energy per bit to noise power spectral density ($E_{b(opt)}/N_0$) compared to ADO-OFDM 4-QAM. Furthermore, VAO-OFDM exhibits better PE compared to traditional modulation schemes such as DCO-OFDM, ACO-OFDM, and ADO-OFDM over a wide range of bit rates or normalized bandwidths.

Experimental results confirmed the simulation findings and demonstrated that VAO-OFDM outperformed ADO-OFDM in terms of BER for different transmitter-receiver separations in centimetres. It is also noted that both VAO-OFDM and ADO-OFDM with a signal bandwidth of 1 MHz outperform those with a signal bandwidth of 2 MHz. However, even with different signal bandwidths, VAO-OFDM consistently achieved better BER performance compared to ADO-OFDM. Additionally, VAO-OFDM offers the advantage of low CC compared to traditional ADO-OFDM. Moreover, the experimental setup includes a driver circuit that reduces the system cost by eliminating the need for an additional bias tee.

Chapter 6

Conjugate-symmetric Sequency-ordered Complex Hadamard Coded Modulation for VLC Systems

6.1 Introduction

In the context of Visible Light Communications (VLC), a novel modulation scheme called Variably-biased Asymmetrically-clipped Optical-OFDM (VAO-OFDM) has been initiated in the previous chapter, by introducing a new bias which depends on the specific sample amplitudes. The frequency domain version of the new bias signal will occupy the pre-defined subcarriers. This new bias design ensures that the biased signals do not interfere with the originally transmitted symbols, resulting in improved PE. However, the VAO-OFDM is generated by employing the fast Fourier Transform.

Fourier transform-based OFDM techniques are known to generate continuous waveforms with high amplitude fluctuations [101]. This means that the signal amplitudes can vary significantly, leading to challenges in maintaining linearity. Non-linearities can introduce distortions and impair the performance of the system [102]. Consequently, these OFDM techniques are highly sensitive to non-linear effects [103]. In contrast, using a modulation scheme that relies on a discrete set of signal amplitudes offers certain benefits, particularly in terms of implementation. With such a scheme, a limited number of distinct signal amplitudes are used, which simplifies the modulation process. In this context, the discrete scheme can be achieved by employing different light-emitting diodes (LEDs) that can be either switched on or off to represent the discrete signal amplitudes.

By utilizing this discrete modulation scheme, the linearity of the transmitter can be effectively maintained. Instead of dealing with continuous waveforms and their associated non-linearities, the individual signals produced by the LEDs can be superimposed in the transmission medium. This superposition allows for the synthesis of more complex signal waveforms while preserving linearity. By combining the individual signals in a controlled manner, the desired modulated waveform can be achieved. One example of a modulation scheme that embodies these principles is Hadamard Coded Modulation (HCM) [41, 104]. In a recent work [105], researchers introduced a novel approach called asymmetrically clipped optical Hadamard Coded Modulation (ACO-HCM) to enhance PE. This innovative modulation technique combines the advantages of unipolar OFDM with the benefits of Hadamard Coded Modulation (HCM), which operates within a discrete signal range. It is worth noting that the works described in [41, 104, 105] are focused exclusively on Pulse Amplitude Modulation (PAM) because of the traditional HCM does not yield a real output for the complex input signals.

In this chapter, we conceive a novel modulation scheme called Conjugate-Symmetric Sequency-Ordered Complex Hadamard Coded Modulation (CS-CHCM) which is used to generate the new modulation scheme called Variably Biased Asymmetrically Clipped Optical CS-CHCM (VAO-CS-CHCM). VAO-CS-CHCM can be obtained by replacing the FFT with Conjugate Symmetric Sequency-Ordered Complex Hadamard Transform (CS-SCHT) [106] and IFFT with Inverse CS-SCHT (ICS-SCHT) [106] in VAO-OFDM. In this innovative scheme, based on the conjugate symmetry property, CS-CHCM yields real outputs for complex input signals, and also CS-CHCM introduces the concept of utilizing a discrete set of signal amplitudes for improved PE. A significant finding of this study is that the constraints imposed by the modulation scheme render the negative portion of the signal redundant. As a result, one can effectively transfer this redundant information from the Fourier transform domain to the CS-SCHT domain . This transformation not only simplifies the modulation process but also allows for the efficient allocation of resources and optimization of the transmission system. By presenting the VAO-CS-CHCM modulation scheme and highlighting the advantages of incorporating CS-SCHT, this research opens up new possibilities for achieving higher performance and efficiency in optical communications. The proposed scheme has the potential to revolutionize modulation techniques and advance the field of optical data transmission.

The rest of this chapter is structured as : Section 6.2 provides a comprehensive review of CS-SCHT to establish the context and highlight the significance of CS-SCHT in the research area. The system model is explained in section 6.3 which includes the theoretical framework, mathematical formulations, and the architecture of the proposed new waveform based on CS-SCHT. The simulation outcomes and CC analysis are discussed in Section 6.4 which presents the results of their simulations based on the CS-SCHT-based waveform for VLC systems. Section 6.5 provides the summary which often highlights the novelty of the proposed approach and its advantages over existing methods.

6.2 Review of CS-SCHT

The CS-SCHT transform is analogous to DFT, and it is an orthogonal transform technique which differs from the DFT in that the transform matrix is constructed using a different twiddle factor. The only elements in the CS-SCHT transformation matrix are $\{\pm 1, \pm j\}$ where $j = \sqrt{-1}$ which can be purely real or imaginary. Let $\chi(t)$, a periodic function in the time domain, be defined over the interval $0 \leq t < 1$ in [107] as

$$\chi(t) = \begin{cases} 1, & 0 \leq t < 1/4 \\ -j, & t = 1/4 \\ -1, & 1/4 \leq t < 3/4 \\ j, & t = 3/4 \\ 1, & 3/4 \leq t < 1. \end{cases} \tag{6.1}$$

In accordance with the definition given in (6.1), it is obvious that the elements in equation (6.1) are situated on the unit circle in the complex domain, with each element taking a location on either the real or imaginary axes. The following properties are adhered to by the function $\chi(t)$ [107].

1. $\chi(t) = \chi(t+1)$ (6.2)
2. $\chi(t) = \exp\left(ja(t)\right),\ where\ a(t)\ is\ real\ \forall t$ (6.3)
3. $\chi(t) = -\chi(t)$ (6.4)
4. $\chi(-t + 1/2\ ) = -\chi^*(t).$ (6.5)

To generate the $M \times M$ CS-SCHT matrix, it requires a complex periodic function which satisfies all the above-mentioned properties as given in [107]. Let $M = 2^b$, where b is the minimum number of bits needed to indicate the matrix's last index. The CS-SCHT matrix is generated using a basis matrix $\mathbf{U}$, and is built using the periodic function definition. Then, the basis matrix $\mathbf{U}$ can be generated in [107] as

$$\begin{aligned} &U(m,c) = \chi(m2^c/M) = \chi(m2^{c-b}) \\ &for\ 0 \leq c < b\ and\ 0\ \leq m < M \end{aligned} \tag{6.6}$$

Although the argument of the periodic function on the right-hand side exceeds the maximum index of the matrix $M-1$, the periodic property described in (6.2) gives it a viable index, where M is the discrete equivalent of the normalised unit time period. Then, we obtain the b basis in terms of column vectors of U from (6.6). Following that, we can generate a full-rank matrix $\mathbf{F}_M$ in [107] as

$$\begin{aligned} F_M(m,k) &= \prod_{c=0}^{b-1} U(m,c)^{k_c}, 0 \leq m,k < M \text{ and } 0 \leq c < b \\ \langle k \rangle_{10} &= \langle k_{b-1}, k_{b-2}, ...k_1, k_0 \rangle_2 \end{aligned} \tag{6.7}$$

where $\mathbf{F}_M$ represents the $M \times M$ CS-SCHT matrix, and l_c is the binary representation of l.

The generating process of $\mathbf{F}_M$ consists of two steps, which are defined in (6.6) and (6.7). Since (6.6) entails transferring the values of the periodic function to the columns of $\mathbf{U}$ and (6.7) extends the matrix using the product of elements in the columns that preserve the kernel (i.e. $\{\pm 1, \pm j\}$) that reside on the real or imaginary axis of the unit circle in the complex plane. Because the columns of the basis column matrix $\mathbf{U}$ are orthogonal, and the CS-SCHT matrix is also built to preserve orthogonality among its columns, matrix $\mathbf{F}_M$ is orthogonal like the DFT matrix. In addition to orthogonality, the CS-SCHT matrix possesses the following properties [105].

Property 1: Exponential property:- Lets consider an element in the CS-SCHT matrix of arbitrary dimensions $M \times M$ that resides in the location denoted by the m^{th} row and k^{th} column and is represented by the analytical expression for $0\ \leq m,k < M-1$ given in [105] as

$$F_M(m,k) = (-1)^{\sum_{c=0}^{b-1} g_{m_c} k_c} (-j)^{\sum_{c=0}^{b-1} f_{m_c} k_c}, \tag{6.8}$$

where g_{m_c}, f_{m_c}, and k_c are the binary numbers 0 or 1 defined in [105] (Table I). Further, using the exponential function, the closed-form analytical expression (6.8) can be expressed as

$$F_M(m,k) = e^{j\pi\left(\sum_{c=0}^{b-1} g_{m_c}k_c - \frac{1}{2}\sum_{c=0}^{b-1} f_{m_c}l_c\right)}. \tag{6.9}$$

*Property 2: Unitary property:-*All the row vectors in an $M \times M$ CS-SCHT matrix are orthogonal, much like the DFT matrix. The matrix $\mathbf{F}$ is the inverse matrix of its complex conjugate matrix $\mathbf{F}^*$ and the relation can be given in [105] as

$$\mathbf{F}_M^*\mathbf{F}_M = \mathbf{F}_M\mathbf{F}_M^* = M\mathbf{I}_M. \tag{6.10}$$

The product generated a scalar matrix because the definition omitted the normalization factor.

Property 3: Conjugate Symmetry:- In an approach similar to DFT, using CS-SCHT results in the generation of a conjugate symmetric spectrum of a time domain signal. Each of the elements of the CS-SCHT matrix has the following relationship based on the conjugate symmetry property [105] as

$$F_M(M-m,k) = F_M^*(m,k). \tag{6.11}$$

In addition to these properties, this transform also makes it possible to create an algorithm quickly, similar to the FFT technique, which draws additional interest in its applications. To take advantage of one of the CS-SCHT's applications, it is used in place of DFT throughout the entire VLC system in this work, as shown in Fig. 6.1.

6.3 VAO-CS-CHCM System Model using CS-SCHT

In this section, we discribed the VAO-CS-CHCM, which is similar to the VAO-OFDM which is initiated in the previous chapter.

6.3.1 Transmitter

The VAO-OFDM modulation scheme which is initiated in the previous chapter introduces a new structure to further optimize the system performance. In this scheme,

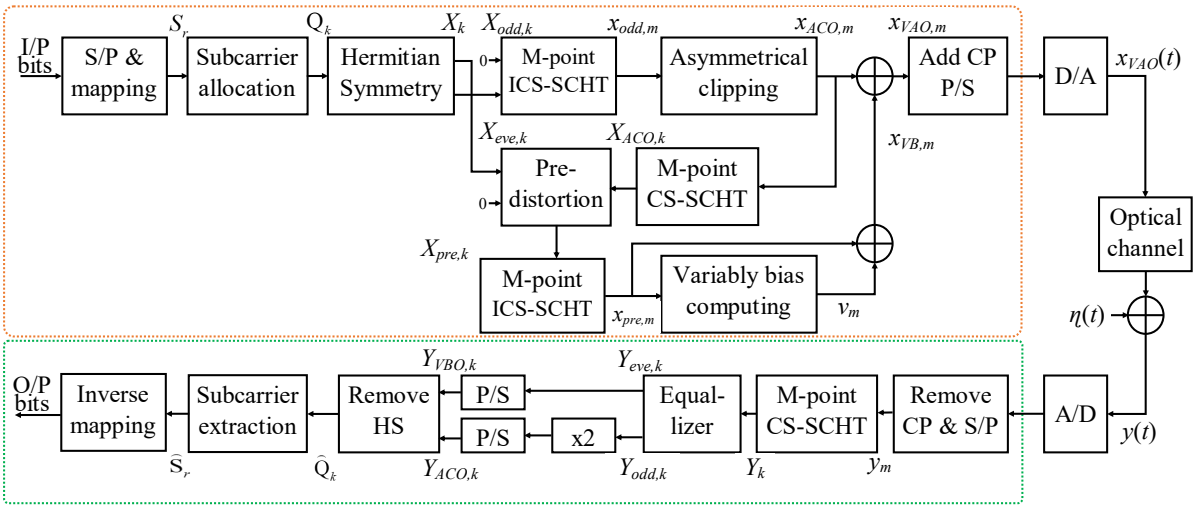

Figure 6.1: Block diagram of VAO-CS-CHCM scheme

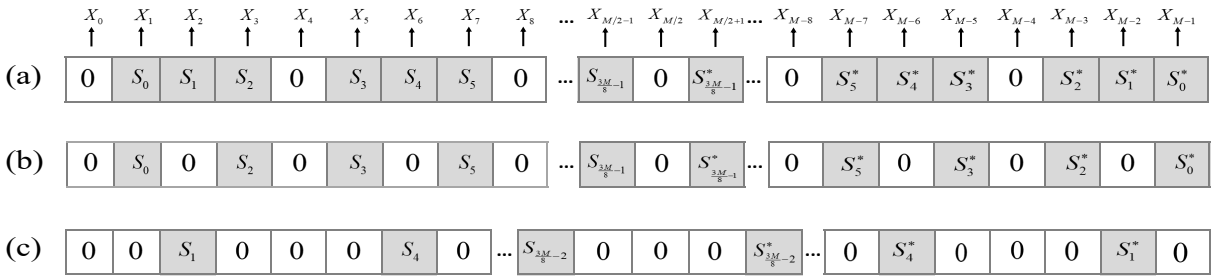

Figure 6.2: Frequency-domain demonstration of the proposed VAO-CS-CHCM: (a) Actual QAM symbol vector $\mathbf{X}$, (b) input symbol vector $X_{odd,k}$ to the ACO-CS-CHCM, (c) input symbol vector $X_{eve,k}$ to the VBO-CS-CHCM.

the upper layer operates similarly to ACO-OFDM in ADO-OFDM which is named as Asymetriclly Clippied Optical Conjugate-symetric Sequence-ordered Complex Hadamrd Coded Modulation (ACO-CS-CHCM), maintaining its role and characteristics. However, a significant change is made in the lower layer. Instead of using DCO-OFDM with a constant DC bias, a Variably Bias-based Optical Conjugate-symetric Sequence-ordered Complex Hadamrd Coded Modulation (VBO-CS-CHCM) is employed. However, the proposed VAO-CS-CHCM system model in this chapter is also similar to VAO-OFDM except for the modulation process where the IFFT operation is replaced by the CS-SCHT in the VAO-OFDM which results in VAO-CS-CHMC as shown in Fig.6.1.

Let $\mathbf{S} = \{S_0, S_1, S_2, ..., S_{3M/8\,-1}\} \in \mathbb{C}^{\left(\frac{3M}{8}\right)\times 1}$ be a quadrature amplitude modulation (QAM) symbol vector obtained from the input bitstream based on the required QAM

order [97], while M denotes the number of subcarriers in a single OFDM symbol, and $\mathbb{C}$ represents the set of complex numbers. For VAO-CS-CHCM, to ensure the real signal in time domain, we imposed Hermation symmetry on frequency domain symbols, which results in a QAM symbols vector $\mathbf{X}$ shown in Fig. 6.2 (a) is divided into the even components $X_{eve,k}$ and the odd components $X_{odd,k}$. Further, the odd components in $X_{eve,k}$ and the even components in $X_{odd,k}$ are fixed to zero such that the Hermitian symmetry can not be affected, where the resulted QAM symbol vector $X_{odd,k}$ is input to the upper layer for and $X_{eve,k}$ is input to the lower layer for are shown in Fig. 6.2 (b) and Fig. 6.2 (c) respectively.

The upper layer is performed with $X_{odd,k}$ signal, which results in $x_{odd,m}$, and it is given in [1] as,

$$x_{odd,m} = \frac{1}{\sqrt{M}} \sum_{k=0}^{M-1} X_{odd,k} e^{j\pi \left(\sum_{c=0}^{b-1} g_{m_c} k_c + \frac{1}{2} \sum_{c=0}^{b-1} f_{m_c} k_c \right)}, \tag{6.12}$$

where, $m = 0, 1, ..., M-1$ and $x_{odd,m}$ follows a half-wave symmetry as $x_{odd,m} = -x_{odd,m+M/2}$ for $0 < \ m \ < M/2$. Therefore, without any loss of information, the negative part can be clipped to guaranty the positivity of the signal. The asymmetrically clipping (AC) operation is given in [89] as,

$$\lfloor x_{odd,m} \rfloor_{clip} = \begin{cases} x_{odd,m}, & x_{odd,m} > 0 \\ 0, & x_{odd,m} < 0 \end{cases} \tag{6.13}$$

where $\lfloor . \rfloor_{clip}$ represents the zero clipping operator. Therefore, the ACO-CS-CHCM time domain signal, $x_{ACO,m}$ can be expressed as,

$$x_{ACO,m} = \lfloor x_{odd,m} \rfloor_{clip}. \tag{6.14}$$

However, the lower layer is modulated with the new modulation called VBO-CS-CHCM where the bias depends on the specific sample amplitudes. Therefore, the VBO-CS-CHCM signal can be generated by pre-distorting frequency domain signal $X_{eve,k}$ with the $X_{ACO,k}$ signals where the clipping noise of $X_{ACO,k}$ is subtracted from the $X_{eve,k}$ over even subcarriers only, and the signals over odd subcarriers remains same. Therefore, the pre-distorted signal $X_{pre,k}$ which is a noise-free signal, and it is defined as,

$$X_{pre,k} = \begin{cases} X_{eve,k} - X_{ACO,k}, & k = 2b \\ X_{eve,k}, & k = 2b+1 \end{cases} \tag{6.15}$$

Further, one can employ an IFFT operator to perform the OFDM modulation on $X_{pre,k}$ signal to obtain the TD signal $x_{pre,m}$, and it can be expressed as,

$$x_{pre,m} = \frac{1}{\sqrt{M}} \sum_{k=0}^{M-1} X_{pre,k} e^{j\pi \left(\sum_{c=0}^{b-1} g_{m_c} k_c + \frac{1}{2} \sum_{c=0}^{b-1} f_{m_c} k_c \right)}, \tag{6.16}$$

where, $m = 0, 1, ..., M-1$ and $x_{pre,m}$ represents the time domain version of the signal $X_{pre,k}$, and it is a bipolar signal which cannot be transmitted through the LED directly due to nonlinear clipping distortion. Therefore, to transmit through the LED, the signal must be unipolar such that the signal can not be affected by the LED nonlinear effect. To obtain the unipolar and non-negative signal, we employed a variably bias in the previous chapetr which depends on the amplitudes of the specific samples of the signal $x_{pre,m}$, unlike the constant DC-bias for all the samples. We compute the variably bias, v_m using *Algorithm-1* whic is given in the previous chapter.

Add the variably bias signal v_m to the time domain signal $x_{pre,m}$, the modulated signal, $x_{VBO,m}$ can be defined as,

$$x_{VBO,m} = x_{pre,m} + v_m, m = 0, 1, ..., M-1 \tag{6.17}$$

Then, the final modulated signal is the sum of ACO-CS-CHCM and VBO–CS-CHCM signals, and it can be represented as,

$$x_{VAO,m} = x_{ACO,m} + x_{VBO,m}, m = 0, 1, ..., M-1 \tag{6.18}$$

where, $x_{VAO,m}$ is the real and non-negative signal.

Then addition of Cyclic Prefix (CP) and then the parallel to serial (P/S), digital to anolog (D/A) conversions are done sequentially to obtain the continuous signal $x_{VAO}(t)$ which is similar to the VAO-OFDM.

6.3.2 Receiver

The receiver of the VAO-CS-CHCM is shown in Fig.6.1 which is similar to the VAO-OFDM except the IFFT/FFT and ICS-SCHT/CS-SCHT operations. Let the received signal be $y(t)$ with the transmitted signal $x_{VAO}(t)$ over the optical channel [81] . Thereafter, in order to detect the received signal $y(t)$, we applied a matching filter.

Further, an analogue-to-digital converter (A/D), serial to parallel (S/P) converter, and a CP remover are then applied to the received signal to produce the discrete time domain signal y_m [1]. Thereafter, the received frequency domain signal Y_k can be obtained by performing an CS-SCHT operation on the time-domain signal y_m [1]. Due to the mutual interference between ACO-CS-CHCM and VBO-CS-CHCM signals being eliminated at the transmitter with the pre-distortion process, we can directly recover each signal from the even and odd sub-carriers of Y_k separately. Further, the signal Y_k can be divided into odd subcarriers $Y_{odd,k}$ and even subcarriers $Y_{eve,k}$ after the equalization processes respectively.

Therefore, the upper layer signal $Y_{ACO,k}$ can be obtained directly from the $Y_{odd,k}$ by multiplying with a factor of two to compensate for the asymmetrical clipping noise, and it is given in [89] as $Y_{\mathrm{ACO,k}} = 2Y_{odd,k}, \forall k$ which is equivalent to,

$$Y_{\mathrm{ACO,k}} = X_{odd,k}, \forall k \tag{6.19}$$

Further, the VBO-CS-CHCM signal $Y_{VBO,k}$ can be obtained directly from the $Y_{eve,k}$ and it can be represented as $Y_{VBO,k} = Y_{eve,k}$. According to *Theorem 1* in previous chapter, the resulted signal occupies only the $4p$-th located subcarriers and hence the resulting signal $Y_{VBO,k}$ can be expressed as,

$$Y_{VBO,k} = \begin{cases} X_{eve,k}, & k = 2p+1 \\ X_{eve,k}, & k = 2(2p+1) \\ V_k, & k = 4p \end{cases} \tag{6.20}$$

where, $p = 0, 1, ..., M/8 - 1$ and V_k represents the IFFT of variably biased sequence v_m. From the symbol structure shown in Fig. 6.2 (c), the odd components of signal $X_{eve,k}$ for $k = 2p + 1$ are set to zero before the transmission taken palce. Therefore, the effective $Y_{VBO,k}$ signal can be directly obtained from the $k = 2(2p + 1)$-th positioned subcarriers which are interference-free caused by the variably biased sequence.

Thereafter, by reframing the $Y_{ACO,k}$ and $Y_{VBO,k}$ and removing the HS, extracting subcarriers, one can obtain the corresponding QAM symbols which can be inversely mapped and further processed for S/P conversion to attain the actual output bit stream.

6.3.3 CC Analysis

The proposed VAO-CS-CHCM offers several advantages over other modulation schemes, including reduced interference between VBO-CS-CHCM and ACO-CS-CHCM, as well as improved PE. In terms of CC, the VAO-CS-CHCM exhibits some trade-offs. The transmitter section experiences a slight increase in CC due to the pre-distortion process, which is necessary to achieve the desired modulation characteristics. On the other hand, the receiver CC is significantly reduced when compared to the traditional VAO-OFDM and ADO-OFDM.

To evaluate the computational requirements of different modulation schemes, we focused on two key operations: CAs and CMs. In M-point FFT/IFFT-based optical OFDM systems, each FFT/IFFT block in the system architecture requires $M\log_2^M$of CAs and $\frac{M}{2}\log_2^M$ CMs. In contrast, M-point CS-SCHT/ICS-SCHT schemes employ a different approach. These schemes consist of $b = \log_2^M$ stages, with each stage requiring a set of additions/subtractions. Each stage needs M additions/subtractions to process the complex input data. The total computational requirements for complex input data are $M\log_2^M$ additions/subtractions and

$$2^0 + 2^1 + 2^2 + ...2^{b-2} = \frac{1-2^{b-1}}{1-2} = 2^{b-1} - 1 = \left(\frac{M}{2} - 1\right) \tag{6.21}$$

number of Complex multiplications are required for each SCHT/ICS-SCHT block in the system architecture.

Considering the overall system architecture, the proposed VAO-CS-CHCM and VAO-OFDM consist of four SCHT/ICS-SCHT and FFT/IFFT blocks, respectively. In contrast, the traditional ADO-OFDM utilizes six FFT/IFFT blocks. Consequently, the VAO-CS-CHCM requires $4M\log_2^M$ CAs and $M\log_2^M$ CMs, while the VAO-OFDM requires $4M\log_2^M$ CAs and $2M\log_2^M$ CMs. The traditional ADO-OFDM, with its six FFT/IFFT blocks, necessitates $6M\log_2^M$ CAs and $3M\log_2^M$ CMs. Overall, the proposed VAO-CS-CHCM exhibits a significant reduction in CC when compared to both VAO-OFDM and traditional ADO-OFDM schemes. Further, the CC reduction ratio is evaluated for the proposed VAO-CS-CHAM with respect to VAO-OFDM and ADO-OFDM for the different number of subcarriers and tabularized in Table 6.1. This reduction in CC makes the VAO-CS-CHCM as an attractive choice for practical implementations.

Table 6.1: Comparison of Computational Complexity in terms of Complex Multiplications (CMs)

Sub. (M)	ADO-OFDM $6\left(\frac{M}{2}\log_2^M\right)$	VAO-OFDM $4\left(\frac{M}{2}\log_2^M\right)$	VAO-CS-CHCM $4\left(\frac{M}{2}-1\right)$	CCRR w.r.t. ADO-OFDM	CCRR w.r.t. VAO-OFDM
64	1152	758	124	89.23	83.64
128	2688	1792	252	90.62	85.93
256	6144	4096	508	91.73	87.93
512	13824	9216	1020	92.62	88.93
1024	3072	20480	2044	93.33	90.01
2048	67584	45056	4092	93.94	90.91

6.4 Results and Discussion

This section presents an analysis of the simulation outcomes for the VAO-CS-CHCM modulation, in contrast to the VAO-OFDM, ADO-OFDM, ACO-OFDM, and DCO-OFDM techniques. The simulation parameters utilized in this evaluation are presented in Table 6.2.

Table 6.2: Simulation parameters

Parameter	**Values**
QAM orders	4, 8, 16, 32, 64, 128, 256
Sub-carriers (M)	128
OFDM Symbols	10^5
CP length	8
DC bias for ADO-OFDM and DCO-OFDM	7 dB

During the simulation process, we utilized a total of 10^5 OFDM symbols. Each OFDM symbol consisted of 128 subcarriers and was loaded with varying QAM orders, namely 4, 8, 16, 32, 64, 128, and 256 symbols. To ensure a fair comparison, Monte-

Carlo simulations were conducted on several modulation schemes, including DCO-OFDM, ACO-OFDM, ADO-OFDM, VAO-OFDM and the proposed VAO-CS-CHCM. In our simulations, we employed a cyclic prefix (CP) with a length of 8. For DCO-OFDM and ADO-OFDM, a DC-bias of $7dB$ was applied. Additionally, we utilized a normalized optical-bit-energy-to-noise-power ratio, denoted as $E_{b(opt)}/N_0$, which was obtained by setting the optical power to unity and also defined the required normalized $E_{b(opt)}/N_0$ for an acceptable bit error rate (BER) of 10^{-3} as $< E_{b(opt)}/N_0 >_{BER}$. The performance evaluation primarily focused on the bit error rate (BER) as a function of the normalized optical-bit-energy-to-noise-power ratio, $E_{b(opt)}/N_0$. Subsequently, the performance of the modulation schemes was assessed in terms of $< E_{b(opt)}/N_0 >_{BER}$ with respect to the constellation orders, while maintaining an acceptable BER of 10^{-3}.

Finally, the performance of the VAO-CS-CHCM and the compared modulation schemes are evaluated in terms of $< E_{b(opt)}/N_0 >_{BER}$ against the bitrate/normalized bandwidth. Whereas the modulation bandwidths of the compared modulation schemes are considered from [1,35]. In VAO-OFDM and VAO-CS-CHCM modulation schemes, the upper and lower layers utilize the $\frac{M}{4}$ and $\frac{M}{8}$ effective subcarriers respectively. Therefore, the bitrate/normalized bandwidth of the VAO-OFDM is obtained as $(2\log_2 N_{ACO} + \log_2 N_{VBO})$ / $4\left(1+\frac{2}{M}\right)$ where N_{ACO} represents the QAM constellation orders of the ACO-OFDM and ACO-CS-CHCM, and N_{VBO} represents the QAM constellation order of the VBO-OFDM and VBO-CS-CHCM.

Figure 6.3 presents a comparison of the simulation results among three modulation techniques: VAO-CS-CHCM, VAO-OFDM, and ADO-OFDM, with respect to the bit error rate (BER) against the $E_{b(opt)}/N_0$. It is evident from Figure 6.3 that the VAO-CS-CHCM outperforms both VAO-OFDM and ADO-OFDM in terms of BER. Analyzing Fig. 6.3 in more detail, we can observe that the VAO-CS-CHCM achieves superior performance compared to VAO-OFDM and ADO-OFDM at a BER value of 10^{-3}. Specifically, the VAO-CS-CHCM demonstrates a signal-to-noise ratio (SNR) improvement of $4dB$ and $14dB$ over VAO-OFDM and ADO-OFDM, respectively. One notable advantage of VAO-CS-CHCM and VAO-OFDM over ADO-OFDM is the absence of error propagation. In ADO-OFDM, errors occurring in the asymmetrically clipped portion of the signal can propagate and degrade the overall performance. In contrast, VAO-CS-CHCM and

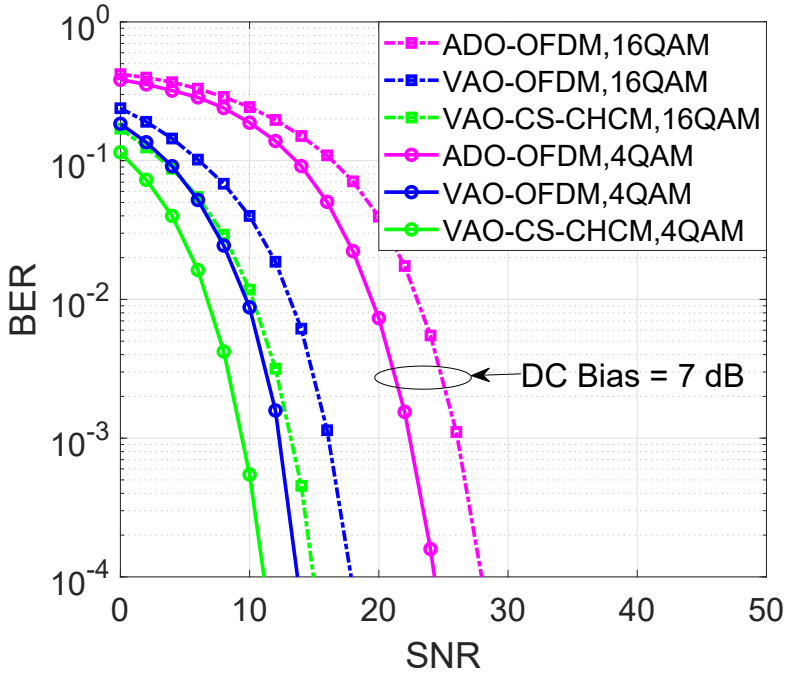

Figure 6.3: Simulation: BER performance of the VAO-CS-CHCM in comparision with VAO-OFDM and ADO-OFDM

VAO-OFDM employ a pre-distortion process where the asymmetrical clipping noise is subtracted from the VBO-CS-CHCM signal in the frequency domain, which is similar to VBO-OFDM. This pre-distortion technique effectively mitigates the mutual interference caused by error propagation, resulting in improved performance for both VAO-CS-CHCM and VAO-OFDM when compared to ADO-OFDM.

Figure 6.4 illustrates the relationship between the average energy per bit to noise power spectral density ratio ($< E_{b(opt)}/N_0 >_{BER}$) and the constellation orders, considering a target bit error rate (BER) of 10^{-3}. In the case of DCO-OFDM and ADO-OFDM, a DC bias of $7dB$ is added to ensure the signal is real and non-negative. From the plot, it is evident that VAO-CS-CHCM and VAO-OFDM exhibit lower $< E_{b(opt)}/N_0 >_{BER}$ values compared to ADO-OFDM, primarily due to the additional DC-bias employed by ADO-OFDM. For example, when using 4-QAM, VAO-CS-CHCM achieves a power gain of $14dB$ and $4dB$ over ADO-OFDM and VAO-OFDM, respectively. Notably, VAO-CS-CHCM outperforms ACO-OFDM, DCO-OFDM, ADO-OFDM, and VAO-OFDM in terms of performance. Furthermore, the plot in Figure 6.4 reveals a linear and parallel trend among the curves, indicating that the rate of change in $< E_{b(opt)}/N_0 >_{BER}$ is similar

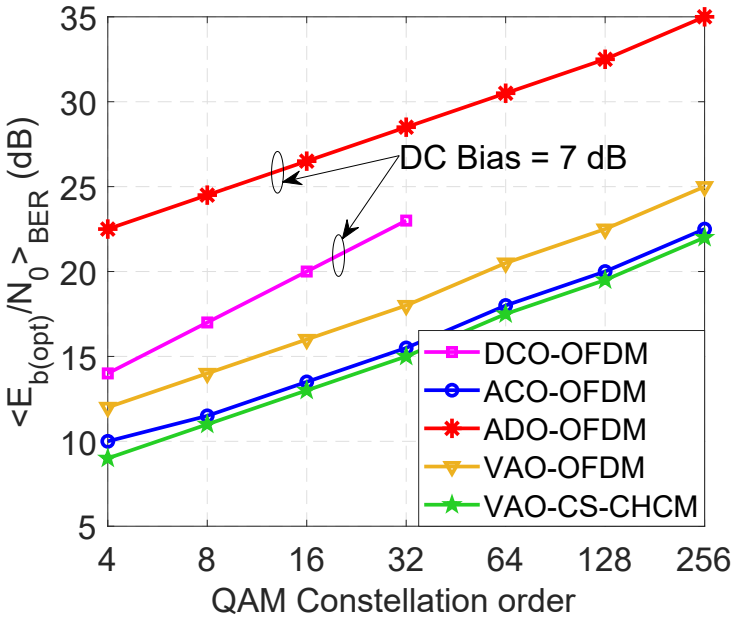

Figure 6.4: Simulation: $< E_{b(opt)}/N_0 >_{BER}$ comarision against distinct constellations.

for DCO-OFDM, ACO-OFDM, ADO-OFDM, VAO-OFDM, and VAO-CS-CHM, respectively.

Figure 6.5 illustrates the plots depicting the relationship between the average energy per bit to noise power spectral density ratio ($< E_{b(opt)}/N_0 > BER$) and the bitrate/normalized bandwidth for various optical OFDM schemes, namely DCO-OFDM, ACO-OFDM, ADO-OFDM, VAO-OFDM, and the proposed VAO-CS-CHCM. In the case of DCO-OFDM and ADO-OFDM, a DC bias of $7dB$ is added to ensure the signal is real and non-negative, thereby eliminating nonlinear clipping distortion. Observing Figure 6.5, it becomes apparent that VAO-CS-CHCM surpasses both VAO-OFDM and ADO-OFDM in terms of $< Eb(opt)/N_0 > BER$. Specifically, to achieve a bitrate/normalized bandwidth of $3bit/s/Hz$, VAO-CS-CHCM requires a lower $< Eb(opt)/N_0 > BER$ of $13dB$ for 16-QAM constellations, while VAO-OFDM and ADO-OFDM require higher $< Eb(opt)/N_0 >_{BER}$ values of $16dB$ and $25dB$ for 16-QAM and 8-QAM constellations respectively. Comparatively, VAO-CS-CHCM outperforms ADO-OFDM and VAO-OFDM, achieving a power gain of $12dB$ and $3dB$, respectively, at a bitrate/normalized bandwidth of 3 bit/s/Hz. Additionally, Figure 6.5 reveals that VAO-CS-CHCM surpasses ACO-OFDM and DCO-OFDM with a DC bias of $7dB$. For instance, to achieve the same bitrate/normalized bandwidth of 3 bit/s/Hz, VAO-CS-CHCM requires a lower

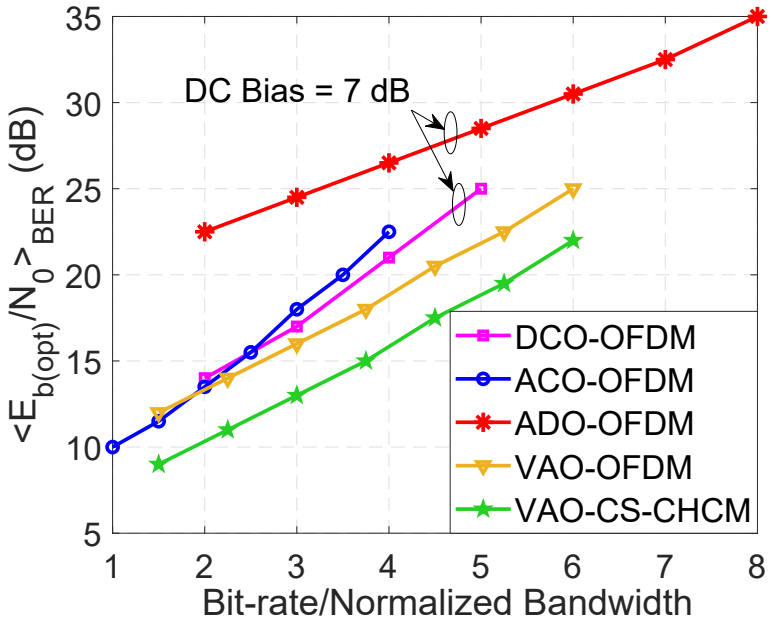

Figure 6.5: Simulation: $< E_{b(opt)}/N_0 >_{BER}$ comparision against bitrate/ normalized bandwidth.

$< E_{b(opt)}/N_0 > BER$ of $13dB$ for 16-QAM constellations, while DCO-OFDM demands a higher $< Eb(opt)/N_0 > BER$ of $17dB$ for 8-QAM constellations, resulting in a power gain of 4 dB for VAO-CS-CHCM over DCO-OFDM. Furthermore, ACO-OFDM requires a higher $< Eb(opt)/N_0 >_{BER}$ of $18dB$ for 64-QAM constellations, indicating that VAO-CS-CHCM achieves a power gain of $5dB$ over ACO-OFDM. Based on these findings, VAO-CS-CHCM demonstrates superior PE compared to ACO-OFDM, DCO-OFDM, ADO-OFDM, and VAO-OFDM, as well as improved SE compared to ACO-OFDM. Although there exists a trade-off between SE and PE, the proposed VAO-CS-CHCM achieves higher bit-rate/normalized bandwidth at lower $< E_{b(opt)}/N_0 >_{BER}$ values when compared to VAO-OFDM, ADO-OFDM, ACO-OFDM, and DCO-OFDM.

6.5 Summary

In this chapter, a novel modulation scheme called VAO-CS-CHCM is proposed for VLC systems. The objective of this scheme is to enhance PE by leveraging the benefits of a discrete set of amplitudes generated through CS-SCHT. VAO-CS-CHCM introduces a new approach to bias design like in VAO-OFDM, where the bias is dependent on specific

sample amplitudes. Additionally, the frequency domain signals of VAO-CS-CHCM are distributed across $4pth$-located subcarriers, similar to the VAO-OFDM scheme which is initiated in the previous chapter. This VAO-CS-CHCM ensures that the originally transmitted symbols remain unaffected by any interference, resulting in significant gains in PE. Simulation results are presented to evaluate the performance of VAO-CS-CHCM. It is observed that VAO-CS-CHCM outperformed both VAO-OFDM and ADO-OFDM schemes at a BER of 10^{-3}. This finding states that VAO-CS-CHCM requires a lower energy per bit to noise power spectral density ratio ($E_{b(opt)}/N_0$) compared to VAO-OFDM and ADO-OFDM. However, it is worth noting that there is a trade-off between SE and PE in VAO-CS-CHCM.

Furthermore, VAO-CS-CHCM exhibits superior PE when compared to traditional modulation schemes such as VAO-OFDM, DCO-OFDM, ACO-OFDM, and ADO-OFDM over a wide range of bit rates and normalized bandwidths. This demonstrates the effectiveness of VAO-CS-CHCM in achieving efficient power utilization in VLC systems. Additionally, the CCof VAO-CS-CHCM is analyzed in comparison to VAO-OFDM and ADO-OFDM. It is found that the CS-SCHT-based VAO-CS-CHCM scheme offers lower CC, particularly in terms of complex multiplications, making it a favourable choice for practical implementation.

Chapter 7

Conclusions and Future Scope

7.1 Conclusions

The innovation of new physical layer waveforms for IM/DD systems, particularly in VLC applications, is crucial to overcome challenges related to SE, PE, flexibility, and quality of service. In this thesis, through extensive investigation and experimentation, we aim to improve the performance and efficiency of optical communication systems, ultimately enhancing the capabilities and reliability of these systems in various practical scenarios.

Primarily, the first contribution which is given in the third chapter of this thesis, is introduced a novel technique called TSDA for reducing PAPR in DCO-OFDM systems. One notable advantage of the TSDA scheme is that it does not require any side information, unlike existing techniques such as SLM and PTS. By eliminating the need for side information, the TSDA technique simplified the implementation process. Furthermore, the TSDA technique not only enhanced PAPR reduction performance but also reduced the computational complexity compared to conventional SLM and PTS techniques. The lower computational complexity of the TSDA scheme makes it more efficient in terms of resource utilization. An implicit advantage of the reduced computational complexity is a decrease in processing delay. This aspect is particularly beneficial in real-time implementations where timely signal transmission is crucial.

Subsequently, the second contribution which is given in the fourth chapter of this

thesis, is proposed a new modulation technique called LADO-OFDM for VLC systems to meet the specifications of 5G networks, including low computing complexity and latency. The main objective of the LADO-OFDM scheme is to address the issue of mutual interference between two existing modulation techniques used in VLC systems, namely, DCO-OFDM and ACO-OFDM. By employing a pre-distortion technique, the LADO-OFDM scheme aims to mitigate this mutual interference. This chapter also investigated the performance of the proposed LADO-OFDM scheme under two generalized LED models. Specifically, the study examined the effects of nonlinear clipping distortion on the LED's dynamic range and bias point. It is observed that a larger dynamic range of LEDs leads to better performance. To achieve a linearized LED dynamic range, the transmitted signal is pre-distorted using a piecewise polynomial model or by increasing the knee factor in Rapp's model. Monte-Carlo simulations are conducted to evaluate the Bit Error Rate (BER) performance of the LADO-OFDM scheme compared to ADO-OFDM and PAM-DMT schemes under the effect of LED nonlinearity. The results show that the proposed LADO-OFDM scheme outperforms the traditional ADO-OFDM and PAM-DMT schemes in terms of BER, computing complexity, and latency in the presence of LED nonlinearity. In summary, this chapter introduces the LADO-OFDM modulation technique for VLC systems, which aims to reduce computing complexity and latency by mitigating mutual interference between DCO-OFDM and ACO-OFDM. The scheme achieved improved BER performance under LED nonlinearity and outperforms traditional modulation schemes in terms of various performance metrics.

Furtherly, the third contribution which is given in the fifth chapter of this thesis proposed a novel modulation scheme called VAO-OFDM for VLC systems. The main aim of this modulation scheme is to improve PE in VLC systems. In VAO-OFDM, a new bias is introduced in such a way that it depends on specific sample amplitudes. The frequency domain signals with this bias are placed on pre-defined subcarriers. This bias design ensures that the biased signals do not interfere with the originally transmitted symbols, resulting in improved PE. Simulation results show that VAO-OFDM outperformed ADO-OFDM. Furthermore, VAO-OFDM exhibits better PE compared to traditional modulation schemes such as DCO-OFDM, ACO-OFDM, and ADO-OFDM over a wide range of bit rates or normalized bandwidths. Experimental results confirm the simulation findings and demonstrated that VAO-OFDM outperformed ADO-OFDM

in terms of BER for different transmitter-receiver separations in centimetres. It is also noted that both VAO-OFDM and ADO-OFDM with a signal bandwidth of 1 MHz outperformed those with a signal bandwidth of 2 MHz. However, even with different signal bandwidths, VAO-OFDM consistently achieved better BER performance compared to ADO-OFDM. Additionally, VAO-OFDM offers the advantage of low computational complexity compared to traditional ADO-OFDM. Moreover, the experimental setup includes a driver circuit that reduces the system cost by eliminating the need for an additional bias tee.

Finally, the fourth contribution which is given in the sixth chapter of this thesis proposed a novel modulation scheme called VAO-CS-CHCM for VLC systems. The main objective of this scheme is to enhance PE by leveraging the benefits of a discrete set of amplitudes generated through CS-SCHT. VAO-CS-CHCM introduced a new approach to bias design like in VAO-OFDM, where the bias is dependent on specific sample amplitudes. Additionally, the frequency domain signals of VAO-CS-CHCM are distributed across pre-defined subcarriers. This VAO-CS-CHCM ensures that the originally transmitted symbols remain unaffected by any interference, resulting in significant gains in PE. Simulation results are presented to evaluate the performance of VAO-CS-CHCM. It is observed that VAO-CS-CHCM outperformed both VAO-OFDM and ADO-OFDM schemes. However, it is worth noting that there is a trade-off between SE and PEin VAO-CS-CHCM. Furthermore, VAO-CS-CHCM exhibits superior PE when compared to traditional modulation schemes such as VAO-OFDM, DCO-OFDM, ACO-OFDM, and ADO-OFDM over a wide range of bit rates and normalized bandwidths. This demonstrates the effectiveness of VAO-CS-CHCM in achieving efficient power utilization in VLC systems. Additionally, the computational complexity of VAO-CS-CHCM is analyzed in comparison to VAO-OFDM and ADO-OFDM. It is found that the CS-SCHT-based VAO-CS-CHCM scheme offers lower computational complexity, particularly in terms of complex multiplications, making it a favourable choice for practical implementation.

7.2 Future Scope

Although the thesis explores proposed modulations to enhance PE and reduce the computational complexity in IM/DD-based VLC systems, there are several other unresolved issues that require further investigation. The following are key areas that necessitate future research:

- Spectrally efficient and low-complexity transceiver solutions for the modulation schemes need exploration to address the trade-off between improved PE and reduced SE, memory requirements, and signal processing costs.
- The performance of the proposed modulation schemes should be assessed in realistic channel conditions, particularly under sunlight. Additionally, the feasibility of employing MIMO systems with these modulations requires substantial attention in future studies.
- To enhance the experimental testbed, it is crucial to explore the development of a more sophisticated driver circuit capable of driving LEDs at higher frequencies.
- The improvement of data rates relies on the utilization of advanced LEDs with enhanced modulation bandwidth capabilities and highly sensitive photodiodes that can mitigate noise effects. Therefore, further research is necessary in the design of LEDs and photodiodes to address this aspect.

Furthermore, the VAO-CS-CHCM concept can be extended in various directions. Some potential extensions include: Spectrally-enhanced unipolar OFDM techniques, such as ACO-OFDM, PAM-DMT, and Flip-OFDM, can be explored to improve SE by minimizing rate loss. Methods like layered ACO-OFDM (LACO-OFDM) have shown promise and can be further investigated [28].

- ACO-CS-CHCM, obtained by replacing IFFT with CS-SCHT in the ACO-OFDM modulation, presents a novel modulation scheme where parallel data streams are first ACO-OFDM modulated and then processed.
- LACO-OFDM utilizes a partitioning of subcarriers into distinct layers, each modulated by various types of ACO-OFDM, and these layers are merged for concurrent

transmission [30]. The CS-SCHT can also adopt a similar approach: by partitioning the Complex Hadamard matrix into multiple layers, each layer can be modulated using different dimensions of ACO-CS-CHCM, and eventually combined for simultaneous transmission. This innovative technique is referred to as LACO-CS-CHCM.

- Hybrid methods like HACO-OFDM, which combines ACO-OFDM on odd subcarriers and PAM-DMT on even subcarriers, can be explored to improve bandwidth efficiency. Similar ideas can be explored by combining ACO-CS-CHCM with PAM-DMT.

- ACO-CS-CHCM and VAO-CS-CHCM are well-suited for integration with the spatial summation architecture, where different layers are transmitted via separate light sources and superposition occurs in the medium. This architectural aspect is worth exploring in future work [34], [35].

Publications

List of International Journals:

1. **Ganesh Miriyala** and V. V. Mani, "A new PAPR reduction technique in DCO-OFDM for visible light communication systems", *Optics Communications*, Volume 474, 2020, 126064. (**SCI-Elsevier**)

2. **Ganesh Miriyala** and V. V. Mani, "A nonlinear Modelled Low-complex ADO-OFDM for Visible Light Communication Systems", *Optik*, Volume 246, 2021, 167831, ISSN 0030-4026, https://doi.org/10.1016/j.ijleo.2021.167831. (**SCI-Elsevier**)

3. **Ganesh Miriyala** and V. V. Mani, "Real-Time Implementation of a Variably Biased Asymmetrically Clipped Optical OFDM with Pre-Distortion for VLC Systems", *IEEE Trans. on Green Comm. and Networking.* (**Under Review**)

4. **Ganesh Miriyala** and V. V. Mani, "Conjugate-symmetric Sequency-ordered Complex Hadamard Coded Modulation for VLC Systems", *IEEE Wireless Communications Letters.* (**Communicated**)

List of International Conferences:

1. **Ganesh Miriyala** and V. V. Mani, "Peak Sample Detection based PAPR Reduction Algorithm in Optical-OFDM for VLC Systems," 2021 *24th Intl. Symposium on Wireless Personal Multimedia Commu. (WPMC)*, Okayama, Japan, 2021, pp. 1-6, doi: 10.1109/WPMC52694.2021.9700470.(**IEEE Conf.**)

2. **Ganesh Miriyala**, and V. V. Mani, "Demonstration of a Variably Biased Asymmetrically Clipped Optical OFDM for VLC Systems," 28th IEEE Asia-Pacific Conference on Communications (APCC) (**Under Review**)

Appendix A

Theorem 1 Proof

In this appendix, we will provide the proof of the *Theorem 1.*

The time domain signal $\{v_m\}_{m=0}^{M-1}$ satisfies the new bias structure given in (5.12). And the frequency domain signals representation of the $\{v_m\}_{m=0}^{M-1}$ can be obtained by taking the IFFT of $\{v_m\}_{m=0}^{M-1}$ signal, and it is expressed as,

$$V_k = \frac{1}{\sqrt{M}} \sum_{m=0}^{M-1} v_m W_M^{km}, \text{ for } k = 0, 1, ..., M-1, \tag{A.1}$$

where $W_M = \exp\left(\frac{-j2\pi}{M}\right)$ is the twiddle factor in FFT. Further (A.1) can be equivalently simplified as,

$$V_k = \frac{1}{\sqrt{M}} \sum_{m=0}^{\frac{M}{4}-1} \left(v_m W_M^{km} + v_{m+\frac{M}{4}} W_M^{\left(m+\frac{M}{4}\right)k} + v_{m+\frac{M}{2}} W_M^{\left(m+\frac{M}{2}\right)k} + v_{m+\frac{3M}{4}} W_M^{\left(m+\frac{3M}{4}\right)k} \right). \tag{A.2}$$

Further (A.1) can be equivalently simplified as,

$$V_k = \frac{1}{\sqrt{M}} \sum_{m=0}^{\frac{M}{4}-1} W_M^{km} \left(v_m + v_{m+\frac{M}{4}} W_M^{\left(\frac{M}{4}\right)k} + v_{m+\frac{M}{2}} W_M^{\left(\frac{M}{2}\right)k} + v_{m+\frac{3M}{4}} W_M^{\left(\frac{3M}{4}\right)k} \right). \tag{A.3}$$

From (5.12), (A.3) can be expressed as,

$$V_k = \frac{1}{\sqrt{M}} \sum_{m=0}^{\frac{M}{4}-1} v_m W_M^{km} \left(\sum_{p=0}^{3} W_M^{\left(\frac{pM}{4}\right)k} \right). \tag{A.4}$$

Let's consider the portion of (A.4) and expressed as,

$$\sum_{p=0}^{3} W_M^{\left(\frac{pM}{4}\right)k} = W_M^0 + W_M^{\left(\frac{M}{4}\right)k} + W_M^{\left(\frac{M}{2}\right)k} + W_M^{\left(\frac{3M}{4}\right)k}. \tag{A.5}$$

By substiting the $W_M = \exp\left(\frac{-j2\pi}{M}\right)$ in (A.5) results in

$$\sum_{p=0}^{3} W_M^{\left(\frac{pM}{4}\right)k} = \exp(0) + \left(\exp\left(\frac{-j\pi}{2}\right)\right)^k + (\exp(-j\pi))^k + \left(\exp\left(\frac{-j3\pi}{2}\right)\right)^k. \quad \text{(A.6)}$$

Putting $\exp(0) = 1$, $\exp\left(\frac{-j\pi}{2}\right) = -j$, $\exp(-j\pi) = -1$ and $\exp\left(\frac{-j3\pi}{2}\right) = j$ in (A.6) results in

$$\sum_{p=0}^{3} W_M^{\left(\frac{pM}{4}\right)k} = 1 + (-j)^k + (-1)^k + (j)^k. \quad \text{(A.7)}$$

For odd values of k, i.e., $k = 2r + 1$ for $r = 0, 1, ..., M/2 - 1$, the (A.7) resulted in

$$\begin{aligned}\sum_{p=0}^{3} W_M^{\left(\frac{pM}{4}\right)k} &= 1 + (-j)^{2r+1} + (-1)^{2r+1} + (j)^{2r+1} \\ &= 1 - j - 1 + j \\ &= 0 \text{ for odd } k. \end{aligned} \quad \text{(A.8)}$$

For $k = 2(2r + 1)$ where $r = 0, 1, ..., M/8 - 1$, the (A.7) results,

$$\begin{aligned}\sum_{p=0}^{3} W_M^{\left(\frac{pM}{4}\right)k} &= 1 + (-j)^{2(2r+1)} + (-1)^{2(2r+1)} + (j)^{2(2r+1)} \\ &= 1 + \left((-j)^2\right)^{(2r+1)} + \left((-1)^2\right)^{(2r+1)} + \left((j)^2\right)^{(2r+1)} \\ &= 0 \text{ for } k = 2(2r + 1). \end{aligned} \quad \text{(A.9)}$$

For $k = 4r$ where $r = 0, 1, ..., M/8 - 1$, the (A.7) resulted in

$$\begin{aligned}\sum_{p=0}^{3} W_M^{\left(\frac{pM}{4}\right)k} &= 1 + (-j)^{4r} + (-1)^{4r} + (j)^{4r} \\ &= 1 + \left((-j)^2\right)^{2r} + \left((-1)^2\right)^{2r} + \left((j)^2\right)^{2r} \\ &= 4 \text{ for } k = 4r. \end{aligned} \quad \text{(A.10)}$$

Putting the (A.8), (A.9), and (A.10) in the (A.4) can be resulted as,

$$V_k = \frac{4}{\sqrt{M}} \sum_{m=0}^{\frac{M}{4}-1} v_m W_M^{km}, k = 4r, \text{ for } r = 0, 1, ..., M/8 - 1. \quad \text{(A.11)}$$

From (A.8) and (A.9), we can conclude that the signal V_k is the FD signal of v_m is attained zeros at the odd and $2(2p + 1)$-th positioned subcarriers, and (A.10) show that the FFT results of v_m only fall on the $4p$-th positioned subcarriers.

Bibliography

[1] S. D. Dissanayake, K. Panta, and J. Armstrong, "A novel technique to simultaneously transmit aco-ofdm and dco-ofdm in im/dd systems," in *2011 IEEE GLOBECOM Workshops (GC Wkshps)*, 2011, pp. 782–786.

[2] International Telecommunication Union (ITU), "IMT Traffic estimates for the years 2020 to 2030," *retrieved from https://www.itu.int/pub/R-REP-M.2370-2015*, July-2015.

[3] Indianexpress, "5g spectrum auction slated for mar-apr; dot panel rules against reserve price cut," *retrieved from https://indianexpress.com/article/business/economy/5g-spectrum-auction-slated-for-mar-apr-dot-panel-rules-against-reserve-price-cut-6177804/*, 22 December 2019.

[4] V. Chandrasekhar, J. G. Andrews, and A. Gatherer, "Femtocell networks: a survey," *IEEE Communications Magazine*, vol. 46, no. 9, pp. 59–67, 2008.

[5] T. Cogalan and H. Haas, "Why would 5g need optical wireless communications?" in *2017 IEEE 28th Annual International Symposium on Personal, Indoor, and Mobile Radio Communications (PIMRC)*, 2017, pp. 1–6.

[6] A. N. Uwaechia and N. M. Mahyuddin, "A comprehensive survey on millimeter wave communications for fifth-generation wireless networks: Feasibility and challenges," *IEEE Access*, vol. 8, pp. 62 367–62 414, 2020.

[7] F. Gfeller and U. Bapst, "Wireless in-house data communication via diffuse infrared radiation," *Proceedings of the IEEE*, vol. 67, no. 11, pp. 1474–1486, 1979.

[8] C. Lee, C. Shen, C. Cozzan, R. M. Farrell, S. Nakamura, A. Y. Alyamani, B. S. Ooi, J. E. Bowers, S. P. DenBaars, and J. S. Speck, "Semipolar GaN-based laser diodes for Gbit/s white lighting communication: devices to systems," in *Gallium Nitride Materials and Devices XIII*, J.-I. Chyi, H. Fujioka, and H. Morkoç, Eds., vol. 10532, International Society for Optics and Photonics. SPIE, 2018, p. 105321N. [Online]. Available: `https://doi.org/10.1117/12.2315791`

[9] N. Holonyak and S. F. Bevacqua, "Coherent (visible) light emission from ga(as 1 x p x) junctions," *Applied Physics Letters*, vol. 1, no. 4, pp. 82–83, 1962. [Online]. Available: `https://app.dimensions.ai/details/publication/pub.1057814151`

[10] I. Eliashevich, Y. Li, A. Osinsky, C. A. Tran, M. G. Brown, and R. F. Karlicek, "Ingan blue light-emitting diodes with optimized n-gan layer," in *SPIE Proceedings*, vol. 3621. SPIE, April 1999, pp. 28–36.

[11] S. Rajagopal, R. D. Roberts, and S.-K. Lim, "IEEE 802.15.7 visible light communication: modulation schemes and dimming support," *IEEE Communications Magazine*, vol. 50, no. 3, pp. 72–82, 2012.

[12] M. P. S. L. S. C. N. K. D. C. G. P. A. M. C. J. M. F. M. R. V. J. D. K. N. Sera movski, R. Lacroix and H. Haas, "Light communications for wireless local area networking," *IEEE 5G Tech Focus*, vol. 2, May 2018.

[13] J. Kahn and J. Barry, "Wireless infrared communications," *Proceedings of the IEEE*, vol. 85, no. 2, pp. 265–298, 1997.

[14] J. Armstrong and B. J. Schmidt, "Comparison of asymmetrically clipped optical ofdm and dc-biased optical ofdm in awgn," *IEEE Communications Letters*, vol. 12, no. 5, pp. 343–345, 2008.

[15] D. Tsonev, S. Sinanovic, and H. Haas, "Novel unipolar orthogonal frequency division multiplexing (u-ofdm) for optical wireless," in *Proc. of the IEEE 75th Vehicular Technology Conference (VTC Spring)*, 2012, pp. 1–5.

[16] N. Fernando, Y. Hong, and E. Viterbo, "Flip-ofdm for unipolar communication systems," *IEEE Transactions on Communications*, vol. 60, no. 12, pp. 3726–3733, 2012.

[17] N. Huang, J.-B. Wang, J. Wang, C. Pan, H. Wang, and M. Chen, "Receiver design for pam-dmt in indoor optical wireless links," *IEEE Photonics Technology Letters*, vol. 27, no. 2, pp. 161–164, 2015.

[18] R. Zhang and L. Hanzo, "Multi-layer modulation for intensity-modulated direct-detection optical ofdm," *Journal of Optical Communications and Networking*, vol. 5, no. 12, pp. 1402–1412, 2013.

[19] D. Tsonev, S. Videv, and H. Haas, "Unlocking spectral efficiency in intensity modulation and direct detection systems," *IEEE Journal on Selected Areas in Communications*, vol. 33, no. 9, pp. 1758–1770, 2015.

[20] H. Elgala, R. Mesleh, and H. Haas, "Predistortion in optical wireless transmission using ofdm," in *2009 Ninth International Conference on Hybrid Intelligent Systems*, vol. 2, 2009, pp. 184–189.

[21] S. P. valluri and V. V. Mani, "Demonstration of effect of oversampling on jitter removal for multitaper gfdm system using sdr," in *2018 International Conference on Advanced Technologies for Communications (ATC)*, 2018, pp. 168–173.

[22] N. Shuji and G. Fasol, "The Blue Laser Diode : Gan Based Light Emitters and Lasers." Berlin: Springer, 1997. [Online]. Available: `https://doi.org/10.1007/978-3-662-03462-0`

[23] Y. Tanaka, S. Haruyama, and M. Nakagawa, "Wireless optical transmissions with white colored led for wireless home links," in *11th IEEE International Symposium on Personal Indoor and Mobile Radio Communications. PIMRC 2000. Proceedings (Cat. No.00TH8525)*, vol. 2, 2000, pp. 1325–1329 vol.2.

[24] H. Haas, L. Yin, Y. Wang, and C. Chen, "What is lifi?" *Journal of Lightwave Technology*, vol. 34, no. 6, pp. 1533–1544, 2016.

[25] D. Karunatilaka, F. Zafar, V. Kalavally, and R. Parthiban, "Led based indoor visible light communications: State of the art," *IEEE Communications Surveys & Tutorials*, vol. 17, no. 3, pp. 1649–1678, 2015.

[26] I. S. Ramirez-Iniguez, R. and Z. Sun, "Optical Wireless Communications: IR for Wireless Connectivity." Auerbach Publications, 2008. [Online]. Available: https://doi.org/10.1201/9781420013443

[27] S. Randel, F. Breyer, S. C. J. Lee, and J. W. Walewski, "Advanced modulation schemes for short-range optical communications," *IEEE Journal of Selected Topics in Quantum Electronics*, vol. 16, no. 5, pp. 1280–1289, 2010.

[28] S. H. Lee, S.-Y. Jung, and J. K. Kwon, "Modulation and coding for dimmable visible light communication," *IEEE Communications Magazine*, vol. 53, no. 2, pp. 136–143, 2015.

[29] Y. Zeng, Y. Chen, H. Zhao, and X. Wang, "Multiple pulse amplitude and position modulation for optical wireless channel," in *2015 Seventh International Conference on Ubiquitous and Future Networks*, 2015, pp. 132–134.

[30] D. J. F. Barros, S. K. Wilson, and J. M. Kahn, "Comparison of orthogonal frequency-division multiplexing and pulse-amplitude modulation in indoor optical wireless links," *IEEE Transactions on Communications*, vol. 60, no. 1, pp. 153–163, 2012.

[31] M. A. Kashani and M. Kavehrad, "On the performance of single- and multi-carrie modulation schemes for indoor visible light communication systems," in *2014 IEEE Global Communications Conference*, 2014, pp. 2084–2089.

[32] C. Wu, H. Zhang, and W. Xu, "On visible light communication using led array with dft-spread ofdm," in *2014 IEEE International Conference on Communications (ICC)*, 2014, pp. 3325–3330.

[33] P. A. Haigh, S. T. Le, S. Zvanovec, Z. Ghassemlooy, P. Luo, T. Xu, P. Chvojka, T. Kanesan, E. Giacoumidis, P. Canyelles-Pericas, H. L. Minh, W. Popoola, S. Rajbhandari, I. Papakonstantinou, and I. Darwazeh, "Multi-band carrier-less amplitude and phase modulation for bandlimited visible light communications systems," *IEEE Wireless Communications*, vol. 22, no. 2, pp. 46–53, 2015.

[34] L. Cimini, "Analysis and simulation of a digital mobile channel using orthogonal frequency division multiplexing," *IEEE Transactions on Communications*, vol. 33, no. 7, pp. 665–675, 1985.

[35] S. D. Dissanayake and J. Armstrong, "Comparison of aco-ofdm, dco-ofdm and ado-ofdm in im/dd systems," *Journal of Lightwave Technology*, vol. 31, no. 7, pp. 1063–1072, 2013.

[36] S. C. J. Lee, S. Randel, F. Breyer, and A. M. J. Koonen, "Pam-dmt for intensity-modulated and direct-detection optical communication systems," *IEEE Photonics Technology Letters*, vol. 21, no. 23, pp. 1749–1751, 2009.

[37] M. S. Islim, D. Tsonev, and H. Haas, "On the superposition modulation for ofdm-based optical wireless communication," in *Proc. of the IEEE Global Conference on Signal and Information Processing (GlobalSIP)*, 2015, pp. 1022–1026.

[38] A. W. Azim, Y. Le Guennec, and G. Maury, "Performance analysis of precoded layered aco-ofdm for visible light communication systems," *Optics Communications*, vol. 440, pp. 49–60, 2019. [Online]. Available: `https://www.sciencedirect.com/science/article/pii/S0030401819301002`

[39] H. Elgala and T. D. C. Little, "See-ofdm: Spectral and energy efficient ofdm for optical im/dd systems," in *2014 IEEE 25th Annual International Symposium on Personal, Indoor, and Mobile Radio Communication (PIMRC)*, 2014, pp. 851–855.

[40] M. Svaluto Moreolo, R. Munoz, and G. Junyent, "Novel power efficient optical ofdm based on hartley transform for intensity-modulated direct-detection systems," *Journal of Lightwave Technology*, vol. 28, no. 5, pp. 798–805, 2010.

[41] M. Noshad and M. Brandt-Pearce, "Hadamard coded modulation: An alternative to ofdm for wireless optical communications," in *2014 IEEE Global Communications Conference*, 2014, pp. 2102–2107.

[42] W. Huang, C. Gong, and Z. Xu, "System and waveform design for wavelet packet division multiplexing-based visible light communications," *Journal of Lightwave Technology*, vol. 33, no. 14, pp. 3041–3051, 2015.

[43] E. Monteiro and S. Hranilovic, "Design and implementation of color-shift keying for visible light communications," *Journal of Lightwave Technology*, vol. 32, no. 10, pp. 2053–2060, 2014.

[44] H. Elgala, R. Mesleh, and H. Haas, "An led model for intensity-modulated optical communication systems," *IEEE Photonics Technology Letters*, vol. 22, no. 11, pp. 835–837, 2010.

[45] S. Dimitrov and H. Haas, "Information rate of ofdm-based optical wireless communication systems with nonlinear distortion," *Journal of Lightwave Technology*, vol. 31, no. 6, pp. 918–929, 2013.

[46] S. Dimitrov, S. Sinanovic, and H. Haas, "Clipping noise in ofdm-based optical wireless communication systems," *IEEE Transactions on Communications*, vol. 60, no. 4, pp. 1072–1081, 2012.

[47] E. Setiawan, T. Adiono, I. N. O. Osahon, and W. O. Popoola, "Experimental demonstration of visible light communication using white led, blue filter and soc based test-bed," in *2019 International Symposium on Electronics and Smart Devices (ISESD)*, 2019, pp. 1–4.

[48] M. S. Islim and H. Haas, "An Experimental Demonstration of an Energy Efficient DMT Technique for LiFi Systems," in *2019 IEEE International Conference on Communications Workshops (ICC Workshops)*, 2019, pp. 1–5.

[49] S. P. Valluri and V. V. Mani, "Investigation of blind cfo estimation for gfdm system using universal software radio peripheral: Theory, simulations and experiments," vol. 13, no. 13, p. 19361944, aug 2019. [Online]. Available: `https://doi.org/10.1049/iet-com.2018.5867`

[50] P. A. Haigh and I. Darwazeh, "Real time implementation of cap modulation with better-than-nyquist pulse shaping in visible light communications," *IEEE Communications Letters*, vol. 24, no. 4, pp. 840–843, 2020.

[51] Q. C. Li, H. Niu, A. T. Papathanassiou, and G. Wu, "5G Network Capacity: Key Elements and Technologies," *IEEE Vehicular Technology Magazine*, vol. 9, no. 1, pp. 71–78, March 2014.

[52] T. Komine and M. Nakagawa, "Fundamental Analysis for Visible-light Communication System using LED Lights," *IEEE Transactions on Consumer Electronics*, vol. 50, no. 1, pp. 100–107, Feb 2004.

[53] H. Zhang, Y. Yuan, and W. Xu, "Papr reduction for dco-ofdm visible light communications via semidefinite relaxation," *IEEE Photonics Technology Letters*, vol. 26, no. 17, pp. 1718–1721, 2014.

[54] Y. Hei, J. Liu, W. Li, X. Xu, and R. T. Chen, "Branch and bound methods based tone injection schemes for papr reduction of dco-ofdm visible light communications," *Opt. Express*, vol. 25, no. 2, pp. 595–604, Jan 2017. [Online]. Available: `https://opg.optica.org/oe/abstract.cfm?URI=oe-25-2-595`

[55] J. G. Doblado, A. C. O. Oria, V. Baena-Lecuyer, P. Lopez, and D. Perez-Calderon, "Cubic Metric Reduction for DCO-OFDM Visible Light Communication Systems," *Journal of Lightwave Technology*, vol. 33, no. 10, pp. 1971–1978, May 2015.

[56] J. Bai, Y. Li, Y. Yi, W. Cheng, and H. Du, "PAPR Reduction Based on Tone Reservation Scheme for DCO-OFDM Indoor Visible Light Communications," *Opt. Express*, vol. 25, no. 20, pp. 24 630–24 638, Oct 2017. [Online]. Available: `http://www.opticsexpress.org/abstract.cfm?URI=oe-25-20-24630`

[57] Z. Yu, R. J. Baxley, and G. T. Zhou, "Iterative Clipping for PAPR Reduction in Visible Light OFDM Communications," in *2014 IEEE Military Communications Conference*, Oct 2014, pp. 1681–1686.

[58] W. O. Popoola, Z. Ghassemlooy, and B. G. Stewart, "Pilot-Assisted PAPR Reduction Technique for Optical OFDM Communication Systems," *Journal of Lightwave Technology*, vol. 32, no. 7, pp. 1374–1382, April 2014.

[59] L. Deng, Y. Fan, and Q. Zhao, " A Novel PAPR Reduction Scheme for VLC DCO-OFDM Systems ," *Optics Communications*, vol. 426, pp. 164 – 169, 2018. [Online]. Available: `http://www.sciencedirect.com/science/article/pii/S0030401818304401`

[60] S. H. Muller and J. B. Huber, "OFDM with Reduced Peak-to-average Power Ratio by Optimum Combination of Partial Transmit Sequences," *Electronics Letters*, vol. 33, no. 5, pp. 368–369, Feb 1997.

[61] G. Lu, P. Wu, and C. Carlemalm-Logothetis, "Enhanced Interleaved Partitioning PTS for Peak-to-average Power Ratio Reduction in OFDM Systems," *Electronics Letters*, vol. 42, no. 17, pp. 983–984, August 2006.

[62] Y. Xiao, M. Chen, F. Li, J. Tang, Y. Liu, and L. Chen, " PAPR Reduction Based on Chaos Combined with SLM Technique in Optical OFDM IM/DD System ," *Optical Fiber Technology*, vol. 21, pp. 81 – 86, 2015. [Online]. Available: http://www.sciencedirect.com/science/article/pii/S106852001400131X

[63] M. Z. Farooqui, P. Saengudomlert, and S. Kaiser, "Average transmit power reduction in ofdm-based indoor wireless optical communications using slm," in *International Conference on Electrical & Computer Engineering (ICECE 2010)*, 2010, pp. 602–605.

[64] W.-W. Hu and D.-H. Lee, "Papr reduction for visible light communication systems without side information," *IEEE Photonics Journal*, vol. 9, no. 3, pp. 1–11, 2017.

[65] Y. Li, H. Qiu, X. Chen, and J. Fu, "A Novel PAPR Reduction Algorithm for DCO-OFDM/OQAM System in Underwater VLC ," *Optics Communications*, vol. 463, p. 125449, 2020. [Online]. Available: http://www.sciencedirect.com/science/article/pii/S0030401820301103

[66] Chin-Liang Wang and Yuan Ouyang, "Low-complexity Selected Mapping Schemes for Peak-to-average Power Ratio Reduction in OFDM Systems," *IEEE Transactions on Signal Processing*, vol. 53, no. 12, pp. 4652–4660, Dec 2005.

[67] C. Li, S. Wang, and C. Wang, "Novel Low-Complexity SLM Schemes for PAPR Reduction in OFDM Systems," *IEEE Transactions on Signal Processing*, vol. 58, no. 5, pp. 2916–2921, May 2010.

[68] E. Alsusa and L. Yang, "A Low-Complexity Time-Domain Linear Symbol Combining Technique for PAPR Reduction in OFDM Systems," *IEEE Transactions on Signal Processing*, vol. 56, no. 10, pp. 4844–4855, Oct 2008.

[69] T. Uday, A. Kumar, and L. Natarajan, "Low papr coding scheme for uniform illumination in mimo vlc," in *2018 IEEE Globecom Workshops (GC Wkshps)*, 2018, pp. 1–6.

[70] X.-Y. Xu, Q. Zhang, and D.-W. Yue, "Orthogonal frequency division multiplexing with index modulation based on discrete hartley transform in visible light communications," *IEEE Photonics Journal*, vol. 14, no. 3, pp. 1–10, 2022.

[71] u. Thummaluri, A. Kumar, and L. Natarajan, "Flicker mitigating high rate rll codes for vlc with low complexity encoding and decoding," in *2018 IEEE International Symposium on Smart Electronic Systems (iSES) (Formerly iNiS)*, 2018, pp. 209–214.

[72] R. Jensen and Q. Shen, *Set Theory*. IEEE, 2008, pp. 13–37. [Online]. Available: `https://ieeexplore.ieee.org/document/5236664`

[73] V. Kishore and V. Mani, " Spectrally Efficient Revised PAM-DMT for IM/DD Optical Wireless Communication systems ," *Optics Communications*, vol. 465, p. 125568, 2020. [Online]. Available: `http://www.sciencedirect.com/science/article/pii/S0030401820301772`

[74] L. Chen, B. Krongold, and J. Evans, "Performance Analysis for Optical OFDM Transmission in Short-Range IM/DD Systems," *Journal of Lightwave Technology*, vol. 30, no. 7, pp. 974–983, April 2012.

[75] K. Vejandla, S. Valluri, V. M. Vakamulla, and A. Kumar, "A Tunable Energy Signal for Intensity Modulation and Direct Detection Systems: Theory, Simulations, and Experiments," *IEEE Photonics Journal*, vol. 12, no. 1, pp. 1–12, Feb 2020.

[76] J. Armstrong, "Analysis of New and Existing Methods of Reducing Intercarrier Interference due to Carrier Frequency Offset in OFDM," *IEEE Transactions on Communications*, vol. 47, no. 3, pp. 365–369, March 1999.

[77] S. P. Valluri, V. Kishore, and V. M. Vakamulla, "A New Selective Mapping Scheme for Visible Light Systems," *IEEE Access*, vol. 8, pp. 18 087–18 096, 2020.

[78] S. Valluri and V. Mani, " A Novel Approach for Reducing Complexity in the SLM-GFDM System ," *Physical Communication*, vol. 34, pp. 188 – 195, 2019. [Online]. Available: http://www.sciencedirect.com/science/article/pii/S1874490718304397

[79] Z. Ghassemlooy, S. Arnon, M. Uysal, Z. Xu, and J. Cheng, " Emerging Optical Wireless Communications-Advances and Challenges," *IEEE Journal on Selected Areas in Communications*, vol. 33, no. 9, pp. 1738–1749, 2015.

[80] H. Elgala, R. Mesleh, and H. Haas, "Indoor Broadcasting via White LEDs and OFDM," *IEEE Transactions on Consumer Electronics*, vol. 55, no. 3, pp. 1127–1134, 2009.

[81] J. R. Barry, J. M. Kahn, W. J. Krause, E. A. Lee, and D. G. Messerschmitt, "Simulation of Multipath Impulse Response for Indoor Wireless Optical Channels," *IEEE Journal on Selected Areas in Communications*, vol. 11, no. 3, pp. 367–379, 1993.

[82] A. M. Khalid, G. Cossu, R. Corsini, P. Choudhury, and E. Ciaramella, "1-Gb/s Transmission Over a Phosphorescent White LED by Using Rate-Adaptive Discrete Multitone Modulation," *IEEE Photonics Journal*, vol. 4, no. 5, pp. 1465–1473, 2012.

[83] V. Kishore and V. Mani, "A novel Timing Synchronization Method for OFDM Based VLC Systems," *Optik*, vol. 244, p. 167206, 2021. [Online]. Available: https://www.sciencedirect.com/science/article/pii/S0030402621008676

[84] Z. Yu, H. Chen, M. Chen, S. Yang, and S. Xie, "Bandwidth Improvement Using Adaptive Loading Scheme in Optical Direct-Detection OFDM," *IEEE Journal of Quantum Electronics*, vol. 52, no. 10, pp. 1–6, 2016.

[85] O. Saied, Z. Ghassemlooy, S. Rajbhandari, and A. Burton, "Optical Single Carrier-interleaved Frequency Division Multiplexing for Visible Light Communication Systems," *Optik*, vol. 194, p. 162910, 2019. [Online]. Available: https://www.sciencedirect.com/science/article/pii/S0030402619307739

[86] F. Tithi and S. Majumder, "Performance Analysis of a DCO-CO-OFDM Optical Transmission System with Distributed Raman Amplifier using Coherent

Heterodyne Receiver," *Optik*, vol. 210, p. 164481, 2020. [Online]. Available: https://www.sciencedirect.com/science/article/pii/S0030402620303156

[87] T. Adiono, A. Pradana, R. V. W. Putra, W. A. Cahyadi, and Y. H. Chung, "Physical Layer Design with Analog Front end for Bidirectional DCO-OFDM Visible Light Communications," *Optik*, vol. 138, pp. 103–118, 2017. [Online]. Available: https://www.sciencedirect.com/science/article/pii/S0030402617303066

[88] G. Miriyala and V. Mani, "A new PAPR Reduction Technique in DCO-OFDM for Visible Light Communication Systems ," *Optics Communications*, vol. 474, p. 126064, 2020. [Online]. Available: http://www.sciencedirect.com/science/article/pii/S0030401820304818

[89] J. Armstrong and A. J. Lowery, "Power Efficient Optical OFDM," *Electronics Letters*, vol. 42, no. 6, pp. 370–372, 2006.

[90] R. Islam and M. R. H. Mondal, "Hybrid DCO-OFDM, ACO-OFDM and PAM-DMT for dimmable LiFi," *Optik*, vol. 180, pp. 939–952, 2019. [Online]. Available: https://www.sciencedirect.com/science/article/pii/S0030402618318746

[91] X. Li, R. Mardling, and J. Armstrong, "Channel Capacity of IM/DD Optical Communication Systems and of ACO-OFDM," in *2007 IEEE International Conference on Communications*, 2007, pp. 2128–2133.

[92] G. Miriyala, A. Kakumanu, M. P. Swapna, and P. S. Shankar, "Joint Estimation of Channel Response, Frequency Offset and Phase Noise in OFDM Systems," in *2018 Second International Conference on Intelligent Computing and Control Systems (ICICCS)*, 2018, pp. 1299–1303.

[93] G. Miriyala, A. Kaul, and R. Nath, "Reduced Complexity channel Estimation Method for Multi Input Multi Output-Orthogonal Frequency Division Multiplexing Systems by Subspace Tracking," in *2013 3rd IEEE International Advance Computing Conference (IACC)*, 2013, pp. 470–475.

[94] R. Mesleh, H. Elgala, and H. Haas, "LED Nonlinearity Mitigation Techniques in Optical Wireless OFDM Communication Systems," *IEEE/OSA Journal of Optical Communications and Networking*, vol. 4, no. 11, pp. 865–875, 2012.

[95] S. R. Z. Ghassemlooy, W. Popoola, *Optical Wireless Communications: System and Channel Modelling with MATLAB*, 1st ed. CRC Press, 2012. [Online]. Available: http://gen.lib.rus.ec/book/index.php?md5=d28002ccffdf8462f6de2b5a15bc132f

[96] G. Miriyala, M. Vakkalagadda, and M. Narsing Yadav, "MIMO-OFDM System Analysis over Distinct Fading Channels with Different Modulation Techniques," in *2018 3rd IEEE International Conference on Recent Trends in Electronics, Information Communication Technology (RTEICT)*, 2018, pp. 1332–1335.

[97] G. Miriyala and V. V. Mani, "Peak Sample Detection based PAPR Reduction Algorithm in Optical-OFDM for VLC Systems," in *2021 24th Intl. Symp. on Wirel. Pers. Multi. Commu. (WPMC)*, 2021, pp. 1–6.

[98] S. Kruse, C. Kress, A. Memedi, C. Tebruegge, M. S. Amjad, C. Scheytt, and F. Dressler, "Design of an Automotive Visible Light Communications Link using a Off-The-Shelf LED Headlight," in *ANALOG 2018 16. GMM/ITG-Fachtagung*. IEEE, 2018.

[99] V. Kishore, S. P. Valluri, V. M. Vakamulla, M. Sellathurai, A. Kumar, and T. Ratnarajah, "Performance Analysis Under Double Sided Clipping and Real Time Implementation of DCO-GFDM in VLC Systems," *Journal of Lightwave Technology*, vol. 39, no. 1, pp. 33–41, 2021.

[100] S. P. Valluri, "Investigation of Blind CFO Estimation for GFDM System using Universal Software Radio Peripheral: Theory, Simulations and Experiments," *IET Comm.*, vol. 13, pp. 1936–1944(8), August 2019.

[101] D. Demmer, R. Zakaria, R. Gerzaguet, J.-B. Dor, and D. Le Ruyet, "Study of ofdm precoded filter-bank waveforms," *IEEE Transactions on Wireless Communications*, vol. 18, no. 6, pp. 2889–2902, 2019.

[102] K. Ying, Z. Yu, R. J. Baxley, H. Qian, G.-K. Chang, and G. T. Zhou, "Nonlinear distortion mitigation in visible light communications," *IEEE Wireless Communications*, vol. 22, no. 2, pp. 36–45, 2015.

[103] J.-P. M. G. Linnartz, X. Deng, and P. Van Voorthuisen, "Impact of dynamic led non-linearity on dco-ofdm optical wireless communication," *IEEE Communications Letters*, vol. 25, no. 10, pp. 3335–3339, 2021.

[104] M. Noshad and M. Brandt-Pearce, "Hadamard-coded modulation for visible light communications," *IEEE Transactions on Communications*, vol. 64, no. 3, pp. 1167–1175, 2016.

[105] H. Schulze and P. A. Hoeher, "Asymmetrically clipped optical hadamard coded modulation (aco-hcm)," *IEEE Photonics Journal*, vol. 15, no. 1, pp. 1–12, 2023.

[106] A. Aung, B. P. Ng, and S. Rahardja, "Conjugate symmetric sequency-ordered complex hadamard transform," *IEEE Transactions on Signal Processing*, vol. 57, no. 7, pp. 2582–2593, 2009.

[107] S.-C. Pei, C.-C. Wen, and J.-J. Ding, "Conjugate symmetric discrete orthogonal transform," *IEEE Transactions on Circuits and Systems II: Express Briefs*, vol. 61, no. 4, pp. 284–288, 2014.